AFDELINGEN FOR
BÆRENDE KONSTRUKTIONER
DANMARKS TEKNISKE HØJSKOLE

STRUCTURAL RESEARCH LABORATORY
TECHNICAL UNIVERSITY OF DENMARK

Egil Borchersen

MOIRÉ PATTERN DEFORMATION THEORY AND OPTICAL FILTERING TECHNIQUES

RAPPORT NR. R 43 1974

MOIRÉ PATTERN DEFORMATION THEORY
AND
OPTICAL FILTERING TECHNIQUES.

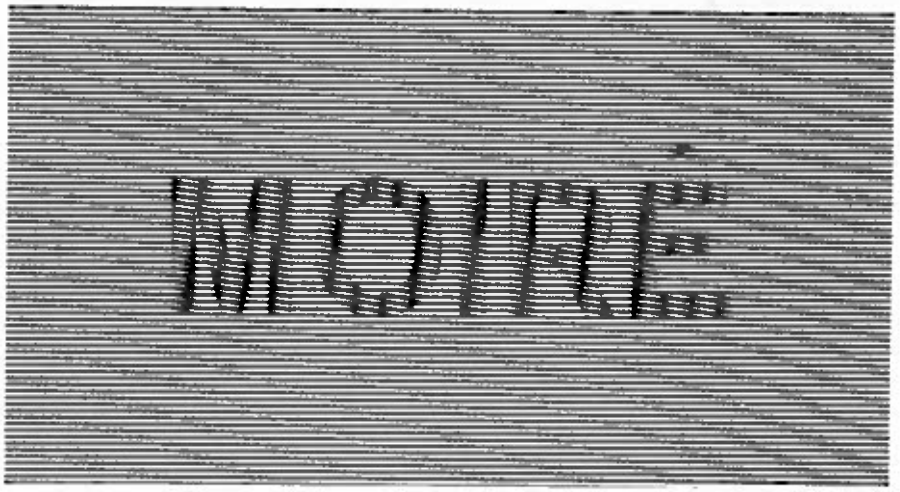

BY

EGIL BORCHERSEN

1974

Institute of Building Design
Technical University of Denmark

PREFACE

This report is a slightly revised version of a thesis submitted in November, 1972, for the degree of Lic.Tech.(Ph.D.) in structural engineering.

The subject for the research was:

1) to give a general presentation of the theory for moiré-technique applied to deformation measurements,
2) to carry out moiré-tests with a view to determining the accuracy and suitability for the method for the solution of specific problems.

The post-graduate research has been carried out at the Structural Research Laboratory, The Technical University of Denmark, under Professor, Dr.Tech. K.W. Johansen and Professor Vagn Askegaard.

The translation into English has been done by Mrs. Pauline Katborg and granted by the Structural Research Laboratory, and the type-writing has been done by Miss Birgit Rossil at the Institute of Building Design.

All this help is hereby gratefully acknowledged.

Institute of Building Design
June 1974

Egil Borchersen

CONTENTS

	PAGE
PREFACE	I
CONTENTS	II
SUMMARY	V
EXPLANATORY NOTE	V
NOTATION	VI
1. INTRODUCTION	1-1
1.1 What is Moiré ?	1-1
1.2 The Principle of Moiré-Technique	1-2
1.3 On the Moiré Literature	1-4
1.4 Contents of the Report	1-6
2. THE MOIRÉ-EFFECT	2-1
2.1 The Gratings Applied	2-1
2.2 The Moiré-Effect of Two Parallel Line Gratings	2-2
2.3 The Moiré-Effect of Two Crossed Line Gratings	2-8
2.4 Influence of the Grating Geometry	2-11
2.5 Bright and Dark Fringes or Vice Versa	2-13
3. GENERAL MOIRÉ-PATTERN THEORY	3-1
3.1 Contour Lines and Diagonal Systems	3-1
3.2 General Moiré-Pattern Theory for Two Gratings of the Known Geometry	3-6
3.3 General Moiré-Pattern Theory in Deformation Measurements	3-12
4. GENERAL MOIRÉ-PATTERN THEORY OF LINE GRATINGS	4-1
4.1 The Displacement and Deformation of the Model Grating	4-1
4.2 Parametric Description of the Moiré-Pattern	4-10
5. ANALYSIS OF THE UNDEFORMED MOIRÉ-PATTERN FORMED BY TWO LINE GRATINGS	5-1
5.1 The Geometrical Relationship	5-1
5.2 Comparison the Two Line Gratings	5-9
5.3 Two Undeformed Line Gratings Used for Displacement Measurements	5-11

	PAGE
6. ANALYSIS OF THE "DEFORMED" MOIRÉ-PATTERN BETWEEN TWO LINE GRATINGS	6-1
6.1 Parametric Description of the Moiré-Pattern	6-1
6.2 Variation of the Grating Displacement Function	6-3
6.3 Tangent Method. Variation in the Derivatives of the Grating Displacement Function	6-8
6.4 Variation in Moiré-Line Parameter	6-15
6.5 Moiré-Line Density. "Mismatch". Geometrical Multiplication	6-18
6.6 The Moiré-Surface. The Surface Slope Method	6-25
6.7 Super-Moiré. Moiré of Moiré. Second-Order Moiré	6-28
6.8 For How Great Displacements and Displacement Gradients is the Theory Valid ?	6-31
7. ACCURACY IN DETERMINATION OF DEFORMATION	7-1
7.1 Accuracy in Determination of Displacement	7-2
7.2 Accuracy in the Tangent Method	7-3
7.3 Accuracy with the Surface-Slope Method	7-8
7.4 Accuracy in Super-Moiré Method	7-13
8. OPTICAL METHODS IN MOIRÉ-PATTERN ANALYSIS	8-1
8.1 The Optical Arrangement	8-1
8.2 The Diffraction Pattern of a Line Grating and the Optical Filtering of its Image	8-3
8.3 Diffraction Pattern for a Moiré-Pattern and its Optical Filtering	8-9
8.4 Interpolation by Means of Measurements of Light Intensity	8-13
8.5 Optical Multiplication of a Moiré-Pattern	8-17
8.6 Other Applications of Optical Filtering Technique	8-23
8.7 Other Applications of the Diffraction Effect of the Gratings	8-24

APPENDIX	PAGE
A. REFERENCES	A-1
B. DIFFRACTION THEORY. CALCULATION OF DISTRIBUTION OF LIGHT INTENSITY	B-1
B.1 Basic Concepts of Physical Optics	B-1
B.2 On Fourier Series, Fourier Transforms and Dirac's Delta Function	B-4
B.3 Fourier Analysis of the Diffraction Pattern	B-8
B.4 The Diffraction Pattern of a Line Grating	B-11
B.5 Optical Filtering of a Line Grating	B-15
B.6 The Diffraction Pattern of Two Crossed Line Gratings	B-20
B.7 Optical Filtering of a Moiré Pattern	B-23
C. BRIGHT AND DARK MOIRÉ-FRINGES, OR VICE VERSA	C-1

SUMMARY

The report deals mainly with the moiré-pattern formed by two superposed line gratings. The deformation of one of the gratings can be described by a displacement function, and by means of this, a parametric description of the moiré-fringes can be established. On this basis, a number of methods for determining the displacement function and its derivatives from the geometry of the moiré-fringes are developed and evaluated.

Within recent years, interest has concentrated on developing the use of optical filtering and multiplication of moiré-patterns. The theoretical background for this is examined at the end of the report.

RESUMÉ

I rapporten behandles hovedsageligt moiré-mønsteret, som to overlejrede liniegitre danner. Det ene gitters deformation kan beskrives ved en flytningsfunktion, og ved hjælp af denne opstilles en parameterbeskrivelse for moiréstriberne. På grundlag heraf udvikles og vurderes en række metoder til bestemmelse af flytningsfunktionen og dennes afledede udfra moiré-stribernes geometri.

Inden for de senere år har udviklingen koncentreret sig om brugen af optisk filtrering og multiplikation af moirémønstrene. Den teoretiske baggrund for dette gøres der rede for sidst i rapporten.

EXPLANATORY NOTE

The report consists of 8 chapters and 3 appendices, which are divided into numbered sections, e.g. 3.1. The formulae are numbered consecutively within each section, e.g. (6.2-5), and the same applies to tables and figures. References to the literature are given in square brackets, e.g. [68-10], where the first figure is the year of publication, and the second, its number in the bibliography in appendix A.

NOTATION

Part of the notation is used throughout, while the remainder is only used locally in a few chapters. The former is as follows:

A_m and A_r : Coordinates to the grating lines m = 0 and r = 0 (section 4.2).

e : Relative difference in line-spacing (5.1-10).

f, f_x, f_y : Interfringe spacing (5.1).

F, F_x, F_y : Relative interfringe spacing (5.1-1, 5.1-2, and 5.1-3).

m : Model-grating-parameter (4.2).

M{x,y} : Moiré-surface (6.6).

MG : Model grating.

MP : Moiré pattern.

n : Moiré-line parameter (4.2-4).

p : Pitch (2.1).

p_r : Reference grating pitch (4.2).

p_m : Model grating pitch (4.2).

r : Reference grating parameter (4.2).

RG : Reference grating.

T : Transmittance (2.2-2).

v{x,y} : Grating displacement function (4.1).

V : Visibility (2.4).

β : Relative space-width (2.1).

δ : Relative model grating pitch (4.2-5).

θ : Angle between grating lines (2.2 or 4.2).

φ : Moiré-line inclination (3.2 or 5.1).

1. INTRODUCTION

1.1 What is Moiré ?

If two superposed line-systems are dense and almost periodic, they often form an interference pattern known as a MOIRÉ-PATTERN. The word "moiré" is derived from the French name for a silk fabric in which the threads are oriented in such a way that they form patterns similar to the above-mentioned interference-pattern. The interference-phenomenon, which is due to a simple shadow effect, is sometimes called GEOMETRICAL or MECHNICAL INTERFERENCE (Weller & Shepard [48-1], Kaczer & Kroupa [52-1]), as distinct from optical interference, which is due to the wave-nature of light.

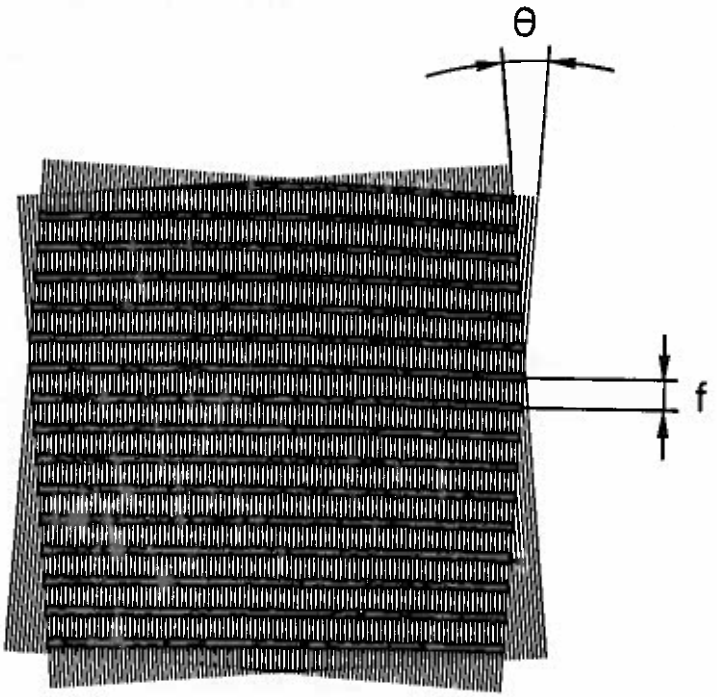

The interference-pattern between two identical line-gratings turned an angle θ in relation to each other

Figure 1.1-1

1.2 The Principle of Moiré-Technique

In experimental strain analysis, MOIRÉ-TECHNIQUE is defined as the utilization of the interference-effect between two dense line-systems (called GRATINGS). It is, of course, a condition that the geometrical properties of the two superposed line-systems produce a moiré-pattern.

The principle of the moiré-technique is as follows: the state (i.e. the position of a structural member or its state of deformation), the change in which is to be determined, is characterized by a grating (denoted the MODEL GRATING). It is assumed that there is an unambiguous relationship between the geometry of the model grating and the state of the specimen, which means that determination of the change in the geometry of the model grating is sufficient for determination of the corresponding change in the state of the specimen.

In order to determine the geometry of the model grating, a second grating (called the REFERENCE GRATING) is superposed on it, whereby a moiré-pattern is produced.

In order to determine the changes in the state of the specimen it is necessary to know the relationship between the model grating, the reference grating, and the moiré-pattern, and the relationship between the model grating and the state of the specimen.

The first relationship is general and does not depend particularly on the state to be measured, but solely on the mutual geometry of the two gratings. The analysis of this relationship is called THE MOIRÉ-PATTERN THEORY.

On the other hand, the relationship between the geometry of the model grating and the state of the specimen differs from one method to another. The analysis of this relationship is called THE MOIRÉ-METHOD THEORY, and it is only treated briefly in this report. In Section 4.1 the moiré-method theory for three well-known methods is described, namely, direct-moiré, shadow-moiré, and reflection-moiré.

In the following, a more rigorous division of the moiré-theory is given on the basis of the following common features of the moiré-methods:

a. In all the moiré-methods, a moiré-pattern is formed in the focal plane of the reproducing system (camera).

b. The moiré-pattern in a. is formed by superposing two reproduced gratings.

c. The deformation of one of the gratings can be unambiguously expressed by means of one or more of the parameters describing the deformation of the specimen.

The relationship c. also depends on the position of the reproducing system (camera) in relation to the specimen. Thus, the same deformation of the specimen will produce different moiré-patterns if the position of the reproducing system is altered. However, it is possible to take this factor into account in the relationship c., and the author has therefore decided, for the purpose of the present report, to differentiate as follows between moiré-pattern theory and moiré-method theory.

The moiré-pattern theory comprises the geometrical relationship between two gratings reproduced on the same focal plane and their moiré-pattern.

The moiré-method theory comprises the theoretical relationship between the deformation of a specimen and the reproduction of a grating on the focal plane of an optical reproduction system (camera).

The report concentrates mainly on the moiré-pattern theory, which is the part of the theory of moiré-technique that is common to all moiré-methods. With this approach, the treatment differs from current papers on moiré-technique, in which it is usual to describe only the combination of pattern-theory and method-theory that is valid for the method under consideration.

It appears to the author that it is more logical to differentiate between the two theories when all the moiré-methods are to be treated as a whole, in addition to which, this approach facilitates comparison of the individual methods.

1.3 On the Moiré Literature

There are at present more than 400 papers on moiré-technique, and new papers continue to appear, although at a slower rate. The most recent survey is provided by Theocaris [69-1], who has reviewed about 300 of them.

In the following, the historical background of the moiré-pattern theory is outlined in brief.

According to Guild [56-1], Lord Rayleigh seems to have been the first to describe his observation of a moiré-pattern. "This phenomenon might be made useful as a test". However, it was not until 70-80 years later that the observation was utilized for the measurement of deformations.

Weller and Shepard [48-1] described displacement measurements using two identical line-gratings and establish the fact that if two identical line-gratings are superposed with their lines parallel, a deformation of one of the gratings will result in the formation of a moiré-pattern with the following characteristics: 1) Points in the deformed grating situated on the same moiré-fringe are displaced the same distance in the direction perpendicular to the original line orientation. 2) The difference in displacement between points on neighbouring fringes (two bright or two dark ones) is equal to the pitch of the undeformed grating.

Kaczer and Kroupa [52-1] gave the first formulae expressing the geometrical relationship between two undeformed line-gratings with different pitches and their moiré-pattern.

One of the most important contributions to the moiré-pattern theory is that of Dantu [58-1], which is a continuation of

[54-1]. Dantu interprets the moiré-fringes as contour-curves for the displacement function in the direction perpendicular to the orientation of the grating line, and on the basis of this approach, he evaluates formulae for determination of the strain-state from the moiré-pattern. Both the linear and the angular mismatch techniques are included in the approach, and a number of other topics, e.g. moiré of moiré, are considered.

Dantu's approach, also known as the displacement approach, has not gained as much ground as that used by Kaczer and Kroupa, which is known as the geometrical approach. Durelli, Sciammarella, and Parks have used Dantu's approach in a couple of papers [61-1] and [63-1], but have since shown a preference for the geometrical approach. Post [65-5], Košťák [68-2], Martin and Ju [69-2][70-3],and Danh and Taylor [70-4] have used the displacement approach because it has proved advantageous in the analysis of finite deformations.

The geometrical approach initiated by Kaczer and Kroupa has been elaborated by Crisp [57-1], who has analysed the accuracy of the method. A more significant analysis is given by Morse, Durelli, and Sciammarella [60-2], in which curves are shown from which the strain components can be read directly after measurement of the inter-fringe spacing and the fringe inclination. An analogous analysis in respect of finite deformations is given by Vinckier and Dechaene [63-3], and the mismatch phenomenon has been analysed by means of the geometrical approach by Tanaka and Nakashima [60-4], Chiang [65-4], and Vafiadakis and Lamble [67-3]. Finally, Chiang [69-3] has used the geometrical approach to analyse the sign of the strain components.

There are only a few papers on the general moiré-pattern theory; those of Pirard [60-1] and Košťák [68-2] form the basis for chapter 3 of the present work and are discussed there.

In 1969, when work started on the present report, the literature on moiré-technique consisted mainly of papers in which only special topics within the field of moiré were

analysed. There was no single paper in which all the results were summarized in a way that would enable a beginner in moiré-technique to utilize all the report results together, without reading the main part of the papers. It, therefore, became the main purpose of the author's work as post-graduate student to summarize the existing literature on moiré.

In the meantime, two books have been published that deal particularly with the utilization of the moiré-effect in strain analysis. The first, by Theocaris, "MOIRÉ FRINGES IN STRAIN ANALYSIS" [69-1] deals mainly with moiré-methods. Theocaris is responsible for a large number of the papers on moiré-technique, and his book is primarily a reprint of these papers, supplemented by a few papers by other authors. The second book, "MOIRÉ ANALYSIS OF STRAIN" [70-1], by Durelli and Parks, deals to a greater extent with the moiré-pattern theory, and the only method described is direct-moiré.

Although the books have in some measure supplied the need for a summarizing paper, there are still a number of problems that require analysis. Furthermore, some problems have been solved since publication of the above-mentioned books, and interest has focused particularly on the utilization of the grating-diffraction effect, so the need has arisen for a summarizing treatment of these topics too.

These factors, together with the further generalization of the moiré-pattern theory that has proved possible, form the background of this report. The preliminary work consists of two lecture notes [70-2] and [71-1] and a number of unpublished, internal reports.

1.4 Contents of the Report

The report is divided into two parts, moiré-pattern theory and optical filtering technique.

The first part, which includes chapters 2.-7., begins with chapter 2 on the moiré-effect, i.e. the conditions causing a moiré-pattern to appear when two line-systems are superposed.

The discussion on the moiré-pattern theory commences with a generel review in chapter 3. Items of new interest are dealt with particularly in section 3.3 of this chapter. In chapter 4, the theory is specialized to deformation measurement by means of two superposed line-gratings, one of which has undergone deformations and displacement. At the end of this chapter, a parametric description of the moiré-pattern is drawn up.

Chapters 5 and 6 contain an analysis of this parametric description. In chapter 5, the "undeformed moiré-pattern" is analysed, i.e. the moiré-pattern formed by two undeformed line-gratings, mutually inclined and displaced.

In chapter 6, the most important of the report, the analysis deals with the case in which one of the gratings is deformed. The procedure for complete determination of the deformation from the geometry of the moiré-pattern is described. The analysis, in particular, differs from those given elsewhere.

In chapter 7, which completes the first part of the report, the accuracy of the deformation measurement is estimated. The contents of this chapter are also new.

After this treatment of the so-called classical moiré-pattern theory, chapter 8 deals with the possibilities offered by the optical filtering technique for extracting further information from the moiré-pattern. This exposition of the latest developments in the field is also new.

A number of appendices conclude the report.

2. THE MOIRÉ-EFFECT

2.1 The Gratings Applied

As mentioned above, the line-systems under consideration are called gratings. Some authors distinguish between moiré-gratings and diffraction-gratings, but this is unnecessary as the latter can also form moiré-patterns. The term "grid" is also used for the line-systems, but here it is reserved for the line-systems applied in the grid method, which is not a moiré-method.

The grating most frequently utilized is the line-grating. Its structure, which is shown in fig. 2.1-1, consists of parallel, dark and bright lines (rules), bars and spaces. The centre-lines of the bars are denoted the GRATING LINES, and the distance between them is known as the PITCH. In the figure, p denotes the pitch, and β the ratio between the space width and the pitch. The relative space width β adopts values in the interval $0 < \beta < 1$.

The grating can work either as a TRANSMISSION GRATING or as a REFLECTION GRATING. In the first case, the spaces are transparent, while in the second, they are reflecting. In both cases, the bars absorb all the light received. In the following, only transmission gratings are considered, but it will be evident that the theory is also valid in respect of reflection gratings.

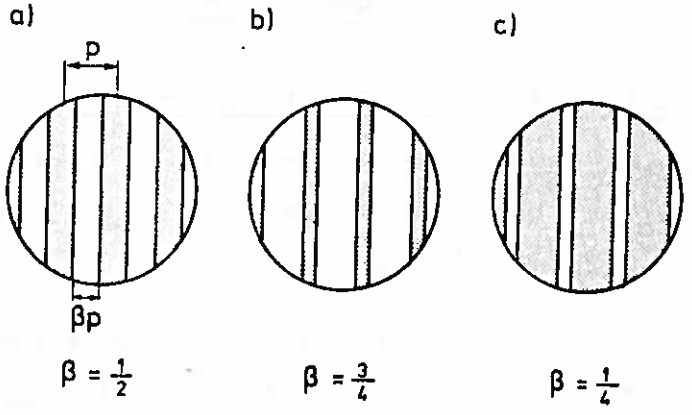

Examples of line grating structures

Figure 2.1-1

The gratings normally utilized in moiré-technique have line densities of about 1-40 lines per millimetre (ℓ/mm), while the diffraction gratings have densities of more than 400 ℓ/mm. This could provide grounds for differentiating between the two categories of gratings, because moiré-patterns formed by low-density gratings can be observed with the naked eye, while in the case of higher densities, the gratings have to be placed in a spectroscope (Guild [56-1]). The difference arises due to the wave-nature of light, which makes the diffraction effect of a grating dominate at high line densities.

Even though line gratings have proved to have many applications, there are cases in which another grating structure is more convenient. The applications of circular and radial gratings have been described by, inter alios, Theocaris [65-1], and the applications of spiral gratings, by Košťák and Popp [66-1]. Finally, fig. 2.1-2 shows other gratings derived from the line grating.

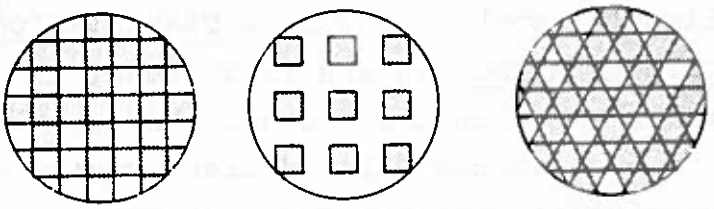

Line grating combinations .

Figure 2.1-2

2.2 The Moiré Effect of Two Parallel Line Gratings

The three standard combinations of two line gratings are shown in fig. 2.2-1. The pitches are p_r and p_m, and the acute angle between the grating lines is θ.

The moiré-pattern consists of equidistant and parallel, dark and bright fringes, which are denoted BRIGHT and DARK MOIRÉ-FRINGES. Their centrelines are the MOIRÉ-LINES or the MOIRÉ-CURVES.

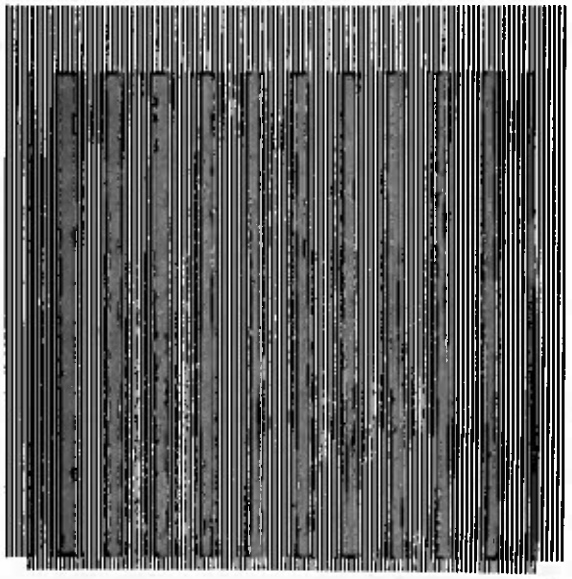

Figure 2.2-1.a

The moiré-pattern between two line gratings with parallel lines but different pitches.

($\theta = 0 \wedge p_r \neq p_m$)

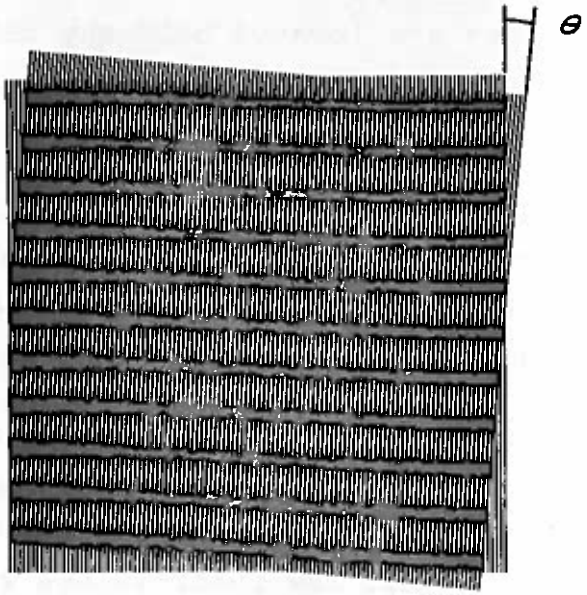

Figure 2.2-1.b

The moiré-pattern between two identical line gratings with the lines inclined the angle θ.

($\theta \neq 0 \wedge p_r = p_m = p$)

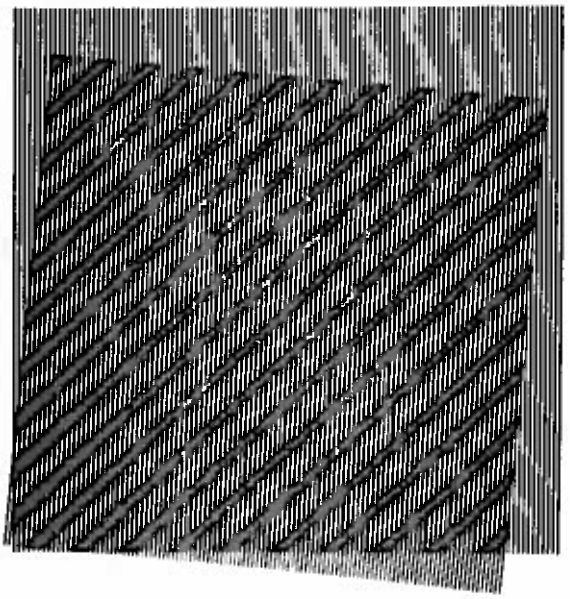

Figure 2.2-1.c

The moiré-pattern between two line gratings with different pitches and with the lines inclined the angle θ.

($\theta \neq 0 \wedge p_r \neq p_m$)

The three cases shown are: a) two gratings with parallel lines but different pitches, b) two identical gratings (i.e. with the same pitch) but with the lines inclined the angle θ, c) two gratings with different pitches and with the lines inclined the angle θ.

In the first case, the moiré-fringes are parallel to the grating lines, while in the second the fringes are parallel to the bisector of the obtuse angle between the grating lines.

2.2.1 Geometrical Interpretation of the Moiré-Effect

If a part of the moiré-pattern in fig. 2.2-1.a is magnified as shown in fig. 2.2-2.a, it will be seen that the moiré-line in one grating coincides with a grating line in the second grating. The dark fringes are located half-way between the bright fringes, i.e. where a grating line in one grating coincides with a space in the second grating.

Geometrically speaking, the difference between the numbers of grating lines in the two gratings is exactly one between two neighbouring fringes. Hence, the grating lines are analogous to the lines of a vernier scale.

In fig. 2.2-2.a, the two gratings are called RG and MG, and their pitches, p_r and p_m ($p_r < p_m$). If the number of pitches (p_r) is n between two bright fringes in the grating RG, then there will be n-1 pitches (p_m) in MG. The inter-fringe spacing (i.e. the shortest distance between two dark or two bright fringes) can then be expressed as

$$f = n\,p_r = (n - 1)\,p_m \qquad (2.2\text{-}1)$$

Eliminating n, we get

$$f = \frac{p_r\,p_m}{p_m - p_r} \qquad (2.2\text{-}2)$$

If $p_r = p_m$, no moiré-pattern will appear as long as the grating lines are parallel.

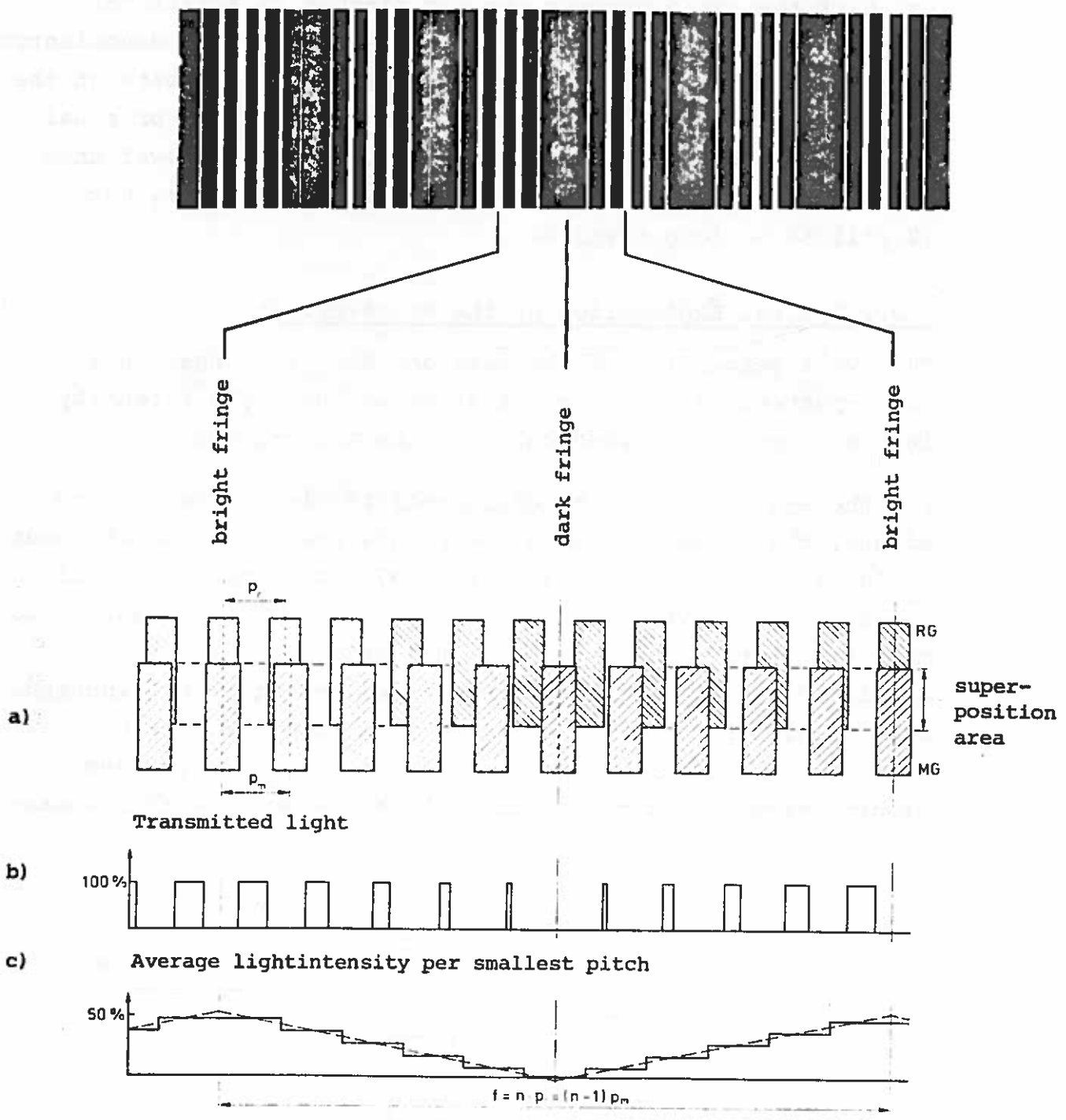
bright fringe
dark fringe
bright fringe
p_r
p_m
RG
MG
super-
position
area
a)
Transmitted light
b)
100 %
c)
Average lightintensity per smallest pitch
50 %
f = n p = (n-1) p_m

Figure 2.2-2

Strictly speaking, the above-mentioned derivation is only valid if the ratio between the two pitches is a rational number and if the difference between nominator and denomiantor is equal to one (unity). This restricts the ratio between the largest and the smallest pitch to values less than or equal to 2. If the pitch ratio is an irrational number lower than 2, then the fringe spacing is also given by (2.2-2), but (2.2-1) is no longer valid.

2.2.2 Optical Explanation of the Moiré-Effect

The eye's perception of the dark and bright fringes in a moiré-pattern is due to a variation in the light intensity in the direction perpendicular to the moiré-lines.

For the eye to be able to differentiate clearly between two points, the visual angle to the points must be at least about 0.0005 radians (Bjerge [64-1] page 97). This means that if the points are 1 metre away from the eye, then their mutual distance must be greater than 0.5 mm. In a line grating with a line density of 2 ℓ/mm the individual lines cannot be distinguished and the grating appears as a grey field because of the eye's impression from each point is equal to the average light-intensity within a circle about the point with diameter 0.5 mm (see fig. 2.2-3).

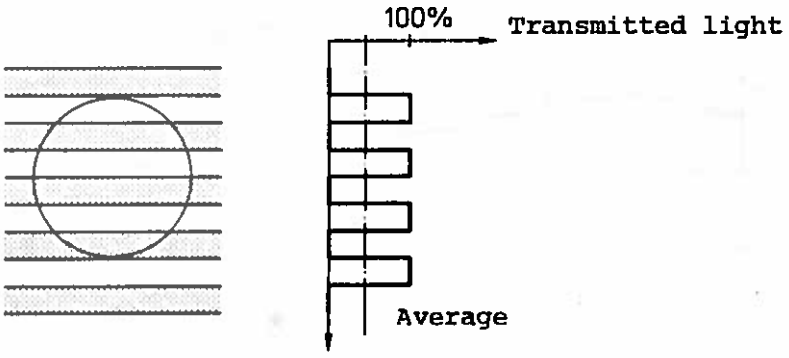

Figure 2.2-3

The average light intensity increases with the relative space width β (fig. 2.1-1) since it increases with the quantity of light transmitted by a transmission grating. Post [67-1] has

therefore chosen to characterize the gratings by a TRANSMITTANCE T, expressing the ratio between transmitted and received light when the light intensity is equally distributed. Hence, the transmittance is equal to the relative space width, i.e.

$$T = \beta \qquad (2.2\text{-}3)$$

Fig. 2.2-2.b and c show the variation in the light intensity in the moiré-pattern in fig. 2.2-1. When observed at normal reading distance, approximately 30 cm, the light distribution is almost as shown in fig. 2.2-2.b. If the observation distance is increased to such an extent that the resolving power of the eye is equal to the smallest pitch, then the average light intensity will be distributed as shown in fig. 2.2-2.c (Durelli and Parks [70-1] p. 32).

Hence, the variation in light intensity at right-angles to the moiré-lines is linear between a number of extreme lines constituting the bright and dark moiré-fringes.

The above considerations are based on geometrical optics, in which the wave-nature of light is neglected. A determination of the variation in the light intensity in accordance with physical optics results in a truer distribution, but is far more complicated. Guild [56-1] has considered the light intensity distribution of two superposed diffraction gratings, while Sciammarella [65-2] has considered the case of coarse gratings. Formally, all gratings are diffraction gratings irrespective of their line densities; the diffraction effect only becomes dominant at large line densities, which is why gratings with such large densities are often called diffraction gratings.

The light intensity distribution determined according to physical optics (se chapter 8) can be expressed as a sum of harmonic terms. The optical system by which the moiré-pattern is observed filters off the higher orders, depending on the line density, the geometry of the optical system, etc. For line densities of the order of 12-20 ℓ/mm, a normal optical system, e.g. a camera, will filter off all orders higher than one; hence, the intensity distribution can be expressed by a sinus curve with maximum values at the bright fringes and

minimum values at the dark ones.

As will have been seen, the light intensity reaches its extreme values at the dark and the bright moiré-lines, irrespective of the optical theory on which the considerations are based. The linear variation shown in fig. 2.2-2.c is thus an approximation. In the so-called "classic" moiré-pattern theory, which is treated in chapters 3 to 7, the moiré-pattern is described solely by the geometry of the moiré-lines and it will therefore be seen that it is sufficient in this connection to base the explanation of the moiré-effect on geometrical optics.

2.3 The Moiré-Effect of two Crossed Line Gratings

If we consider the moiré-pattern in fig. 2.2-1.c, formed by two crossed line gratings in detail, as shown in fig. 2.3-1.a, we can explain the moiré-effect as follows:

The grating lines in the two gratings form parallellograms, one of which is denoted ABCD. The EFFECTIVE or VISUAL MOIRÉ-PATTERN (Pirard [60-1]) proves to be the one in which the bright moiré-fringes coincide with the short diagonals in the parallellograms.

One interpretation, given by Durelli and Parks [67-2], is that the small, transparant parallellograms in that direction have the shortest mutual distance and thus form bright bands that are perceived as bright fringes by the eye.

If we examine the variation in the light intensity, we will find that the distance between the extreme values is maximum in the direction perpendicular to the short diagonals. In fig. 2.3-1. the variation in the light intensity in three different directions is shown.

The supposition that the moiré-fringes follow the short diagonals proves to be valid only when the line densities of the two gratings are nearly equal. The major pitch must not exceed 1.5 times the minor pitch, as is apparent from fig. 2.3-2.

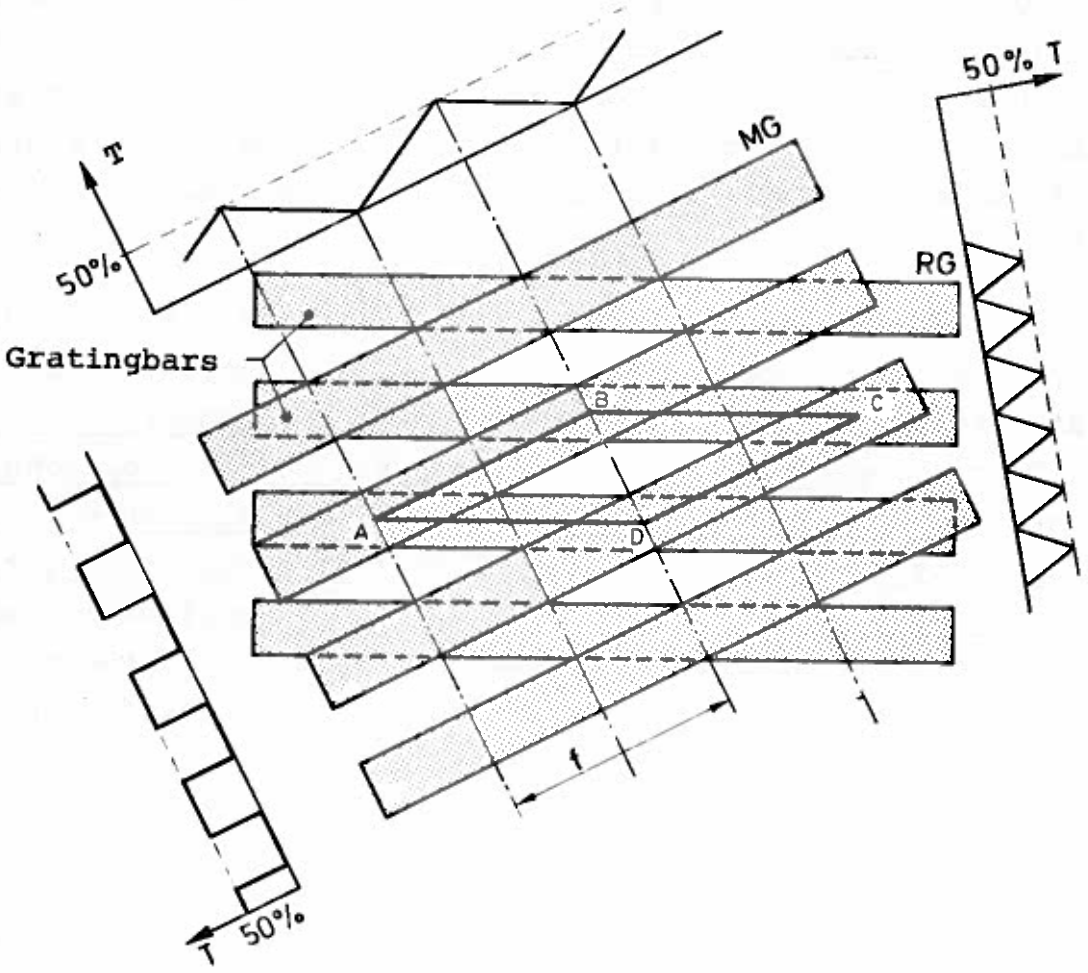

Figure 2.3-1

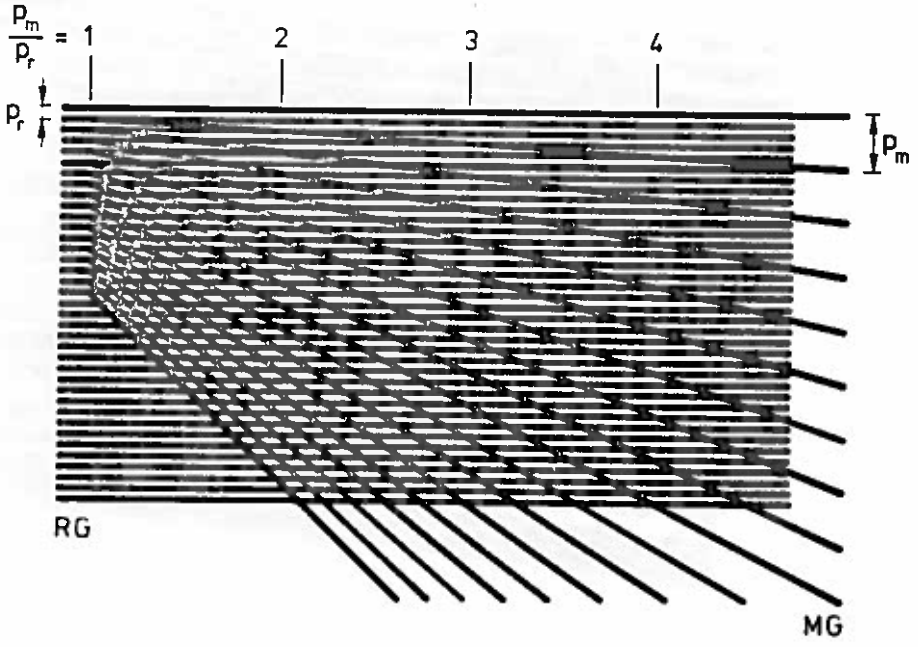

Figure 2.3-2

In the figure, a line grating with pitch p_r is superposed by a second grating with pitch p_m, which increases towards the right. The moiré-pattern can be observed more easily if the figure is tilted around one of the lines in the line grating. An examination of the fringe formation shows that the principle of the short diagonal is only valid in the domain p_m/p_r < about 1.5.

Košťák [63-1] has investigated the fringe formation conditions by considering the variation in the light intensity in different directions. He concludes that a sufficient condition for coincidence between the bright fringes and the short diagonals is that the mutual distance between the diagonal curves following the short diagonals (f in fig. 2.3-1) is bigger than 3 times the minor pitch of the two gratings. Thus, application of the principle of coincidence between the fringes and the short diagonals in respect of a given moiré-pattern is dependent on fulfilment of the Košťák-condition.

Finally, it should be noted that if the grating with the large pitch is replaced by a grating with twice that pitch, the same moiré-pattern will appear if orientation of the grating lines remains unchanged (see fig. 2.3-3), (Durelli and Parks [67-2]).

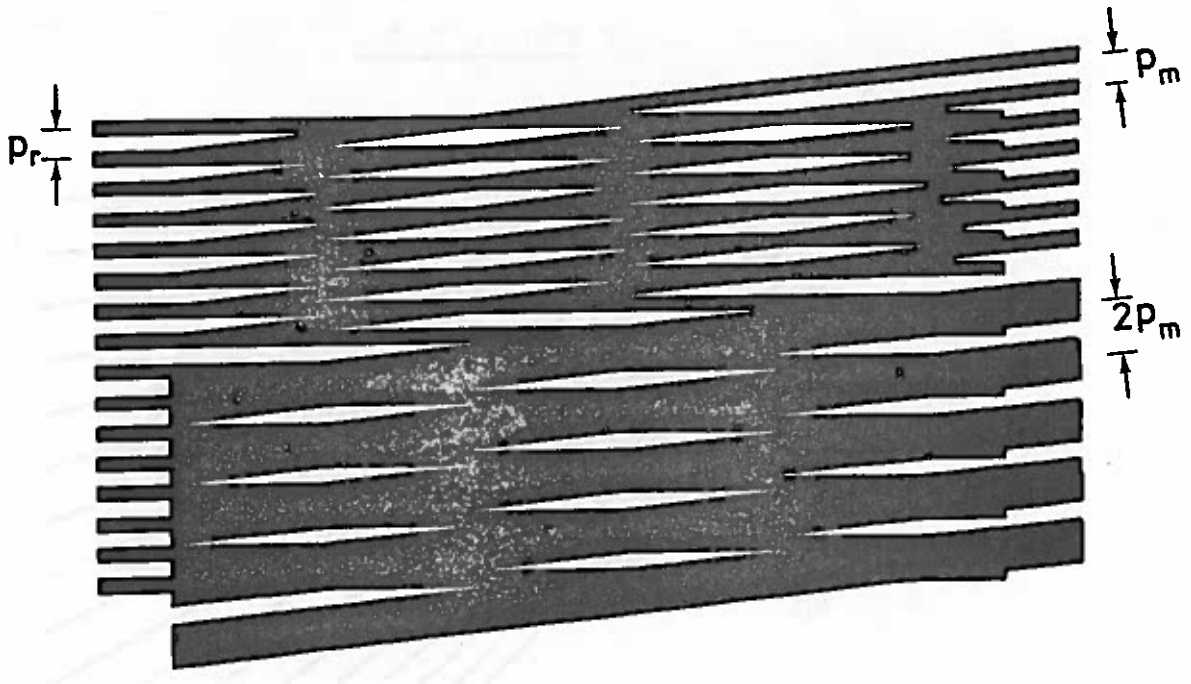

Figure 2.3-3

2.4 Influence of the Grating Geometry

In the above, no assumption has been made about the relative space width β (see fig. 2.1-1). It will be seen from fig. 2.3-2 that β affects the contrast of the pattern. A detailed investigation of this has been carried out by Zandman, Holister, and Brcic [65-3] and Post [67-1].

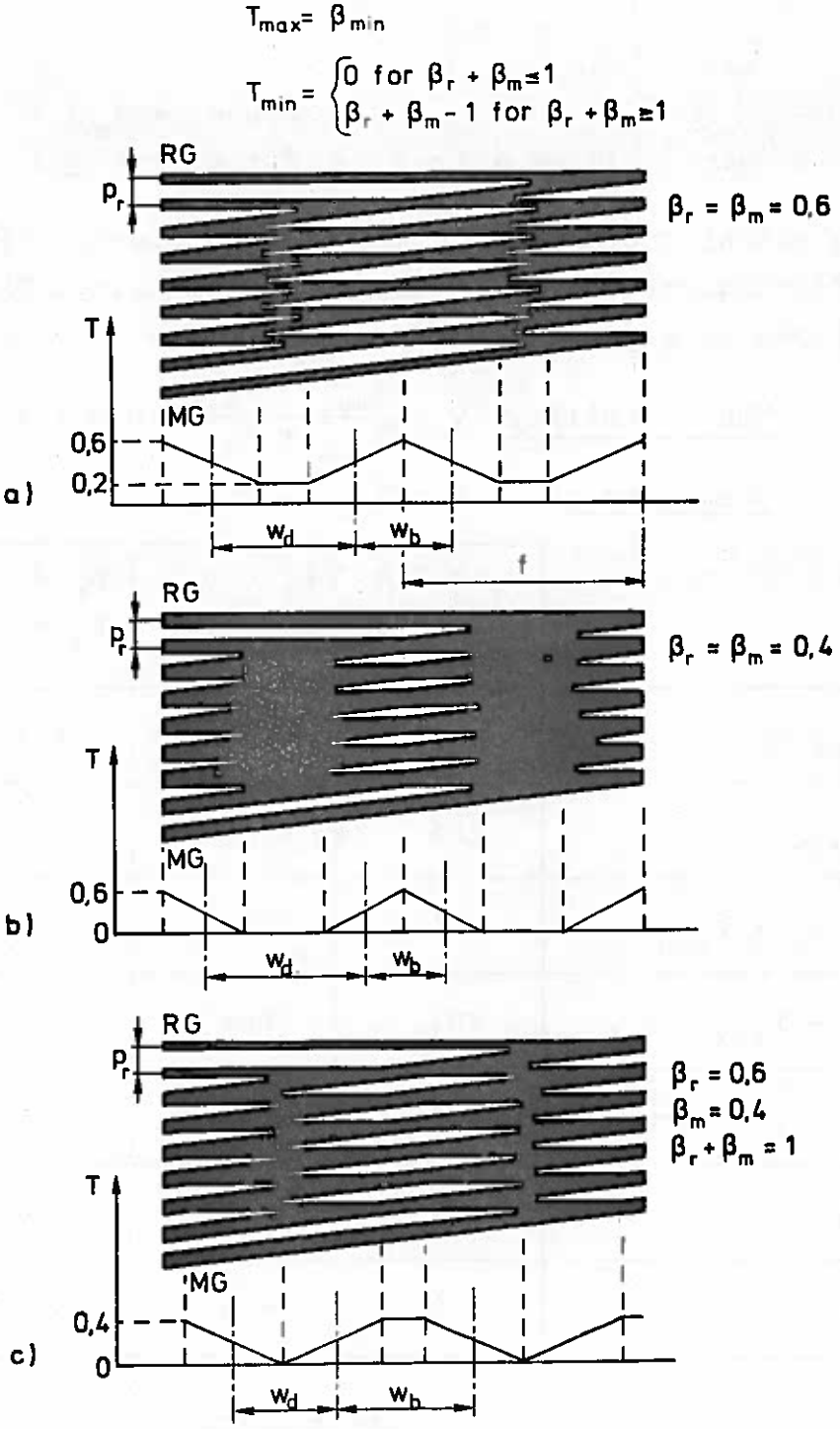

Variation of transmittance T with the relative space width β of the gratings

Figure 2.4-1

Fig. 2.4-1 shows three moiré-patterns formed by two gratings RG and MG with the pitches p_r and p_m. The difference between the patterns are due to the fact that β has different values. The corresponding variation in light intensity, expressed by the transmitted light, is shown for each case.

For the cases under consideration the maximum and minimum values of the transmittance T can be expressed as:

$$T_{max} = \beta_{min} \qquad (2.4\text{-}1)$$

$$T_{min} = \begin{cases} 0 & \text{for } \beta_r + \beta_m \leq 1 \\ (\beta_r + \beta_m) - 1 & \text{for } \beta_r + \beta_m \geq 1 \end{cases} \qquad (2.4\text{-}2)$$

The visual impression of the three patterns differs due to differing variations in the light intensity. These differences can be expressed by the quantities:

The visibility: $V = \dfrac{T_{max} - T_{min}}{T_{max} + T_{min}}$ $(0 \leq V \leq 1)$

The contrast : $K = T_{max} - T_{min}$ $(0 \leq K \leq 50\%)$

	$\beta_r = 0.6$ $\beta_m = 0.6$	$\beta_r = 0.5$ $\beta_m = 0.5$	$\beta_r = 0.4$ $\beta_m = 0.4$	$\beta_r = 0.6$ $\beta_m = 0.4$
T_{max}	60%	50%	40%	40%
T_{min}	20%	0	0	0
$T_{max} + T_{min}$	80%	50%	40%	40%
$K = T_{max} - T_{min}$	40%	50%	40%	40%
$V = \dfrac{T_{max} - T_{min}}{T_{max} + T_{min}}$	0,5	1	1	1
W_b	$< \frac{f}{2}$	$= \frac{f}{2}$	$< \frac{f}{2}$	$> \frac{f}{2}$
W_d	$> \frac{f}{2}$	$= \frac{f}{2}$	$> \frac{f}{2}$	$< \frac{f}{2}$

Table 2.4-1

The table gives the values of these quantities for the three cases in fig. 2.4-1, together with the normal case in which bar and space in the grating are of equal width ($\beta_r = \beta_m = 0.5$) and the values of W_b and W_d.

These quantities, which are due to Post [67-1], are known as THE APPARENT FRINGE WIDTH (W_d for the dark fringes and W_b for the bright ones). The apparent bright moiré-fringe width is defined as the area in which the light intensity exceeds the average intensity of the whole pattern, while the dark fringes constitute the remainder of the pattern (see fig. 2.4-1). The smaller the apparent width, the sharper will be the fringe.

The values to be selected for β depend on the purpose of the moiré-pattern. As will be seen from the table, $\beta_r = \beta_m = 0.5$ gives the best contrast. Furthermore, in this case, the intensity varies linearly from mid-fringe to mid-fringe. If only the bright fringe centrelines are to be determined, gratings with $\beta_m = \beta_r < 0.5$ can be used, since these have the smallest fringe width and maximum visibility. If, on the other hand, it is the dark fringe centrelines that are to be considered, gratings with $\beta_r + \beta_m = 1$ can be recommended. Such pairs are termed COMPLEMENTARY GRATINGS and are characterized by having minimum apparent dark fringe width and maximum visibility.

For most applications, both fringe centrelines have to be determined, for which reason gratings with $\beta = 0.5$ ought to be used. Even though this conclusion is based on the moiré-patterns in fig. 2.4-1, it is in agreement with the conclusions reached in the papers mentioned above. For further explanations, se these papers.

2.5 Bright and Dark Fringes or Vice Versa

When photographic negatives are copied, the fringes defined above as the "dark" fringes sometimes appear brighter than the "bright" fringes.

An example of this phenomenon is shown in fig. 2.5-1, in which the "dark" fringes are dark in one area and bright in another.

Caution must therefore be shown in the use of the terms dark and bright fringes, but as long as the phenomenon and its explanation are borne in mind, mistakes can be avoided. As will be seen in fig. 2.5-1, it is possible to se the grating lines in the formal "bright" fringes, but not in the "dark" ones. An explanation of this phenomenon is given in appendix C.

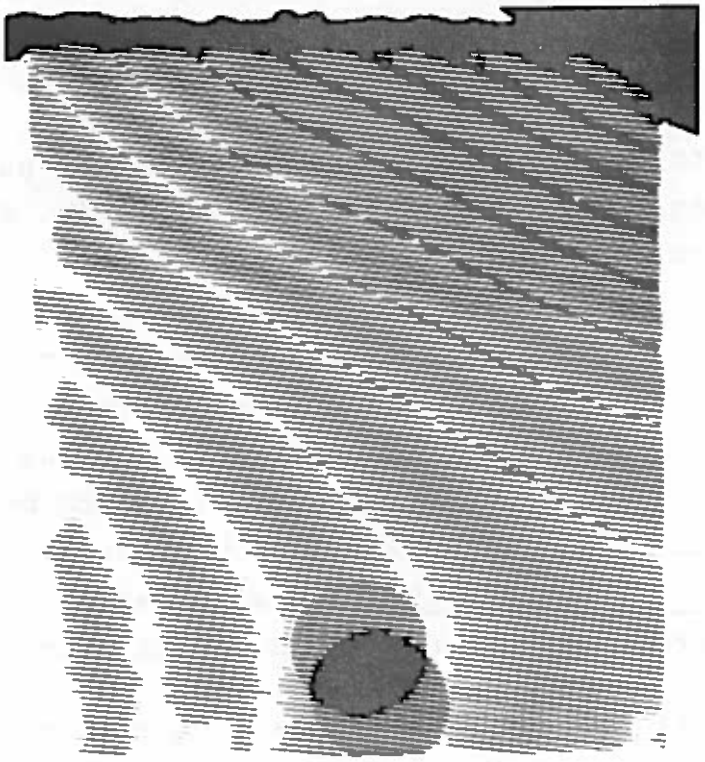

Figure 2.5-1

3. GENERAL MOIRÉ-PATTERN THEORY

Pirard [60-1] was the first to treat the moiré-pattern theory for arbitrary gratings. His results have been reprinted by Theocaris in [69-1] pp 14-18. The following is based partly on Pirard's paper and partly on Kośťák's paper [68-2].

3.1 Contour Lines and Diagonal Systems

When two superposed, undeformed line gratings are considered it is unnecessary to identify the individual grating lines since they have not only the same orientation but also the same spacing. The geometrical relations between the two gratings and their moiré-pattern can be determined by considering a local area; as the system is homogeneous, this will suffice for the whole pattern.

If the grating lines have different geometrical properties, which they may well have in the undeformed state and almost always have following a deformation, it is practical to characterize the individual lines by a parameter (or a number).

Kośťák has chosen to regarding the grating lines as CONTOUR LINES, as each line can be regarded as a curve along which a given function has a certain constant value. It will always be possible to choose this function in such a way that the constant value is an integer, whereby each line can be characterized by a line number or a parameter.

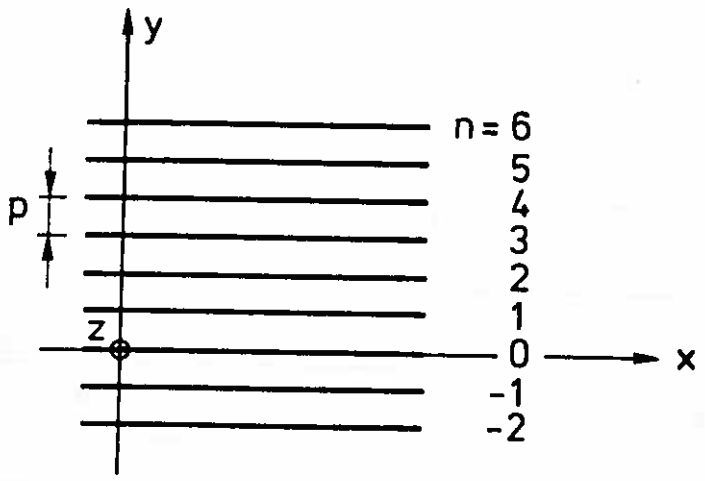

Figure 3.1-1

Consider, as an example, a line grating (fig. 3.1-1) with the pitch p, the lines of which are numbered consecutively with the parameter n. If an x,y-coordinate system is chosen such that the x-axis coincides with the grating line n = 0 and the y-axis is oriented so that the parameter increases in the positive y-direction, it will be seen that each grating line can be expressed by the parametrical equation.

$$y = n\,p \tag{3.1-1}$$

or

$$\frac{y}{p} = n \tag{3.1-2}$$

As a contour line system is the projection on the x-y-plane of the curves of intersection between a surface, $z = G\{x,y\}$ and planes parallel with the x,y-plane, then for any grating there is a corresponding surface for which the grating lines are contour lines. The line grating in fig. 3.1-1 can be regarded as the contour line system of the surface:

$$z = G\{x,y\} = \frac{y}{p} \tag{3.1-3}$$

which is a plane intersecting the x,y-plane along the x-axis. The difference in level from line to line for the chosen surface (3.1-3) is equal to unity, while the choice of $G\{x,y\} = y$ would give a difference equal to the pitch of the grating. The choice of difference in level is, of course, arbitrary, but it has proved more convenient to use the surface that has an integer as the difference.

In general, a grating or curve system can be described as

$$\boxed{G\{x,y\} = n} \tag{3.1-4}$$

which is called <u>the parametrical equation of the grating</u>. For every surface $G\{x,y\}$ there is a corresponding grating and, conversely, it is, in general, possible to determine the grating function $G\{x,y\}$ corresponding to a given grating.

For two contour curves in the same contour curve system it holds that:

a. they will not intersect each other if they have different parameters, and

b. the difference between the parameter values of the two adjacent contour curves is either 0 or 1.

Therefore, cases in which a part of the surface is perpendicular to the x,y-plane are neglected as they are of no interest in the following.

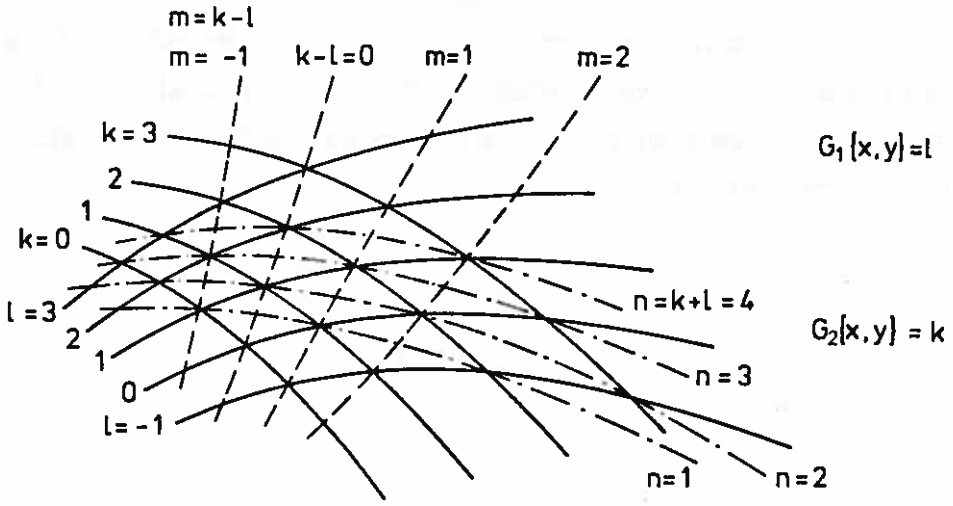

Additive and substractive diagonal curve systems

Figure 3.1-2

Consider two superposed contour curve systems (fig. 3.1-2) with the parameters k and l,

$$G_1\{x,y\} = k \quad \text{and} \quad G_2\{x,y\} = l \qquad (3.1\text{-}5)$$

Through the points of intersections a number of curves can be drawn, which are designated DIAGONAL CURVES and which satisfy certain parametrical conditions. Fig. 3.1-2 shows the diagonal curves that satisfy the following conditions:

$$k - l = m \quad \text{(dotted lines)} \qquad (3.1\text{-}6)$$

$$k + l = n \quad \text{(dot-and-dash lines)} \qquad (3.1\text{-}7)$$

These diagonal curve systems are also known as THE SUBTRACTIVE SYSTEM and THE ADDITIVE SYSTEM, respectively, and it is they that are of principal interest in this report. As the choice of parameter is arbitrary, there are now no restrictions preventing a change of sign for one of the parameters. A change of sign for one of the parameters means that the subtractive system becomes the additive system, and vice versa. Whether a given diagonal system is subtractive or additive thus depends solely on the choice of the parameters and is independent of the geometry of the superposed contour curve systems.

The parametrical conditions for the diagonal systems are not restricted to the two equations mentioned above (3.1-6) and (3.1-7), but may include any linear combination of parameters for the two gratings, hence:

$$n = \lambda_1 k + \lambda_2 l \qquad (3.1\text{-}8)$$

where λ_1 and λ_2, too, are integers.

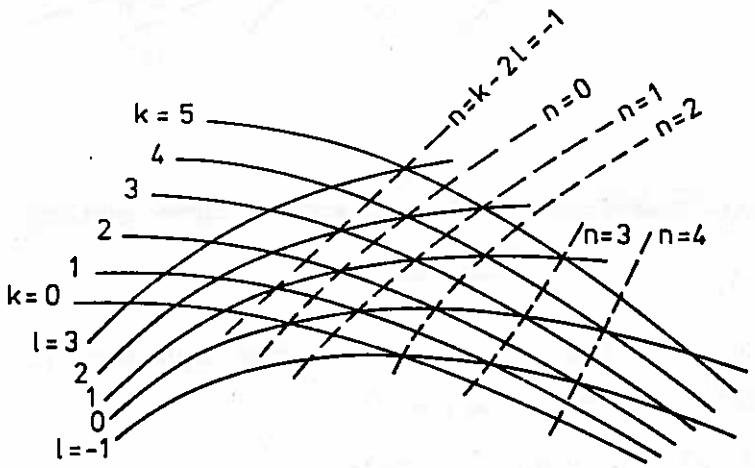

Diagonal curves corresponding to n = k - 2 l

Figure 3.1-3

Thus, fig. 3.1-3 shows diagonal curves corresponding to the parametrical conditions:

$$n = k - 2l \qquad (3.1\text{-}9)$$

In chapter 2 (on the moiré-effect), it was shown that moiré-lines belonging to the bright moiré-fringes correspond to what are here called diagonal curves. To determine the parametrical conditions applying, it is necessary to consider the mutual geometry of the two superposed gratings; if the ratio between the greatest and the smallest pitch in the two superposed line gratings is less than approximately 1.5 (see fig. 2.3-2), then the moiré-lines will follow the short diagonals of the parallelograms, which corresponds to the parametrical conditions (3.1-6) or (3.1-7).

In the following, the term "moiré-lines" will be reserved for the "bright" moiré-lines, since it is these that are determined by the above-mentioned parametrical conditions. The "dark moiré-lines" correspond to parametric values inbetween, such as $-\frac{1}{2}$, $+\frac{1}{2}$, $+1\frac{1}{2}$, $+2\frac{1}{2}$, etc.

In general, the parametrical conditions determining the moiré-lines have to be examined for each moiré-pattern. The results from superposed line gratings can usually be used, as the curvilinear quadrangles formed by the two curve systems can, with good approximation, be treated as parallelograms.

However, it should also be noted that the moiré-lines cannot necessarily be determined by the same parametrical conditions throughout the moiré-pattern, but as moiré-lines corresponding to one parametrical condition do not continue directly into lines corresponding to another parametrical condition, a discontinuity in the moiré-fringes will disclose a change of parametrical condition.

In practice, the coefficients λ_1 and λ_2, (3.1-8) can only determine moiré-patterns with the values ±1, ±2, and ±3. For diagonal systems corresponding to higher values of λ_1 and λ_2, the contrast is too weak for the fringes to be visible (Kosťák [68-2]).

As long as the moiré-lines correspond to one parametrical condition, they can be characterized by a parameter, e.g. m in (3.1-6). This means that the moiré-lines can be treated as

contour-lines as well. The corresponding surface is designated THE MOIRÉ-SURFACE (section 6.6).

Finally, it should be noted that if the moiré-lines are considered as grating lines, then this grating, superposed with one of the two original gratings, will form a moiré-pattern that is identical to the second original grating. This follows directly from the parametrical condition by interchanging two parameters.

Application of this general principle on the addition and substraction of two contour line systems has, for example, been used in two-dimensional photo-elasticity by Mesmer [56-2] and de Lamotte [68-1]. When two thickness-interferograms of a plane specimen (one taken before and the other after the deformation) are superposed, a moiré-pattern results, which is the contour lines for the change in thickness of the specimen. The change is proportional to the sum of the principal stresses in the plane of the specimen.

3.2 General Moiré-Pattern Theory for two Gratings of Known Geometry

In this section, expressions will be derived for the moiré-pattern formed by two superposed, arbitrary gratings of known geometry. The derivation is analogous to that given by Theocaris in [69-1].

Consider two gratings given by the following parametrical equations:

$$R\{x,y\} = r \qquad (3.2\text{-}1)$$

$$S\{x,y\} = m \qquad (3.2\text{-}2)$$

Assuming the moiré-lines to follow the parametrical condition:

$$n = r \pm m \qquad (3.2\text{-}3)$$

the moiré-pattern is given by the equation:

$$M\{x,y\} = R\{x,y\} \pm S\{x,y\} = n \qquad (3.2\text{-}4)$$

If now, an arbitrary contour curve system

$$\boxed{F\{x,y\} = n} \qquad (3.2\text{-}5)$$

is considered, the treatment may be generalized to include gratings as well as moiré-patterns. As n is constant along a contour curve, these can also be described by the differential equation:

$$F_{,x}dx + F_{,y}dy = 0 \qquad (3.2\text{-}6)$$

where comma denotes partial differentiation.

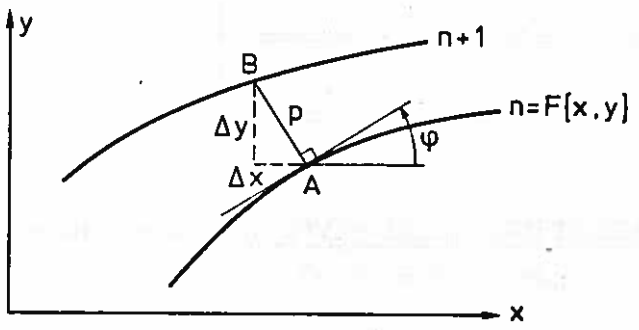

Figure 3.2-1

The slope of the tangent at point A (fig. 3.2-1) on a contour curve is then:

$$\boxed{\tan\varphi = \frac{dx}{dy} = -\frac{F_{,x}}{F_{,y}}} \qquad (3.2\text{-}7)$$

If the contour line spacing (pitch) p at point A is defined as part of the normal at the point that lies between the contour curve and its adjacent curve, then

$$p = \sqrt{(\Delta x)^2 + (\Delta y)^2}$$

The normal is given by

$$-\Delta x\, F_{,y} + \Delta y\, F_{,x} = 0 \qquad (3.2\text{-}8)$$

and the part AB is determined by (3.2-5):

$$\Delta n = 1 = \frac{\Delta F}{\Delta x}\Delta x + \frac{\Delta F}{\Delta y}\Delta y \qquad (3.2\text{-}9)$$

If the curves are so close together that

$$\frac{\Delta F}{\Delta x} \cong F_{,x} \quad \text{and} \quad \frac{\Delta F}{\Delta y} \cong F_{,y}$$

then (3.2-9) takes the form:

$$F_{,x}\,\Delta x + F_{,y}\,\Delta y = 1 \qquad (3.2\text{-}10)$$

If (3.2-8) and (3.2-10) are solved with respect to Δx and Δy, then the contour line spacing (pitch) becomes

$$\boxed{p \cong \frac{1}{\sqrt{(F_{,x})^2 + (F_{,y})^2}}} \qquad (3.2\text{-}11)$$

For an ADDITIVE MOIRÉ-PATTERN, i.e. $n = r + m$, the interfringe spacing f_a takes the form

$$\boxed{f_a = \frac{1}{\sqrt{(R_{,x} + S_{,x})^2 + (R_{,y} + S_{,y})^2}}} \qquad (3.2\text{-}12)$$

and correspondingly, for a SUBTRACTIVE MOIRÉ-PATTERN, f_s takes the form

$$\boxed{f_s = \frac{1}{\sqrt{(R_{,x} - S_{,x})^2 + (R_{,y} - S_{,y})^2}}} \qquad (3.2\text{-}13)$$

Which of the two patterns is the EFFECTIVE MOIRÉ-PATTERN, i.e. the pattern immediately perceived by an observer, can be determined by comparing the two spacings f_a and f_s. The pattern with greater spacing will be the effective pattern, if one can be seen at all.

For the additive and subtractive system the condition is:

$$f_a \gtreqless f_s \iff R_{,x} S_{,x} + R_{,y} S_{,y} \lesseqgtr 0 \qquad (3.2\text{-}14)$$

For the general parametric condition,

$$n = \lambda_1 r + \lambda_2 m \qquad (3.2\text{-}15)$$

the corresponding interfringe spacing is

$$f = [(\lambda_1 R_{,x} + \lambda_2 S_{,x})^2 + (\lambda_1 R_{,y} + \lambda_2 S_{,y})^2]^{-\frac{1}{2}} \qquad (3.2\text{-}16)$$

the coefficients λ_1 and λ_2 determining the effective moriépattern are found by investigating by means of (3.2-16) the combination that results in the biggest spacing f.

3.2.1 Example. Line Grating Superposed with Circular Grating

As an example, the moiré-pattern form by superposing a line grating and a circular grating is considered.

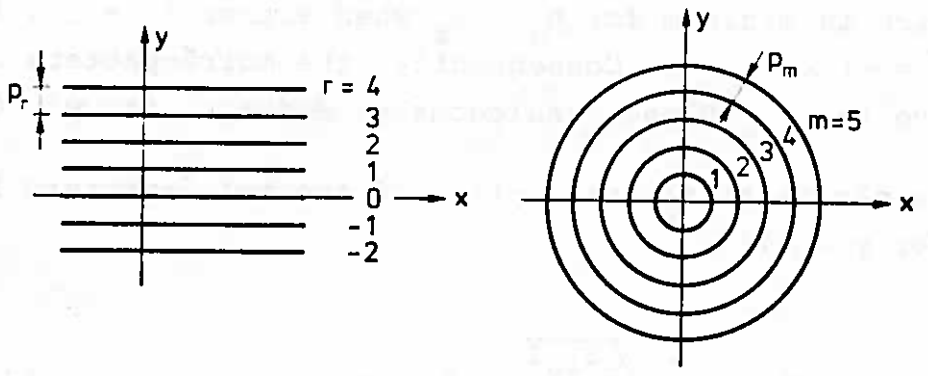

Line grating Circular grating

Figure 3.2-2

Fig. 3.2-2 shows the positions of the gratings in an x,y-coordinate system. The parametrical descriptions of the gratings are:

Line grating : $R\{x,y\} = \frac{y}{p_r} = r$ (3.2-17)

Circular grating : $S\{x,y\} = \frac{\sqrt{x^2+y^2}}{p_m} = m$ (3.2-18)

Calculation of the contour line spacings (pitches) by means of (3.2-11) gives, quite naturally, p_r and p_m. The parametrical description applying to the moiré-pattern is given by (3.2-16):

$$f = \left[\left(\frac{\lambda_2}{p_m}\frac{x}{\sqrt{x^2+y^2}}\right)^2 + \left(\frac{\lambda_1}{p_r} + \frac{\lambda_2}{p_m}\frac{y}{\sqrt{x^2+y^2}}\right)^2\right]^{-\frac{1}{2}}$$

$$= \left[\left(\frac{\lambda_2}{p_m}\right)^2 + \left(\frac{\lambda_r}{p_r}\right)^2 + \frac{2\lambda_1\lambda_2}{p_r p_m}\frac{y}{\sqrt{x^2+y^2}}\right]^{-\frac{1}{2}} \quad (3.2\text{-}19)$$

To maximize f, the expression within the square brackets must be minimized with the restriction that λ_1 and λ_2 must be non-zero integers.

For $y > 0$, this expression is less than

$$\left(\frac{\lambda_2}{p_m}\right)^2 + \left(\frac{\lambda_1}{p_r}\right)^2 + \frac{2\lambda_1\lambda_2}{p_r p_m} = \left(\frac{\lambda_2}{p_m} + \frac{\lambda_1}{p_r}\right)^2$$

which is minimum for $p_m \approx p_r$ when either $\lambda_1 = 1 \wedge \lambda_2 = -1$ or $\lambda_1 = -1 \wedge \lambda_2 = 1$. Consequently, the moiré-pattern is subtractive for $y > 0$ and, analogously, additive for $y < 0$.

The parametrical description of the moiré-pattern is then (for $y > 0$):

$$M\{x,y\} = \frac{\sqrt{x^2+y^2}}{p_m} - \frac{y}{p_r} = n \quad (3.2\text{-}20)$$

which may be rewritten as

$$(p_r^2 - p_m^2)y^2 - 2\,y\,n\,p_r\,p_m + p_r^2 x^2 - p_r^2 n^2 = 0 \quad (3.2\text{-}21)$$

It will be seen that the moiré-curves are conesection curves of a type depending on the two pitches p_r and p_m as follows:

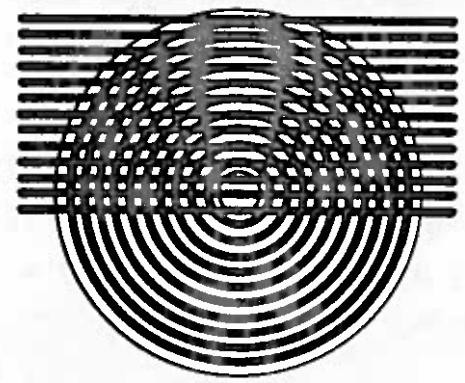

a)

$p_r > p_m$

ellipses

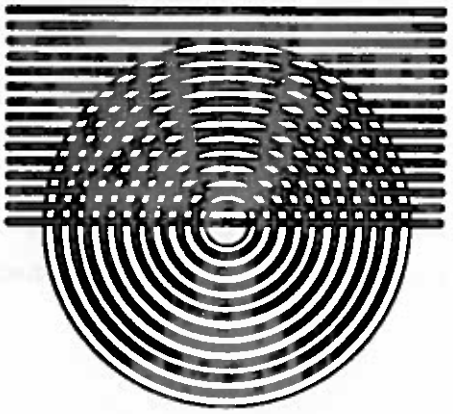

b)

$p_r \leq p_m$

parabolas

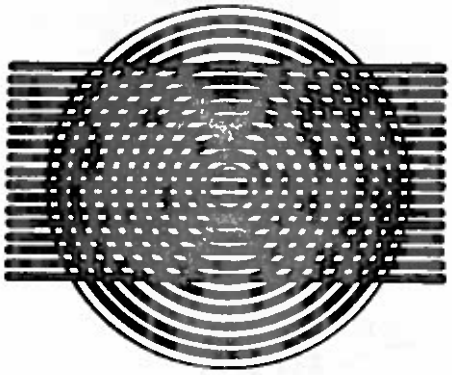

c)

$p_r < p_m$

hyperbolas

Moiré-patterns for a circular grating and a line grating

Figure 3.2-3

The figures illustrate clearly the legitimacy of considering the gratings as contour curves. The circular grating may be considered as the contour curves of a cone. The curves of section between this and the plane for which the line grating is the contour curves are precisely of the type that depends on the ratio between the slope of the plane ($\frac{1}{p_r}$) and the slope of the generator ($\frac{1}{p_m}$).

This means of illustrating section curves between different kinds of surfaces has been used by Oster ([64-2], [64-3], [67-5] and [68-4]), for the purpose of describing a number of optical interference phenomena.

3.3 General Moiré-Pattern Theory in Deformation Measurements

When the moiré-technique is used in deformation measurements, the geometry of one of the gratings is changed from a known state into an unknown state, and it is for determining this new geometry that the moiré-pattern is used.

The grating that deforms is designated the model grating (MG) and its undeformed state is assumed to be determined by the parametrical description,

$$MG^o : S^o\{X,Y\} = m \qquad (3.3\text{-}1)$$

which changes, after deformation into the deformed model grating,

$$MG : S\{x,y\} = m \qquad (3.3\text{-}2)$$

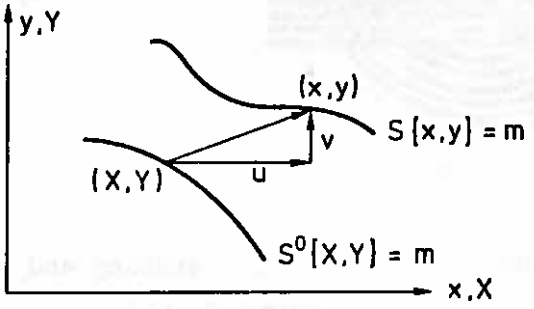

Figure 3.3-1

Fig. 3.3-1 shows the deformation of a single grating line with the parameter m. The deformation is described so that points having the coordinates (X , Y) in the undeformed state are displaced to points having the coordinates (x , y). If (u , v) denotes the components of the displacement vector, the following equations are valid:

$$x = X + u \tag{3.3-3}$$

$$y = Y + v \tag{3.3-4}$$

Equations (3.3-1) and (3.3-2) can then be rewritten as

$$S^{O}\{X,Y\} = S\{X + u,\ Y + v\} = m \tag{3.3-5}$$

The difference between the two functions S^{O} and S is assumed to be determined by a DIFFERENCE- or DEFORMATIONS-FUNCTION $D\{x,y\}$, defined by

$$\boxed{\begin{aligned} D\{x,y\} &= S\{x,y\} - S^{O}\{x,y\} \\ &= S\{x,y\} - S^{O}\{X + u,\ Y + v\} \end{aligned}} \tag{3.3-6}$$

If S^{O} is a differentiable function, then:

$$S^{O}\{X+u,Y+v\} = S^{O}\{X,Y\} + \int_{X}^{X+u} \frac{\partial S^{O}}{\partial x}\,dx + \int_{Y}^{Y+v} \frac{\partial S^{O}}{\partial y}\,dy \tag{3.3-7}$$

and utilizing (3.3-1) and (3.3-2), the difference function takes the form:

$$\boxed{-D\{x,y\} = \int_{X}^{X+u} \frac{\partial S^{O}}{\partial x}\,dx + \int_{Y}^{Y+v} \frac{\partial S^{O}}{\partial y}\,dy} \tag{3.3-8}$$

The difference function is then expressed by the known function $S^{O}\{X,Y\}$ and the unknown displacement components u and v.

When the model gratings are superposed with a reference grating (RG), determined by the parametric discription:

$$RG : R\{x,y\} = r \qquad (3.3\text{-}9)$$

then, in the undeformed state, the undeformed moiré-pattern is given by

$$\boxed{MP^{O} : M^{O}\{X,Y\} = \lambda_1 R\{X,Y\} + \lambda_2 S^{O}\{X,Y\} = n} \qquad (3.3\text{-}10)$$

when the general parametric condition (3.1-8) is used. Assuming that the geometry of both the reference grating and the undeformed model grating is known, it is possible to determine the undeformed moiré-pattern as indicated in section 3.2.

The deformed moiré-pattern formed by superposition of the reference grating and the deformed model grating is given by:

$$\boxed{MP : M\{x,y\} = \lambda_1 R\{x,y\} + \lambda_2 S\{x,y\} = n} \qquad (3.3\text{-}11)$$

when the same parametric condition is assumed to apply as in the case of the undeformed moiré-pattern. If the deformations are large, the parametric condition may have changed, but this can easily be checked by magnifying a section of the pattern.

Using (3.3-6), (3.3-10), and (3.3-11) yield:

$$\boxed{D\{x,y\} = \frac{1}{\lambda_2}[M\{x,y\} - M^{O}\{x,y\}]} \qquad (3.3\text{-}12)$$

and it will be seen that the difference function is also an expression of the change from the undeformed to the deformed moiré-pattern. In the special case $S^{O}\{x,y\} = R\{x,y\}$, i.e.

when the reference grating and the undeformed model grating are identical, $M^{o}\{x,y\} = 0$, the deformed moiré-pattern immediately forms the contour curve system of the difference function.

Furthermore, it will be seen from (3.3-12) that the difference function is determinable to the extent that the geometry of the deformed moiré-pattern is measurable. In the special case of model gratings, with

$$\frac{\partial S^{o}}{\partial x} = \text{constant} = C \quad \text{and} \quad \frac{\partial S^{o}}{\partial y} = 0 \qquad (3.3\text{-}13)$$

it will be seen from (3.3-8) that

$$u = -\frac{1}{C} D\{x,y\} = u\{x,y\} \qquad (3.3\text{-}14)$$

This means that one of the components (u) of the displacement vector is proportional to the difference function if the model grating has the properties (3.3-13). This is the case for line gratings in which the lines are parallel to the y-axis and for circular gratings in which the x-direction is identical to the radial direction.

4. GENERAL MOIRÉ-PATTERN THEORY OF LINE GRATINGS

In this and subsequent chapters, the moiré-pattern formed by two line gratings is dealt with, together with the changes in the pattern resulting from a displacement (with or without deformation) of one of the gratings. Strictly speaking, it is only the images of the displaced and/or deformed gratings that are discussed here, but misunderstandings are hardly likely to arise from the fact that it is said instead that the images of the gratings become deformed or displaced.

The grating whose deformation and displacement are to be determined is designated THE MODEL GRATING (MG). Before displacement, this is assumed to consist of straight and equidistant grating lines, which are transformed, during the displacement, into a number of curves that remain adjacent curves, i.e. they do not intersect each other.

In order that the geometry of the model grating may be determined, both before and after displacement, this is superposed by a second line grating, called THE REFERENCE GRATING (RG). This grating is assumed to consist of straight and equidistant grating lines and its position in relation to a fixed reference configuration is assumed to be known.

First, a displacement function describing the displacement of the model grating will be introduced, after which the parametric description of the moiré-pattern can be formulated. The analysis of the moiré-pattern is then divided into two parts, 1. the cases (chapter 5) in which the model grating undergoes a displacement without deforming, i.e. pure translation and pure rotation, and 2. the cases (chapter 6) in which it is the deformation itself that is to be determined. In the analysis, methods are specified for determining a number of the parameters describing the deformation, and the accuracy of these methods is investigated in chapter 7.

4.1 The Displacement and Deformation of the Model Grating

The displacement and deformation of a grating line can be illustrated as shown in fig. 4.1-1. The straight line ℓ_o is

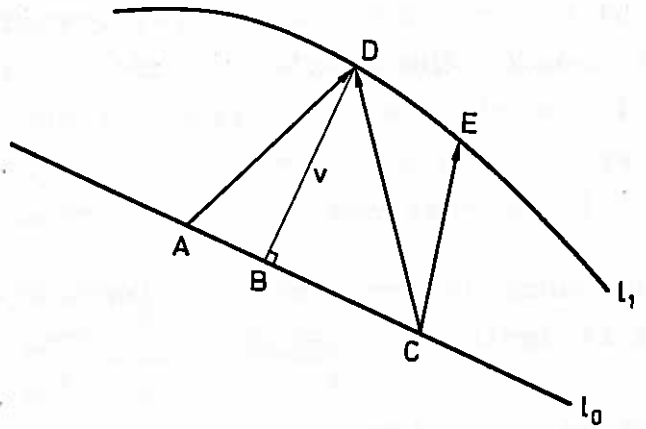

Figure 4.1-1

transformed into the curve ℓ_1. The question is, to what extent the deformation of the line ℓ_o can be determined assuming that the geometry of the curve ℓ_1 is determined by means of the moiré-pattern.

If the individual points on line ℓ_o cannot be identified separately, it is impossible to determine the point to which a point on ℓ_o is displaced, except, of course, that it must be to one of the points on ℓ_1. For example, the point C may be displaced to D or to E, or to a third point on ℓ_1.

If, on the other hand, the points on the deformed curve ℓ_1 are considered, it is possible to determine the component of the displacement vector perpendicular to ℓ_o. It will be seen from fig. 4.1-1 that whether point D is displaced from A, B or C, all the displacement vectors $\vec{AD}$, $\vec{BD}$ and $\vec{CD}$ will have the same component $\vec{BD}$ in the direction perpendicular to ℓ_o.

This expresses the general property of line gratings: that they can only be used to determine the displacement component perpendicular to the direction of the grating lines in the

undeformed state, and at that, only at the positions of the points after the deformation.

It is, of course, only possible to determine the displacement components perpendicular to the grating lines for points lying on these lines. However, with normal line density, it will suffice to know the value of the displacement function at the points on the lines in order to get an impression of the overall behaviour of the displacement function. In the following it is therefore assumed that the displacement function is continuous, whereby it is possible to think in terms of the deformation of the grating plane instead of just the deformation of the grating lines.

In the following sections the relationship between the grating displacement function and the deformation of the specimen is analysed for three characteristic moiré-methods.

4.1.1 Direct-Moiré

A direct-moiré method means a method in which a grating is fastened directly to the surface of the specimen, thereby following its surface deformations. Determination of the deformation of the grating then immediately gives the surface deformation of the specimen.

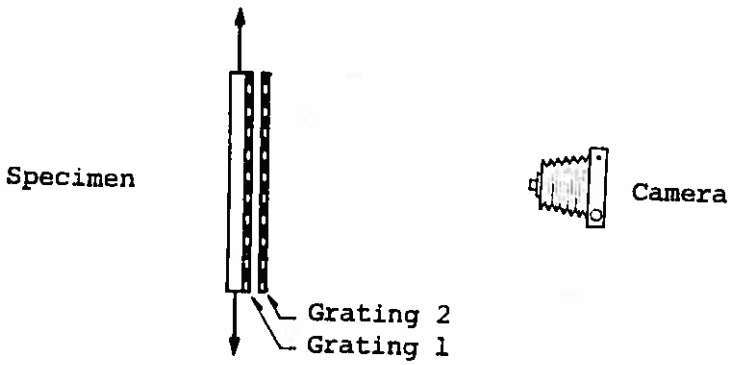

Direct-Moiré

Figure 4.1-2

If a second grating (grating 2) is placed in fromt of the surface with the first grating (see fig. 4.1-2), the images of two gratings, producing a moiré-pattern, will be formed on the focal plane of the camera. The image of grating 1 represents the model grating, and that of grating 2, the reference grating.

The deformation of the model grating is similar to that of the surface of the specimen when the focal plane is parallel to the surface. The similitude factor is equal to the magnification of the reproducing optical system, and for the sake of simplicity, this is set at unity in the following. The grating displacement function is thus identical to the displacement function by which the deformation of the surface of the specimen can be described.

The in-plane deformation is illustrated in fig. 4.1-3.

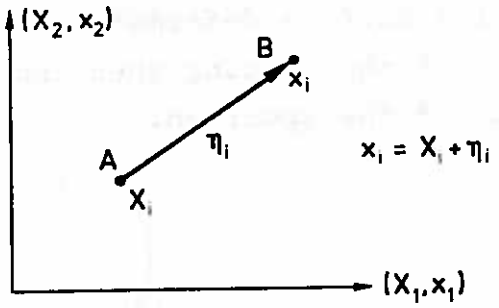

Figure 4.1-3

Due to the deformation, point A, with coordinates X_i, is displaced to point B with coordinates x_i. Describing the deformation by means of the displacement vector η_i, we get

$$x_i = X_i + \eta_i \qquad (i = 1,2) \qquad (4.1\text{-}1)$$

The components η_1 and η_2 of the displacement vector may be regarded as functions of either the initial coordinates X_i or of the final coordinates x_i. In strain analysis, these

two types of description are known as the Lagrangean and the Eulerian description, respectively.

The Lagrangean displacement functions are:

$$\eta_i = U_i = U_i\{X_j\} \qquad (i,j = 1.2) \qquad (4.1\text{-}2)$$

and the corresponding Eulerian functions are:

$$\eta_i = u_i = u_i\{x_j\} \qquad (i,j = 1.2) \qquad (4.1\text{-}3)$$

These are related as follows:

$$u_i\{X_j + U_j\} = U_i\{X_j\} \qquad (4.1\text{-}4)$$

$$U_i\{x_j - u_j\} = u_i\{x_j\} \qquad (4.1\text{-}5)$$

The deformation state is normally described by means of strain tensors. Corresponding to the two types of description we have Green's strain tensor E_{ij} and Almansi's strain tensor e_{ij}, respectively, defined by

$$E_{ij} = \frac{1}{2}\left[\frac{\partial U_i}{\partial X_j} + \frac{\partial U_j}{\partial X_i} + \frac{\partial U_k}{\partial X_i}\frac{\partial U_k}{\partial X_j}\right] \qquad (4.1\text{-}6)$$

$$e_{ij} = \frac{1}{2}\left[\frac{\partial u_i}{\partial x_j} + \frac{\partial u_j}{\partial x_i} - \frac{\partial u_k}{\partial x_i}\frac{\partial u_k}{\partial x_j}\right] \qquad (4.1\text{-}7)$$

For infinitesimal strain, the last product terms in the brackets can be neglected, and the deviations between the components of the two tensors are then usually so small that the two tensors can be regarded as equal. A detailed analysis of these relations is available in Durelli and Park [70-1], chapter 4, or [64-4].

It is evident from section 4.1 that if one axis of the coordinate system is parallel to the grating lines, the grating displacement function will correspond to one of the two Eulerian displacement functions. Therefore, in order to obtain a complete determination of the deformation state, it is necessary to determine the grating displacement functions in two different directions.

In the direct-moiré method, if v stands for the grating displacement function and the magnification of the image-forming system is equal to unity, it then holds that

$$\boxed{\begin{array}{ll} v = u_1 & \text{when the grating lines} \neq x_2\text{-axis} \\ v = u_2 & \text{when the grating lines} \neq x_1\text{-axis} \end{array}} \qquad (4.1\text{-}8)$$

4.1.2 Shadow-Moiré

The shadow-moiré method discussed in this section is treated principally by Dykes [70-5].

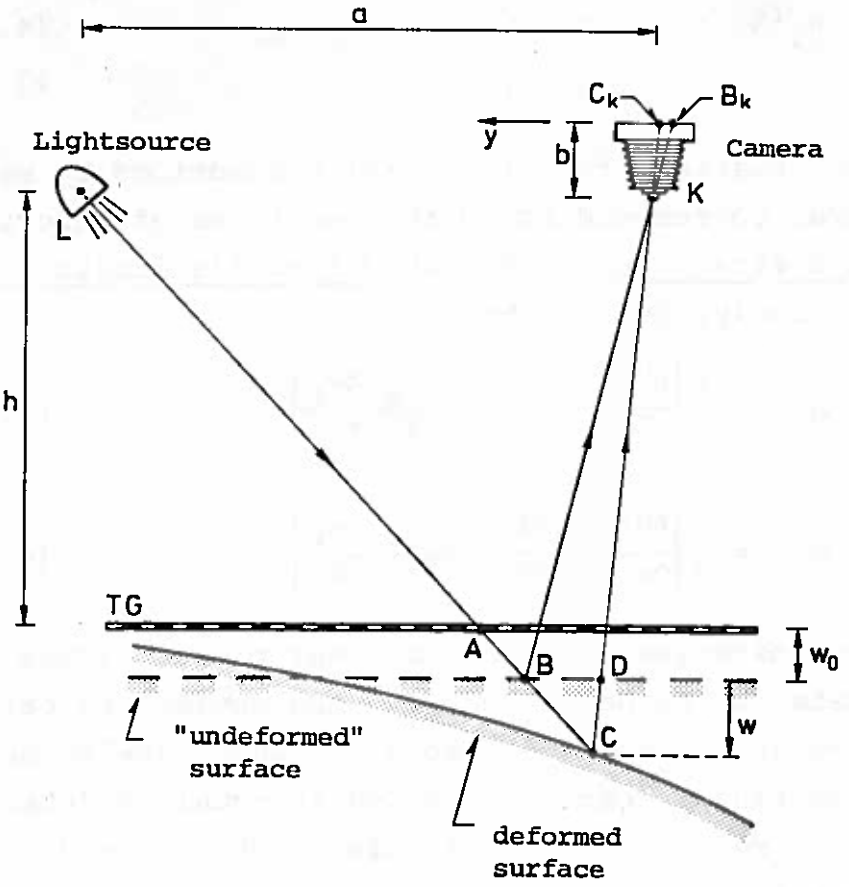

Shadow-Moiré

Figure 4.1-4

The principle of the method is outlined in fig. 4.1-4, which shows a section perpendicular to the grating plane and the grating lines of a transmission line grating (TG) placed in front of (above) the matt measuring area. A light source L

and a camera are placed at the same distance h from the grating plane. The distance h is measured from the optical midpoint K of the lens of the camera.

From the point of observation (the camera), both the grating TG and its shadow on the measuring area can be seen. The image in the camera can be regarded as a similar image of a central projection on the grating plane through the point K. In order to obtain a sufficiently sharp image of both the grating TG and the shadow grating, it must be assumed that the distance $w_o + w$ between the grating plane and the surface of the specimen is small in relation to the distance h of the camera from the grating plane.

The image of the transmission grating TG is an undeformed line grating, which is taken as the reference grating since its geometry can be determined in advance.

The image of the shadow grating, on the other hand, normally appears as a deformed line grating because it consists of a curvilinear line-system. This depicted grating can thus be regarded as the model grating whose geometry is to be determined. If the surface of the specimen is plane and parallel to the plane of TG, the image of the shadow grating will have the form of an undeformed line grating, and this is regarded as the undeformed model grating.

The relationship between the deformation of the surface of the specimen and the displacement function of the model grating is as follows. The grating line at A casts a shadow on the undeformed surface of the specimen at line B and at line C after the deformation. In the focal plane of the camera these are depicted at B_k and C_k, respectively, i.e. line B_k is displaced to C_k during the deformation. From similar triangles it will be seen that

$$v = C_k B_k = \frac{b}{h} BD = \frac{b}{h} \frac{a\, w}{h + w_o + w}$$

With the above-mentioned assumption $w_o + w \ll h$, we then get

$$\boxed{v \simeq \frac{b}{h} \frac{a}{h} w} \qquad (4.1\text{-}9)$$

The grating displacement v is thus proportional to the deflection w of the measuring area in relation to its undeformed state and measured perpendicular to the plane of the transmission grating.

4.1.3 Reflection-Moiré

The third moiré-method to be discussed utilizes as model grating the image of a grating reflected in the specimen surface. The method is due to Ligtenberg [52-2] and [55-1].

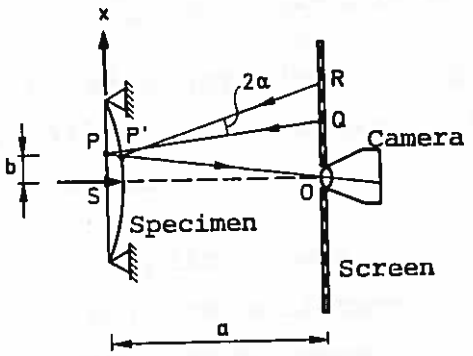

Reflection-Moiré

Figure 4.1-5

Fig. 4.1-5 shows a section perpendicular to the grating plane and the grating lines on a screen. The reflection of the screen grating in the specimen surface is observed through a hole in the screen. If the specimen deforms, the reflection changes and, with it, the model grating.

The relation between the deformation of the specimen and the change in the model grating is as follows: Before deformation, a reflection of point Q on the grating-screen is seen at point P on the specimen. After deformation, it is seen at point P' (with the same visual ray as P). That it is now another point on the screen that is observed is due to the fact that deformation has resulted in a change of slope, α, at P'. This means that the rays (arriving rays) QP and RP' must form a

mutual angle 2α in order to be reflected in the same direction.

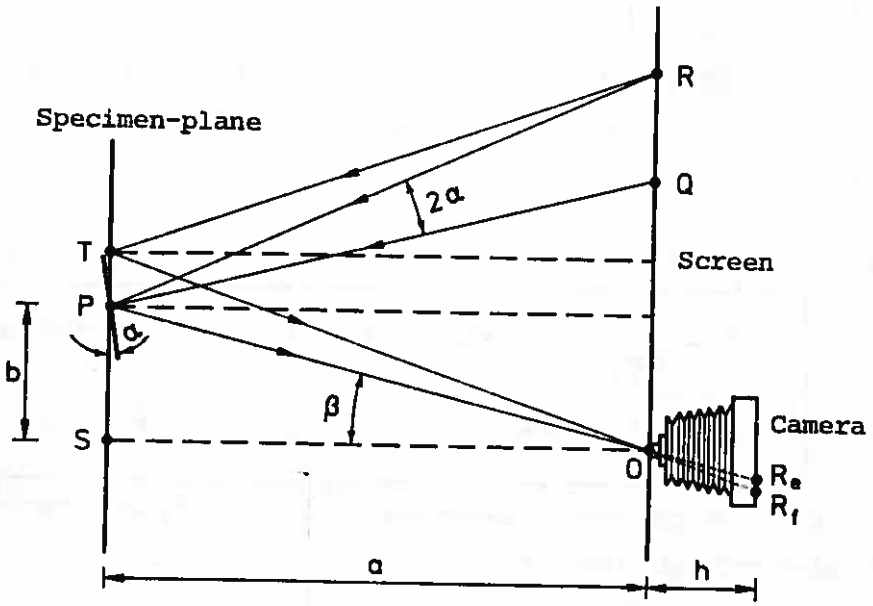

Figure 4.1-6

Fig. 4.1-6 is a simplified version of fig. 4.1-5, for use in the determination of the relationship between the change in angle and the deformation of the model grating. Here, the deflection is assumed to be sufficiently small to allow us, with good approximation, to regard P as coinciding with P'. The case considered is then the one in which the specimen only undergoes a change of slope at point P.

Before the deformation, points R and Q on the screen are reflected at R_f and R_e, respectively, on the focal plane of the camera, and after deformation, R is reflected at R_e. The angular rotation at P due to the deformation has thus caused a displacement of the grating line through R_f to R_e. The distance R_f-R_e is then an expression of the deformation of the model grating and is the image of the distance R-Q prior to the deformation.

If the change in slope is considered small compared with unity, then,

$$RQ = a\left(1 + \frac{b^2}{a^2}\right)\tan 2\alpha \simeq a\left(1 + \frac{b^2}{a^2}\right) 2\alpha$$

If, furthermore, b ≪ a, we get

$$\boxed{RQ \cong 2\,a\,\alpha}$$

The displacement $v = R_f R_e$ of the grating in the focal plane of the camera is thus seen to be proportional to the slope of the specimen surface.

If a coordinate system is inserted in the model plane, then

$$\boxed{\begin{array}{l} v = C\,\frac{\partial w}{\partial x} \quad \text{when the grating lines} \neq \text{y-axis} \\ \\ v = C\,\frac{\partial w}{\partial y} \quad \text{when the grating lines} \neq \text{x-axis} \end{array}} \qquad (4.1\text{-}10)$$

where C is a constant depending on the test arrangement, and w is the deflection of the model surface.

In order to keep this report within reasonable limits, the practical application of the methods will not be treated. In the author's post-graduate studies, particular attention has been paid to the reflection-moiré method, and the results of these investigations will be published later.

Particular reference is made to the following authors for details of the application of the methods:

Direct-moiré	: Sciammarella & Durelli [61-1] and Durelli & Parks [70-1].
Shadow-moiré	: Dykes [70-5] and Meadows, Johnson & Allen [70-12].
Reflection-moiré	: Ligtenberg [55-1], Bradley [59-1] and Beranek [68-14].

4.2 Parametric Description of the Moiré-Pattern

In the previous sections it has been shown that when certain conditions are fulfilled there will be proportionality between the grating displacement function and the displacement component, deflection or surface slope of the specimen, respectively. The next step is thus to establish the relations between the grating displacement function and the geometry of the moiré-pattern.

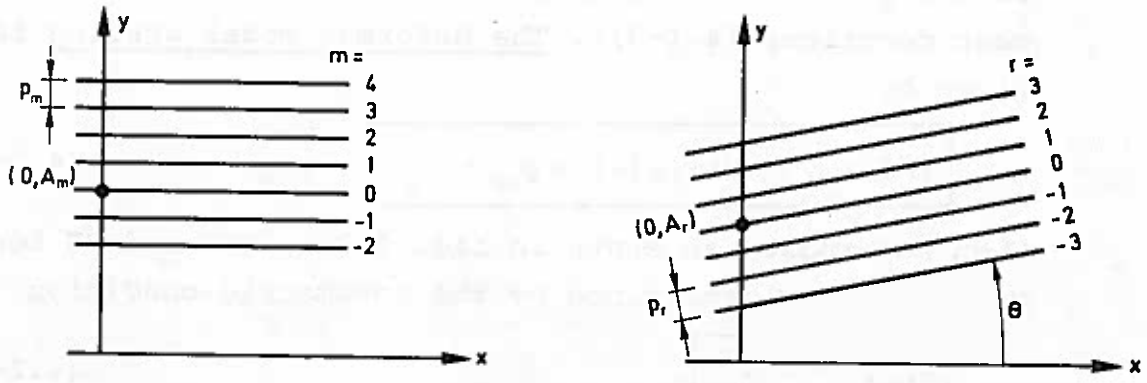

a) MG^O

Undeformed model grating

b) RG

Reference grating

Figure 4.2-1

The undeformed model grating (MG^O) has the pitch p_m, and the reference grating (RG), the pitch p_r. The coordinate system used for describing the gratings is assumed to have its x-axis parallel to the grating lines in MG^O (fig. 4.2-1.a), while the orientation of RG depends on the acute angle θ ($-90^O < \theta < 90^O$) between the x-axis and the grating lines. The angle is measured in an anticlockwise direction from the x-axis.

m and r are used as parameters for the grating lines, and they are so oriented that they increase in the positive y-direction. The grating lines with the parameters r = 0 and m = 0 intersect the y-axis at the points $(0, A_r)$ and $(0, A_m)$, respectively.

The two gratings then have the following parametric descriptions:

$$MG^O : y = m\,p_m + A_m \qquad (4.2\text{-}1)$$

$$RG : y = r\,\frac{p_r}{\cos\theta} + x\tan\theta + A_r \qquad (4.2\text{-}2)$$

In (4.2-2) the possibility of $\theta = 90^O$ is neglected since this does not normally give rise to a visible moiré-pattern.

The parametric description of the deformed model grating (MG) is obtained directly from (4.2-1) by adding the grating displacement function $v = v\{x,y\}$, which is the displacement in the y-direction. ($v\{x,y\}$ is one of the Eulerian displacement functions (4.1-3)). The deformed model grating is then given by

$$\boxed{MG : y = v\{x,y\} + m\,p_m + A_m} \qquad (4.2\text{-}3)$$

When superposed as shown in fig. 4.2-2, MG^o and RG form a moiré-pattern determined by the parametric condition

$$\boxed{n = r - m} \qquad (4.2\text{-}4)$$

This parametric condition is valid as long as the moiré-lines follow the short diagonals (section 2.3). In section 5.1 it is demonstrated that it is a sufficient condition for this to be the case, when

$$-20^o < \theta < 20^o$$

$$\frac{3}{4} < \frac{p_m}{p_r} < \frac{4}{3}$$

In the following these conditions are assumed to be fulfilled.

Solving (4.2-1) and (4.2-2) with respect to m and r and inserting these in (4.2-4), we get

$$n = y\left(\frac{\cos\theta}{p_r} - \frac{1}{p_m}\right) - x\frac{\sin\theta}{p_r} - \frac{A_r}{p_r}\cos\theta + \frac{A_m}{p_m}$$

Introducing, in addition, the relative pitch δ defined as the ratio between the two pitches:

$$\boxed{\delta = \frac{p_m}{p_r}} \qquad (4.2\text{-}5)$$

then the parametric description of the undeformed moiré-pattern takes the form:

$$\boxed{n\,p_m = y(\delta\cos\theta - 1) - x\,\delta\sin\theta - A_r\,\delta\cos\theta + A_m} \qquad (4.2\text{-}6)$$

When the deformed model grating (4.2-3) and the reference grating (4.2-2) are superposed, the same parametric condition (4.2-4) is assumed to apply. The parametric description of the deformed moiré-pattern is then:

$$n\,p_m = v\{x,y\} + y(\delta\cos\theta - 1) - x\,\delta\sin\theta - A_r\,\delta\cos\theta + A_m \qquad (4.2\text{-}7)$$

The validity of the parametric condition (4.2-4) for a given moiré-pattern must, of course, be investigated (se remarks in chapter 3). Generally speaking, it is valid as long as the deformation does not exceed a magnitude at which the ratio between the major and the minor pitch is less than 1.5 and at which the parameter of the model grating maintains its orientation in relation to the y-axis. The conditions are usually fulfilled in the moiré-methods dealt with in the report.

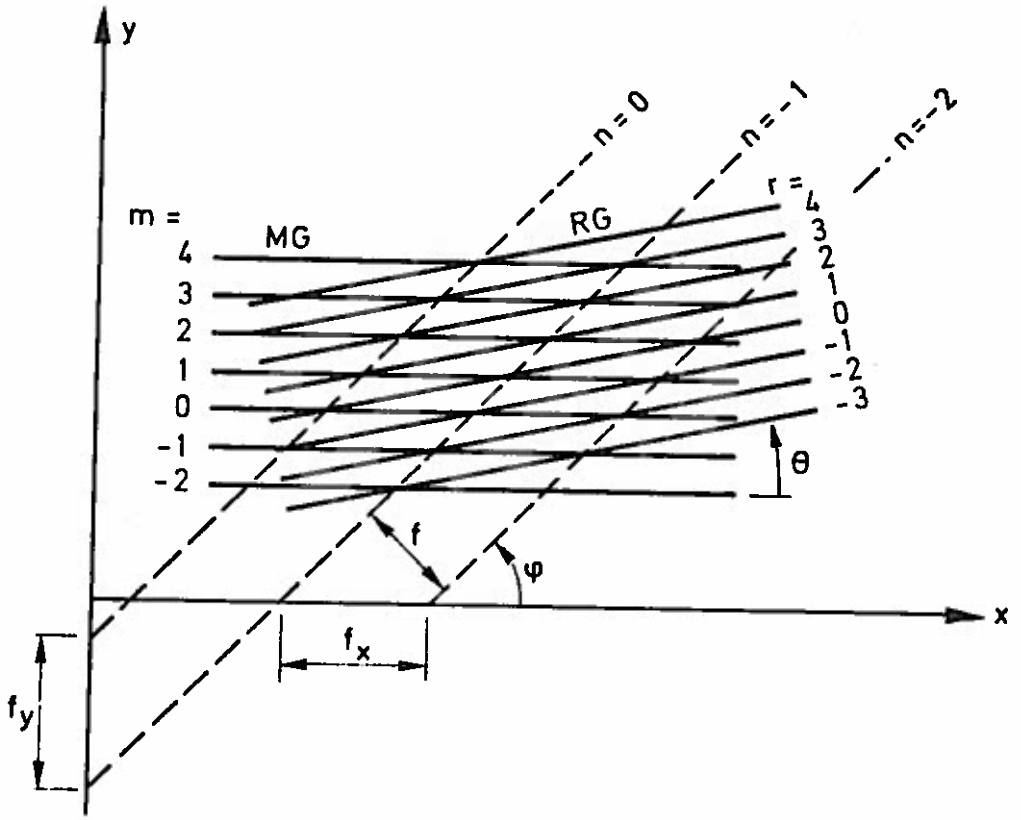

Figure 4.2-2

5. ANALYSIS OF THE UNDEFORMED MOIRÉ-PATTERN FORMED BY TWO LINE GRATINGS

The moiré-pattern to be analysed is that formed by two undeformed line gratings, as given by (4.2-6) and shown in fig. 4.2-2.

5.1 The Geometrical Relationship

Fig. 4.2-2 shows a number of geometrical quantities by which the moiré-pattern can be described. These are the only quantities required for a complete description of the pattern as this consists of straight and equidistant fringes.

The geometrical quantities in question are:

- f : THE INTERFRINGE SPACING, i.e. the distance between two adjacent moiré-lines measured perpendicular to the lines.
- f_x: The distance between two adjacent moiré-lines measured in the x-direction.
- f_y: The distance between two adjacent moiré-lines measured in the y-direction.
- φ : THE MOIRÉ-LINE INCLINATION, i.e. the angle between the x-axis and the moiré-lines measured anti-clockwise ($0 \leq \varphi \leq 180^{\circ}$).

For these quantities, (4.2-6) yields

$$F = \frac{f}{p_r} = \frac{\delta}{\sqrt{1 + \delta^2 - 2\delta\cos\theta}} \qquad (5.1\text{-}1)$$

$$F_x = \frac{f_x}{p_r} = \frac{1}{|\sin\theta|} \qquad (5.1\text{-}2)$$

$$F_y = \frac{f_y}{p_r} = \frac{\delta}{|\delta\cos\theta - 1|} \qquad (5.1\text{-}3)$$

$$\tan\varphi = \frac{\delta\sin\theta}{\delta\cos\theta - 1} \qquad (5.1\text{-}4)$$

in which the relative quantities F, F_x and F_y are introduced.

Fig. 5.1-1 and 5.1-2 show the variation of F and φ , respectively, for various values of δ and $\theta \geq 0^{o}$.

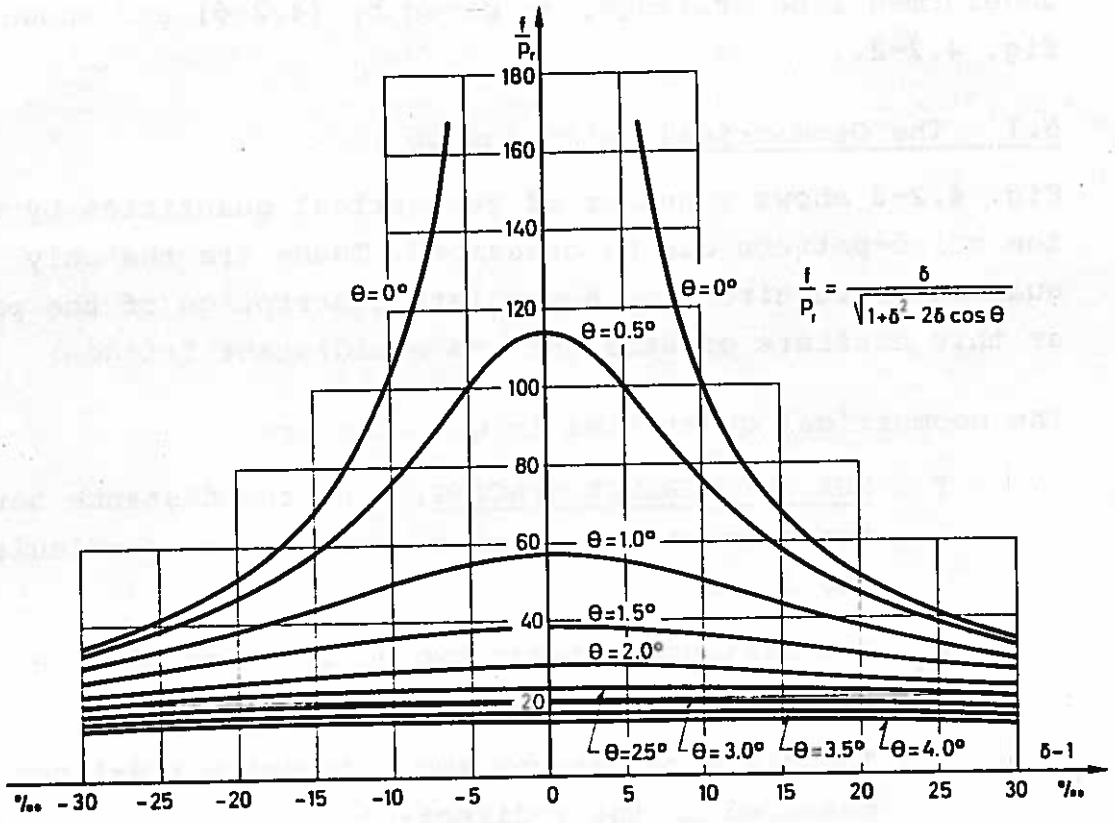

Interfringe Spacing $F = F\{\delta,\theta\}$

Figure 5.1-1

It will be seen from expressions (5.1-1) to (5.1-4) that

$$F\{-\theta\} = F\{\theta\}$$
$$F_x\{-\theta\} = F_x\{\theta\}$$
$$F_y\{-\theta\} = F_y\{\theta\}$$

and

$$\varphi\{-\theta\} = 180 - \varphi\{\theta\}$$

It will further be seen that when $\theta = 0^{o}$, the moiré-lines are parallel to the x-axis ($\varphi = 0$ and $F_x \rightarrow \infty$) and when $\delta \cos\theta - 1 = 0$, the moiré-lines are parallel to the y-axis ($\varphi = 90^{o}$ and $F_y \rightarrow \infty$). In the special case of $\delta = 1$ and $\theta = 0^{o}$, the quantities do not have finite values, but this corresponds to superposing two identical gratings with parallel lines - a case in which no moiré-pattern can be observed.

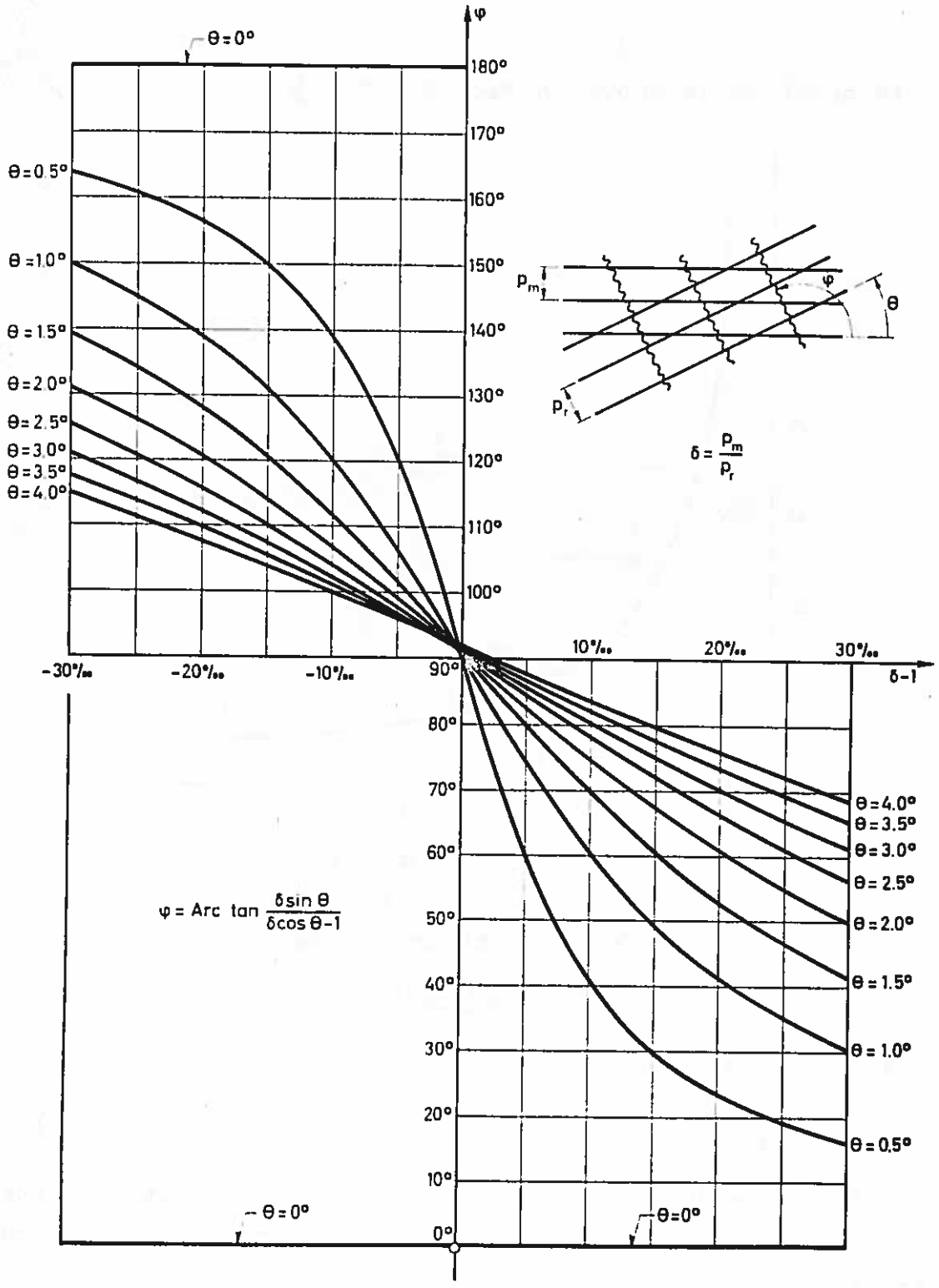

Inclination of Moiré-Lines $\varphi = \varphi\{\delta, \theta\}$

Figure 5.1-2

Example 5.1-1 ($\delta = 1 \wedge \theta \neq 0$).

If the two gratings are identical but inclined an angle θ in relation to each other, i.e. $p_m = p_r = p \Leftrightarrow \delta = 1$, (5.1-1) yields

$$F = \frac{f}{p} = \frac{1}{\sqrt{2 - 2\cos\theta}} = \frac{1}{2\left|\sin\frac{\theta}{2}\right|} \qquad (5.1\text{-}5)$$

This relation is shown in fig. 5.1-3.

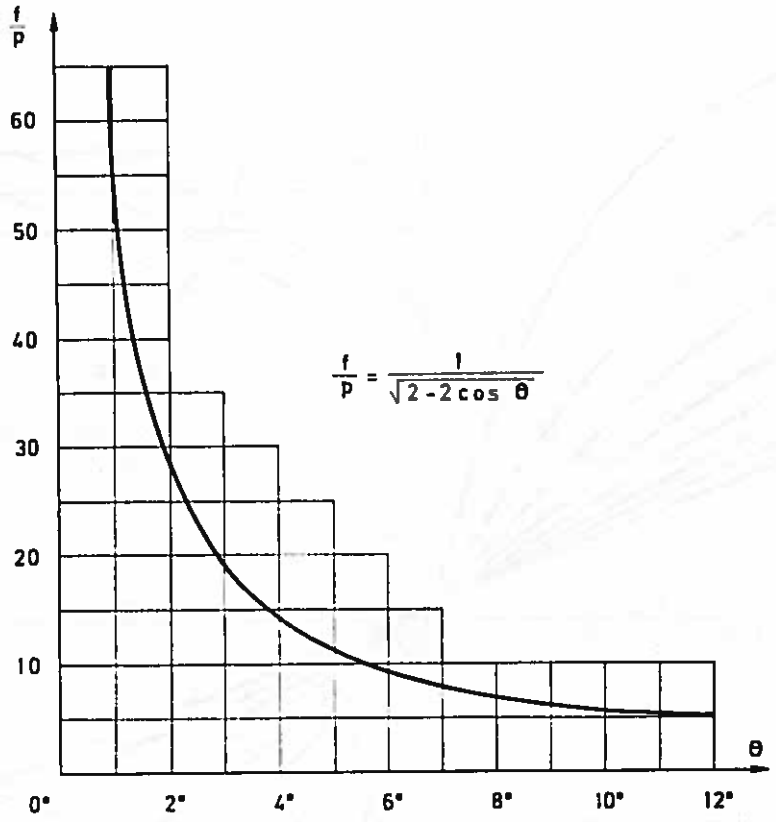

The Interfringe Spacing as
Function of Angular Displacement
of Two Identical Line Gratings

Figure 5.1-3

When θ is small,

$$\theta \simeq \frac{1}{F} \qquad (5.1\text{-}6)$$

It will be seen that F varies considerably for small values of θ and becomes almost constant for larger values of θ than 10^{o}-12^{o}.

For two identical gratings, it will alså be seen from (5.1-4) that

$$\tan\varphi = \frac{\sin\theta}{\cos\theta - 1} = -\cot\frac{\theta}{2} = \tan\left(\frac{\pi}{2} + \frac{\theta}{2}\right) \qquad (5.1\text{-}7)$$

Thus, when two identical gratings are superposed the moiré-lines bisect the obtuse angle between the grating lines.

Example 5.1-2 ($\delta \neq 1 \wedge \theta = 0^{o}$)

Another special case obtains when two parallel line gratings with different pitches are superposed, i.e. $\theta = 0^{o} \wedge p_m \neq p_r \Leftrightarrow \delta \neq 1$. In this case, (5.1-1) yields

$$F = \frac{\delta}{|1 - \delta|} \tag{5.1-8}$$

which, for $p_m > p_r \Leftrightarrow \delta > 1$), gives

$$f = p_r \frac{\delta}{\delta - 1} = \frac{p_r p_m}{p_m - p_r} \tag{5.1-9}$$

as was found by other means in section 2.2 (2.2-2).

It will be seen that the relative pitch-difference e is given by

$$e = \frac{p_m - p_r}{p_r} \cong \frac{p_m - p_r}{p_m} = \frac{\delta - 1}{\delta} = \frac{1}{F} \tag{5.1-10}$$

This expression, together with (5.1-6), was the first step in the development of a moiré-pattern theory (Kazcer and Kroupa [52-1]).

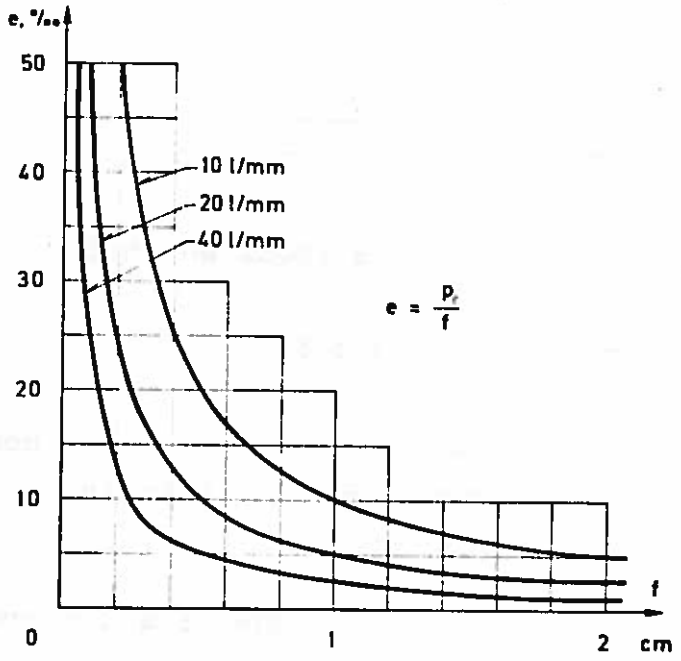

The difference in relative pitch $e = \frac{p_m - p_r}{p_r}$ as a function of the interfringe spacing f.

Figure 5.1-4

The relationship between e and the interfringe spacing f is shown in fig. 5.1-4 for a number of typical line densities. The curves are, of course, of the same character as that shown in fig. 5.1-3.

As mentioned in chapter 2, Košťák [63-1] has established a sufficient condition for ensuring that the moiré-lines follow the short diagonals or, in other words, for ensuring the validity of the parametric condition (4.2-4). Košťák's condition is that the interfringe spacing must be larger than three times the major pitch of the two gratings. The limitations on θ and δ entailed by the condition are as follows:

If $\delta \geq 1$, it is required that $f \geq 3p_m = 3p_r\delta$, and using (5.1-1), this can be written as

$$\frac{\delta p_r}{\sqrt{1 + \delta^2 - 2\delta\cos\theta}} \geq 3p_r\delta$$

$$\Leftrightarrow \quad \sqrt{1 + \delta^2 - 2\delta\cos\theta} \leq \frac{1}{3}$$

Hence,

$$1 \leq \delta \leq \cos\theta + \sqrt{\cos^2\theta - \frac{8}{9}} \qquad (5.1\text{-}11)$$

Similarly, when $\delta \leq 1$ it is required that

$$\frac{9}{8}\left(\cos\theta - \sqrt{\cos^2\theta - \frac{8}{9}}\right) \leq \delta \leq 1 \qquad (5.1\text{-}12)$$

Fig. 5.1-5 shows the area within which the combinations of θ and δ give an interfringe spacing that is larger than three times the major grating pitch.

According to the above conditions, δ and θ are limited to the values

$$\boxed{\begin{aligned} &-20^\circ < \theta < 20^\circ \\ &\frac{3}{4} \leq \delta \leq \frac{4}{3} \end{aligned}} \qquad (5.1\text{-}13)$$

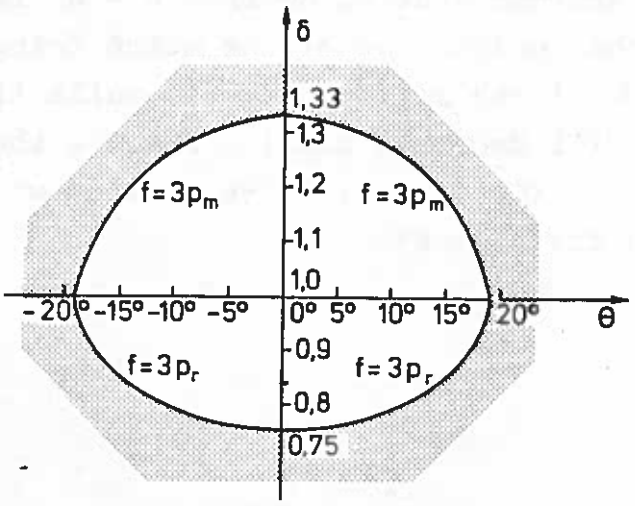

Area within which combinations of
and θ give $f \geq 3 \max\{p_m | p_r\}$

Figure 5.1-5

The conditions are sufficient to obtain moiré-patterns of the type under discussion, but not a necessary one as, for example, it is possible to observe a moiré-pattern when $\delta = 1$ and $\theta = 30^{\circ}$. The limiting area in fig. 5.1-5 should therefore only be regarded as approximate.

When two line gratings are angularly displaced, the inclination of the moiré-lines changes. This relation can be found by differentiating (5.1-4) with respect to θ.

$$\frac{\partial}{\partial\theta}(\tan\varphi) = \frac{\delta(\delta - \cos\theta)}{(\delta\cos\theta - 1)^2} \qquad (5.1\text{-}14)$$

i.e. when $\delta\cos\theta \neq 1$:

$$\cos\theta < \delta \Rightarrow \frac{\partial}{\partial\theta}(\tan\varphi) > 0 \Rightarrow \frac{\partial\varphi}{\partial\theta} > 0$$

$$\cos\theta > \delta \Rightarrow \frac{\partial}{\partial\theta}(\tan\varphi) < 0 \Rightarrow \frac{\partial\varphi}{\partial\theta} < 0$$

This means that if a grating RG is angularly displaced in relation to another grating MG from $\theta = 0^{o}$ in the positive direction, the inclination of the moiré fringe φ will increase with θ when $\delta \geq 1$ (AB in fig. 5.1-6), while if $\delta < 1$, the inclination will decrease until θ reaches the value corresponding to $\cos\theta = \delta$ (CD in fig. 5.1-6), after which it increases again (DE in fig. 5.1-6).

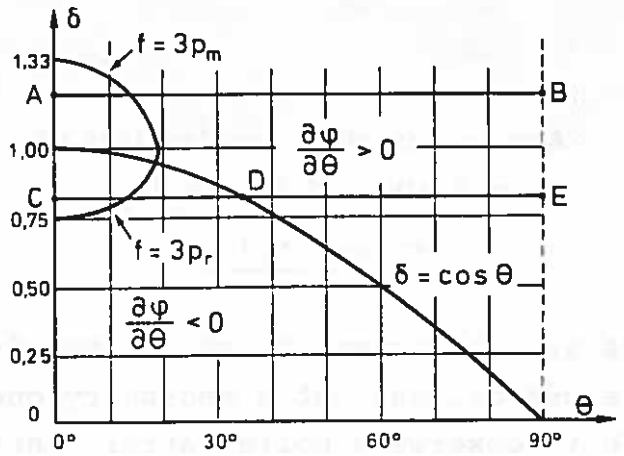

Figure 5.1-6

It is thus always possible to determine which of the two line gratings has the major pitch, since, in accordance with

"THE RULE OF MUTUAL ROTATION"

If a grating is rotated in a small angle from $\theta = 0^{o}$ in relation to a second grating, the first grating will have the minor pitch if the inclination of the moiré-lines follows the rotation, and the major pitch if the lines rotate in the opposite direction.

If δ is slightly less than unity, it will be seen from fig. 5.1-6 that the angle in question has to be correspondingly small. Otherwise, the curve $\delta = \cos\theta$ will be passed during the rotation, and then the rule will no longer be valid. For example,

$$\delta = 0{,}999 = \cos\theta \Rightarrow \theta \cong 2\tfrac{1}{2}^{o}$$

$$\delta = 0{,}990 = \cos\theta \Rightarrow \theta \cong 8^{o}$$

However, the limiting curve in fig. 5.1-5, which is also shown in fig. 5.1-6, also limits δ since the passage of the curve $\delta = \cos\theta$ takes place outside the area when δ is too small.

This δ-value is found by inserting $\cos\theta = \delta$ in (5.1-1), at the same time requiring that $f = 3\,p_r$ (as $\delta < 1$). Then

$$f = F\,p_r = \frac{\delta\,p_r}{\sqrt{1 + \delta^2 - 2\delta^2}} = 3\,p_r$$

$$\Rightarrow \delta = \sqrt{\frac{9}{10}} \simeq 0{,}95$$

i.e. for δ in the interval $0.75 < \delta < 0.95$, the change in the inclination of the moiré-line from the state in which it decreases with θ to that in which it increases with θ cannot be observed. However, doubtful cases in the interval $0.95 < \delta \leq 1$ can also be investigated by means of the "Shifting-rule" (example 5.3-1).

5.2 Comparison the Two Line Gratings

As an example of the applications of the theory developed, let us determine the pitch of a grating MG^{o}, assuming that the pitch of the reference grating (RG) is known. In this case, it must also be assumed that the pitches do not differ so much as to invalidate (5.1-1).

The following procedure can be used. The two gratings are rotated in relation to each other until the moiré-fringes are parallel to the grating lines. By measuring the interfringe spacing f, the pitch p_m of MG^{o} can then be determined by means of (5.1-1) for the case $\theta = 0^{o}$:

$$\delta = \frac{p_m}{p_r} = \begin{cases} \dfrac{f}{f - p_r} = \dfrac{F}{F - 1} > 1 \\ \dfrac{f}{f + p_r} = \dfrac{F}{F + 1} < 1 \end{cases} \qquad (5.2\text{-}1)$$

The "Rule of Mutual Rotation" can be used to determine which of the two cases is the correct result.

The accuracy of the procedure depends mainly on the error in the determination of the interfringe spacing f, since the error in the parallellism between the moiré-fringes and the grating lines can be neglected, because the moiré-fringes rotate through the angle $90^{o} + \frac{\varepsilon}{2}$ ($\varepsilon \ll 1$) when the grating lines are mutually rotated from the angle $\theta = \varepsilon$ to $\theta = 0^{o}$.

The error in the measurement of the interfringe spacing depends on the accuracy of the determination of the position of the fringe centreline (the moiré-line). With the naked eye, the fringe centreline can normally be determined within 1/10 of the interfringe spacing, but as a rule it can be more accurately determined partly on the basis of the "apparent fringe width" (section 2.4) and partly on the basis of the interfringe spacing. The use of a photo-cell for determination of the fringe centreline (minimum or maximum of light-intensity), reduces the error to about 0.01 times the interfringe spacing (Sciammarella et al [65-2]).

If $s\{\delta\}$ denotes the absolute error on δ and $s\{F\}$ the absolute error on $F = \frac{f}{p_r}$, the relative error on δ, calculated from (5.2-1) in accordance with the theory of accumulation of error, will be

$$\frac{s\{\delta\}}{\delta} = \frac{\partial\delta}{\partial F}\,\frac{s\{F\}}{\delta} = \begin{cases} \dfrac{s\{F\}}{F}\,\dfrac{1}{F-1} & \text{for } \delta > 1 \\ \dfrac{s\{F\}}{F}\,\dfrac{1}{F+1} & \text{for } \delta < 1 \end{cases} \qquad (5.2\text{-}2)$$

As the relative error $\frac{s\{F\}}{F}$ on the interfringe spacing can be assumed to be constant, it will be seen that the method gives the best result when $\delta \simeq 1 \Rightarrow F$ is big.

If, instead, we consider the quantity $e = \delta - 1$, i.e. the relative pitch-difference, then

$$\frac{s\{e\}}{e} = \begin{cases} \dfrac{s\{F\}}{F-1} & \text{for } \delta > 1 \Leftrightarrow e > 0 \\ \dfrac{s\{F\}}{F+1} & \text{for } \delta < 1 \Leftrightarrow e < 0 \end{cases} \simeq \frac{s\{F\}}{F} \text{ for } |e| < 10\% \qquad (5.2\text{-}3)$$

It will thus be seen that the relative error on this quantity is constant and equal to the relative error on the difference in the interfringe spacing. With the naked eye, the relative error is $\frac{\sqrt{2}}{10} \simeq 14\%$, whereas, with a photo-cell, it is of the order of magnitude of $\frac{\sqrt{2}}{100} \simeq 1.4\%$.

As the pattern is homogeneous, the accuracy can be further improved by determining the interfringe spacing as the mean (average), taken over several fringes. If F is determined on the basis of N fringes, the relative error (5.2-3) will be $\frac{1}{N}$ of the corresponding value of F determined on the basis of a single interfringe space.

Another way of determining the ratio (δ) between two pitches is to determine the variation in the inclination of the moiré-lines when the two gratings are mutually rotated. Solving (5.1-4) with relation to δ, we get

$$\boxed{\delta = \frac{\tan\varphi}{\cos\theta \tan\varphi - \sin\theta}} \qquad (5.2\text{-}4)$$

from which δ can be determined for related values of θ and δ. Here, the accuracy will depend on the accuracy with which the two angles can be measured.

Finally, δ can also be calculated by means of other combinations of the geometrical quantities characterizing the moiré-pattern. The relative expressions can be derived from (5.1-1 to 5.1-4). A discussion in detail of these expressions has been given by Morse, Durelli, and Sciammarella in [60-2], reprinted in the book [70-1]. Furthermore, Crisp [57-1] has investigated the accuracy of some of the expressions in practice.

5.3 Two Undeformed Line Gratings Used for Displacement Measurements.

An important application of line gratings is their use for the measurement of rigid body displacements (e.g. Guild [60-5]), meaning the mutual movement of two rigid bodies. Each of the bodies is provided with a line grating in such a way that the gratings have an area of superposition where a moiré-pattern can be observed.

If the mutual displacement of the two gratings takes the form of pure translation, no change will occur in the two characteristic quantities discussed in the foregoing, viz. the interfringe spacing and the fringe inclination. On the other hand, there will be a change in the positions of the fringes, and we will now take a look at the relationship between the moiré-fringe displacement and the grating displacement.

As stated in section 4.1, line gratings can be used to determine displacement in the direction perpendicular to the lines in the displaced grating. The displacement is considered in relation to the reference grating RG, i.e. this is fixed, while the other grating, MG, is subjected to pure translation in the y-direction of the order of magnitude of

$$v\{x,y\} = v = \text{constant}$$

It will be seen from the moiré-pattern equation (4.2-7) that the moiré-line with the parameter n is displaced

$$\Delta y = \frac{v}{1 - \delta \cos\theta} \quad \text{in the y-direction} \qquad (5.3\text{-}1)$$

and

$$\Delta x = \frac{v}{\delta \sin\theta} \quad \text{in the x-direction} \qquad (5.3\text{-}2)$$

Here, cases in which one of the denominators is zero, which arise when the moiré-fringes are parallel to one of the axes, are neglected. If $1 - \delta \cos\theta = 0$, no displacement can be observed in the y-direction, and if $\delta \sin\theta = 0$, no displacement can be observed in the x-direction.

If $v = p_m$, i.e. the displacement is equal to the pitch of the grating, then

$$\Delta y = \frac{p_m}{1 - \delta \cos\theta} = \frac{\delta}{1 - \delta \cos\theta} p_r$$

and

$$\Delta x = \frac{p_m}{\delta \sin\theta} = \frac{1}{\sin\theta} p_r$$

Compared with (5.1-2) and (5.1-3), it will be seen that $\Delta y = f_y$ and $\Delta x = f_x$. The displacement of the moiré-pattern per pitch-shift of the grating MG in the x- and y-directions is thus equal to the inter-fringe spacing in the corresponding directions.

Example 5.3-1. The Shifting Rule.

In the case $\theta = 0 \wedge \delta \neq 1$, we have

$$\frac{\Delta y}{v} = \frac{1}{1 - \delta} \quad \text{and } \Delta x = 0 \qquad (5.3\text{-}3)$$

Hence,

$$\delta > 1 \Rightarrow \Delta y < 0$$
$$\delta < 1 \Rightarrow \Delta y > 0$$

In the same way as the "Rule of Mutual Rotation" (section 5.1), this can be used to determine which of two line gratings has the major pitch, since, according to

"THE SHIFTING RULE"

If one of two parallel line gratings is shifted perpendicular to the grating lines, the shifted grating will have the minor pitch if the moiré-fringes move in the same direction as the shifted grating, and the major pitch if they move in the opposite direction.

The ratio (5.3-3) is also denoted the MAGNIFICATION, which indicates by how many times the displacement of the moiré-fringe exceeds that of the grating. If $\delta = 1.001$ and the line density is about 20 ℓ/mm, then a displacement equal to 0.1 mm will result in a displacement of the fringe of $1000 \cdot 0.1 = 10$ cm. If the error in the determination of the fringe-centre is 0.1 f ($= 0.1 \cdot 5$ cm $= 5$ mm), this means that the displacement of the grating can be determined with an error of $\sqrt{2} \cdot 0.1 \text{ mm} \cdot 0.05 = 0.007$ mm .

Displacement measurement by means of two undeformed line gratings has been especially developed in Britain by Ferranti Ltd., in cooperation with NPL (National Physical Laboratories)

and NEL (National Engineering Laboratory). Here, diffraction gratings with high line densities are used on servo-controlled machine tools, the movement of the moiré-pattern being observed by means of a number of photo-cells, which register the variation in light intensity as one grating moves in relation to the other.

The manufacture of gratings for the above purposes is discussed by Burch [60-6] and Dew [62-1]. Guild [60-3] treats the theory relating to a number of measuring systems, and Shepard [63-3] gives a short survey of the latest improvements made to these systems. Systems for light-intensity measurements are described in a number of papers, for example, Wong [63-4] and [63-5], McIlraith [64-5] and [66-3], Sim [65-7], and Russel [66-4].

Example 5.3-2 Calibration Instrument

As an example of the use of photo-cells for displacement measurements based on the fringe-counting principle, the calibration instrument shown in fig. 5.3-1 can be mentioned

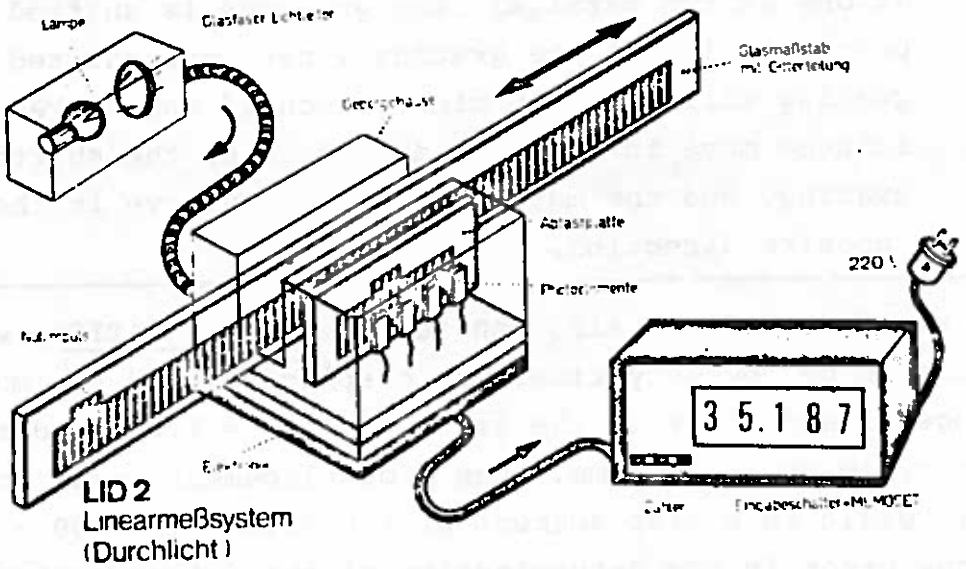

Calibration Instrument (Heidenhain System)

Figure 5.3-1

This instrument, which has been discussed by Askegaard [71-3], is used at the Structural Research Laboratory for calibrating

electrical and mechanical displacement gauges. The gauge length is 30 cm, and the precision is 0.001 mm. As shown in the figure, the instrument is provided with a counter, which registers the movement of the moiré-pattern by means of four photo-cells.

Other applications include a number of mechanical extensometers in which the "dial instrument" is replaced by two superposed gratings. Examples are described in Linge [57-2], Diruy [65-6], Holister, Jones and Luxmoor [66-2] and Vafiadakis [67-6]. These descriptions are all included in Theocaris' book [69-1].

The extensometers are slightly modified versions of existing instruments, and do not, in general, result in greater precision. Their advantage lies in the fact that the displacement of the moiré-pattern is registered electrically, and the instruments can therefore be used for measurements at normally inaccessible locations. In the case of the Diruy, the instrument is also used for measuring dynamic displacements.

A characteristic feature of the extensometers described is that it is necessary to follow the movement of the moiré-pattern during the displacement in order to determine this. Displacements in the direction perpendicular to the grating lines result in the same moiré-pattern if the mutual differences between the displacements are multiples of the pitch. Thus, it is not enough only to observe the initual and the final pattern unless it is known in advance that the displacement is less than the pitch. One method of following the movement of the moiré-pattern is to use fringe-counters, as shown in fig. 5.3-1. Another is to use several sets of gratings with varying line densities simultaneously. Thus, Vafiadakis provides his extensometer [67-6] with both a pair of gratings with a line density of about 4 ℓ/mm and a pair with a line density of about 20 ℓ/mm. This means that provided the grating displacement does not exceed the major pitch, an observation of the initial and the final pattern will suffice for determination of the displacement. The precision, on the other hand, is determined by the pair of gratings with the minor pitch.

In cases in which the movement of the moiré-pattern cannot be followed during displacement, it has proved advantageous to use other types of gratings, in which the moiré-pattern is not repeated for each displacement corresponding to one pitch. Košťák and Popp [66-1] have analysed the change in the moiré-pattern when two spiral gratings are mutually displaced, whereby both translation and rotation can be determined. The former author has also described, in [69-4], an extensometer with circular gratings, which has been used for long-term measurements of the mutual movements of rocks.

6. ANALYSIS OF THE "DEFORMED" MOIRÉ-PATTERN BETWEEN TWO LINE GRATINGS

6.1 Parametric Description of the Moiré-Pattern

If a deformed line grating (MG), in which the grating lines are parallel with the x-axis in the undeformed state, is superposed with a reference grating (RG), the resultant moiré-pattern, expressed by (4.2-7), can be described as follows (slightly rewritten):

$$v\{x,y\} = n\,p_m - y(\delta\cos\theta - 1) + x\,\delta\sin\theta + A_r\,\delta\cos\theta - A_m \qquad (6.1\text{-}1)$$

It is assumed that a number of the parameters describing the moiré-pattern are known:

x and y.....: The coordinate system must be oriented with the x-axis parallel to the grating lines in the undeformed model grating and must remain stationary during deformation of the model grating.

p_m and $\delta = \frac{p_m}{p_r}$: It is assumed that the pitches p_m (in the undeformed model grating) and p_r (in the reference grating) are determined in advance.

θ.....: It is assumed that the angle between the reference grating lines and the x-axis can be determined on the basis of the measuring arrangement.

We are then left with the following unknown parameters:

$v\{x,y\}$.....: The grating displacement function, the variation of which is assumed to be such that the parameter condition (4.2-4) is valid for the moiré-pattern. The order of magnitude of the variation is discussed in section 6.8.

$v\{x,y\}$ is the displacement-function in the y-direction.

n.....: The moiré-line parameter, which is an integer for bright moiré-fringes and is constant along each of these. For the dark fringes, n is equal to an integer + ½.

A_r and A_m....: Coordinate (see fig. 4.2-1) fixing the level of the grating line parameters. However, they can usually be chosen at random as they are only determinative for the absolute value of the moiré-line parameter n.

However, before discussion how the unknown parameters can be determined, let us first consider the moiré-pattern in a significant special case.

Example 6.1-1 ($\theta = 0 \wedge \delta = 1$)

In this case, the two gratings are identical and congruent prior to the deformation.

Therefore, for the known parameters, the following is true:

$$p_m = p_r = p \Leftrightarrow \delta = 1$$

and $\theta = 0$.

Furthermore, $A_m = A_r + k\,p$, where k is an integer. The moiré-pattern is then described by:

$$\boxed{v\{x,y\} = (n - k)p = N\,p} \qquad (6.1\text{-}2)$$

where $N = n - k$.

In this case, the moiré-curves are the contour lines for the grating displacement function v{x,y}, with the difference in level equal to the pitch (p) of the gratings prior to deformation.

This property of the moiré-pattern, for $\delta = 1 \wedge \theta = 0$, was described in the first articles on moiré-pattern theory, e.g.

Dantu [54-1], since it could be derived from simple geometrical considerations.

For the general case ($\theta \neq 0 \wedge \delta = 1$), the parametric description of the form (6.1-1) was first given by Košťák [68-2]. Unlike the so-called geometrical approach (cf. section 1.3), which assumes a homogeneous and infinitesimal state of strain, this provides a simpler method of analysing the moiré-pattern without the restriction of the requirements to a homogeneous and infinitesimal state of strain.

For the moiré-methods discussed in sections 4.1.1-4.1.3, it will be seen that the moiré-patterns for $\delta = 1$ and $\theta = 0$ are also contour-lines for:

Direct moiré : The displacement functions u_1 or u_2.
Shadow moiré : The deflection w.
Reflection moiré: The slope functions $\frac{\partial w}{\partial x}$ or $\frac{\partial w}{\partial y}$.

6.2 Variation of the Grating Displacement Function

For two points in a moiré-pattern with the coordinate differences Δx and Δy and with the parameter difference for the moiré-lines Δn, the difference Δv in the value of the grating displacement function at the two points is found by means of (6.1-1) to be

$$\boxed{\Delta v = \Delta n\, p_m - \Delta y(\delta \cos\theta - 1) + \Delta x\, \delta \sin\theta} \qquad (6.2\text{-}1)$$

Along lines parallel with the axis ($\Delta x = 0, \Delta y = 0$ respectively), the variation can be expressed as

$$\boxed{\begin{aligned} (\Delta v)_{\Delta x=0} &= \Delta n\, p_m - \Delta y(\delta \cos\theta - 1) \qquad (6.2\text{-}2)\\ (\Delta v)_{\Delta y=0} &= \Delta n\, p_m + \Delta x\, \delta \sin\theta \qquad (6.2\text{-}3)\end{aligned}}$$

while, along a moiré-line ($\Delta n = 0$), it becomes

$$\boxed{(\Delta v)_{\Delta n=0} = -\Delta y(\delta \cos\theta - 1) + \Delta x\, \delta \sin\theta} \qquad (6.2\text{-}4)$$

Thus, the difference in the value of v at two points on a moiré-line can be calculated directly from the known or measurable quantities, Δx, Δy, δ and θ.

For $\Delta x \neq 0 \wedge \theta \neq 0$, the variation can also be written

$$(\Delta v)_{\Delta n=0} = \Delta x\, \delta \sin\theta \left(1 - \frac{\Delta y}{\Delta x} \frac{\delta \cos\theta - 1}{\delta \sin\theta}\right) \qquad (6.2\text{-}5)$$

Then, in the special case $\Delta x > 0 \wedge \theta > 0 \wedge \delta \cos\theta \neq 1$, we get

$$(\Delta v)_{\Delta n=0} \begin{matrix} \geq \\ < \end{matrix} 0 \text{ because } \frac{\Delta y}{\Delta x} \begin{matrix} \leq \\ > \end{matrix} \frac{\delta \sin\theta}{\delta \cos\theta - 1} \qquad (6.2\text{-}6)$$

This is illustrated in fig. 6.2-1, which shows one of the moiré-lines considered.

The value of the displacement function along the line in relation to its value v{A} at point A can be determined by drawing a number of curve secants through A. If the secant slope (AB) is equal to the right side of (6.2-6), the displacement function will have the same value at the two points of the curve, i.e. v{A} = v{B}. If the secant slope (AB') is smaller, then v{B'} > v{A} will apply, and analogously, if it is bigger (AB"), then v{B"} < v{A}.

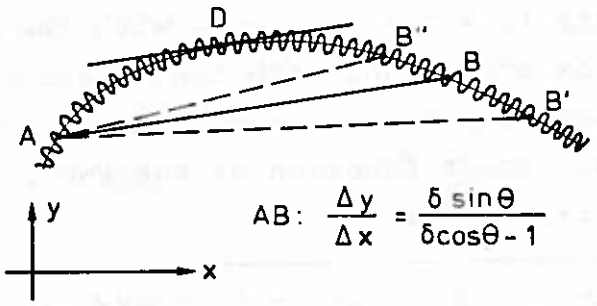

Figure 6.2-1

Continuing this line of reasoning, it will be seen that the displacement function reaches its minimum value along the line at point D where the tangent slope is equal to the right side of (6.2-6).

The slope in question is the same as that of the moiré-fringes prior to the deformation (cf. 5.1-4). This is shown in fig. 6.2-2.

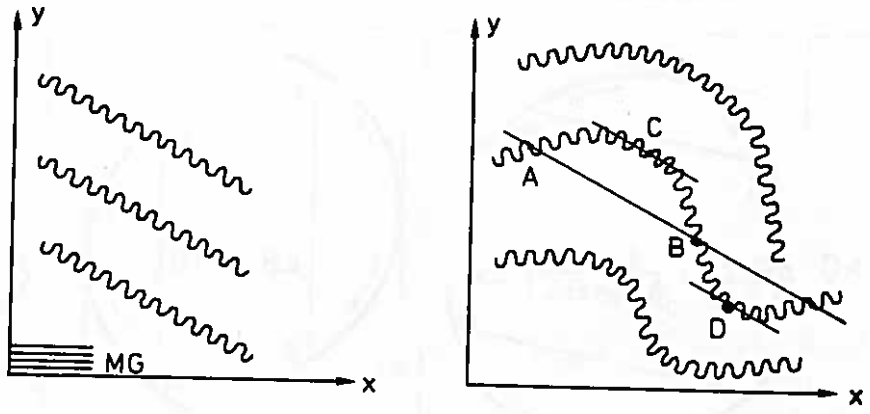

a) Before Deformation b) After Deformation

Figure 6.2-2

The nature of the variation of the displacement function for all possible combinations of θ and δ is shown in fig. 6.2-3. The maximum and minimum points are denoted C and D, while A and B are two points with the same value of the displacement function. Finally, the arrows indicate the directions for increasing value of v{x,y}.

The variation in the value of the displacement function from one moiré-line to another also requires knowledge of the parameter difference Δn for the moiré-lines. With this knowledge, similar considerations apply as for the variation along a moiré-line.

If a secant is drawn with the slope used earlier, as shown in fig. 6.2-4,

$$\frac{\Delta y}{\Delta x} = \frac{\delta \sin\theta}{\delta \cos\theta - 1}$$

then, according to (6.2-1):

$$v\{E\} = v\{F\} = v\{A\} + \Delta n\, p_m \qquad (6.2\text{-}7)$$

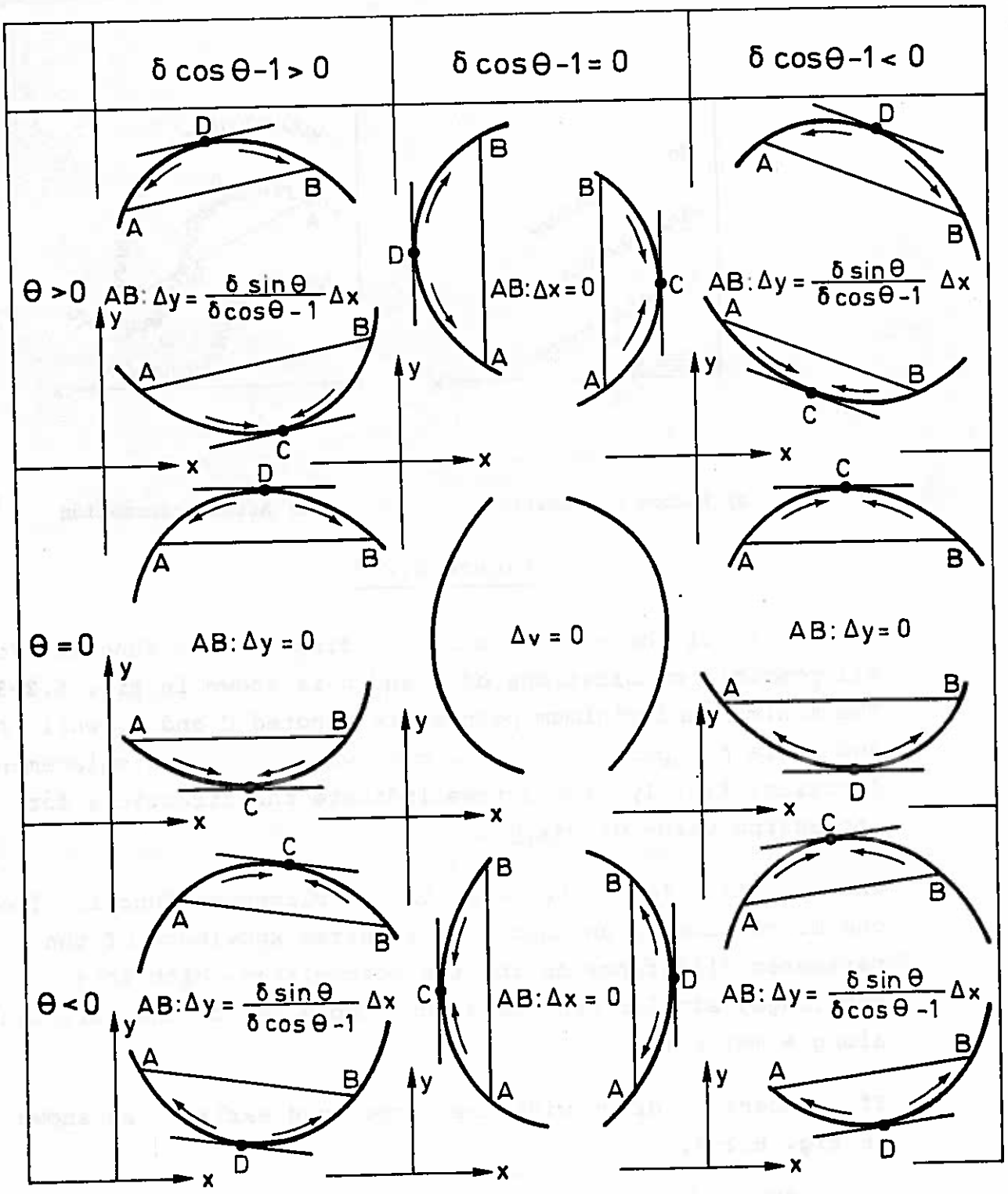

The Variation of the Displacement Function v{x,y}
along a Moiré-line for Various Combinations of θ and δ.
v{max} = v{C} > v{A} = v{B} > v{D} = v{min}

Figure 6.2-3

which means, inter alia, that the variation in the direction in question is independent of the interfringe spacing.

As will be seen from (6.2-1), when the parametric distribution of the moiré-lines and the value of the displacement function at a point are known, it is possible to calculate the displacement function over the whole of the area covered by the moiré-pattern.

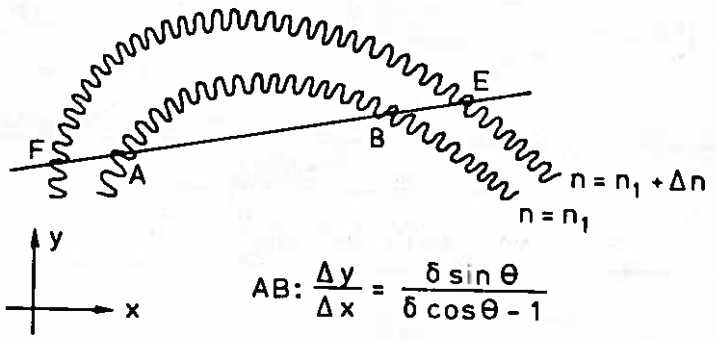

Figure 6.2-4

One method of determining the value of the displacement function at a point is to follow the change in the moiré-pattern while the model grating is deforming. If the distribution of the moiré-line parameter in the "undeformed" moiré-pattern is known, the value of the displacement function at a point will be given by

$$v\{x,y\} = (n_d - n_u)\, p_m \qquad (6.2\text{-}8)$$

where n_u is the moiré-line parameter for the fringe passing through the point in the "undeformed" moiré-pattern and n_d is the parameter for the fringe in the "undeformed" pattern that moves to the point during the deformation.

Another method is to utilize possible knowledge that, in view of the boundary conditions, the conditions of symmetry or

similar, the displacement function has, for example, the value $v = 0$ at certain points.

The variation of the displacement function is mainly only of interest in deflection measurements in shadow-moiré. Both in direct-moiré and in reflection-moiré, on the other hand, interest lies in the derivatives of the grating displacement functions, as these are proportional to components of the strain and curvature tensors, respectively. As it is necessary to know the signs of these derivatives in order to be able to calculate the variation of the moiré-line parameter, the derivatives have to be analysed before the parametric distribution.

6.3 Tangent Method. Variation in the Derivatives of the Grating Displacement Function

Differentiating (6.1-1), we get

$$\boxed{dn\, p_m = \frac{\partial v}{\partial x} dx + \frac{\partial v}{\partial y} dy + (\delta \cos\theta - 1)\, dy - \delta \sin\theta\, dx} \qquad (6.3\text{-}1)$$

Along a moiré-line ($dn = 0$). Therefore,

$$\left(\frac{\partial v}{\partial x} - \delta \sin\theta\right) dx = -\left[\frac{\partial v}{\partial y} - (1 - \delta \cos\theta)\right] dy \qquad (6.3\text{-}2)$$

from which it will be seen that

$$\boxed{\frac{dy}{dx} = 0 \Rightarrow \frac{\partial v}{\partial x} = \delta \sin\theta} \qquad (6.3\text{-}3)$$

and

$$\boxed{\frac{dx}{dy} = 0 \Rightarrow \frac{\partial v}{\partial y} = 1 - \delta \cos\theta} \qquad (6.3\text{-}4)$$

As (6.3-3 and 6.3-4) are independent of the moiré-line parameter, the derivatives of the displacement function have the same value at all points with tangents parallel to the axes. In a moiré-pattern, contour-lines can thus be drawn directly for $\frac{\partial v}{\partial x}$ and $\frac{\partial v}{\partial y}$ with the values determined by θ and δ (cf. figure 6.3-1).

A complete calculation of the derivatives of the displacement function can therefore be carried out by varying δ and/or θ, i.e. either by using reference gratings with different pitches or by rotating the reference grating.

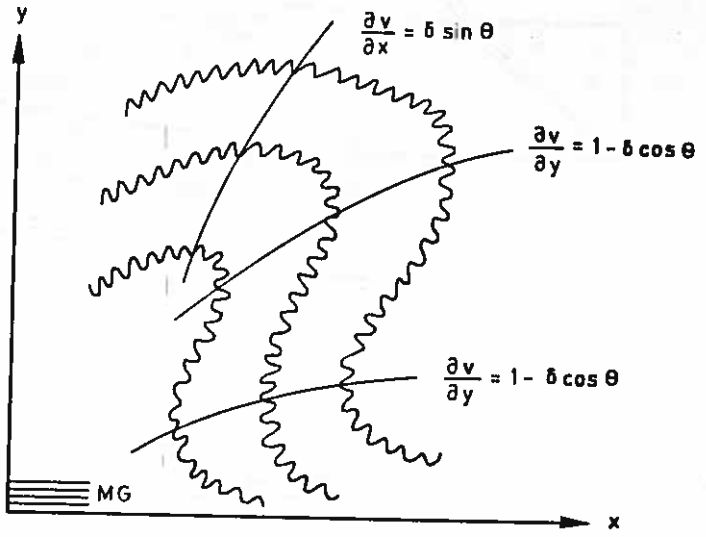

Tangent Method

Figure 6.3-1

Figure 6.3-2 shows a number of typical relationships between θ, δ, $\delta\sin\theta$, and $1 - \delta\cos\theta$. It will be seen that $\delta\sin\theta$ varies slightly with δ and almost proportionally with θ, while $1 - \delta\cos\theta$ varies slightly with θ and almost proportionally with $1 - \delta$. If it is possible to vary both δ and θ, it will be seen that it is most advantageous

and

to vary θ in the determination of $\frac{\partial v}{\partial x}$
to vary δ in the determination of $\frac{\partial v}{\partial y}$

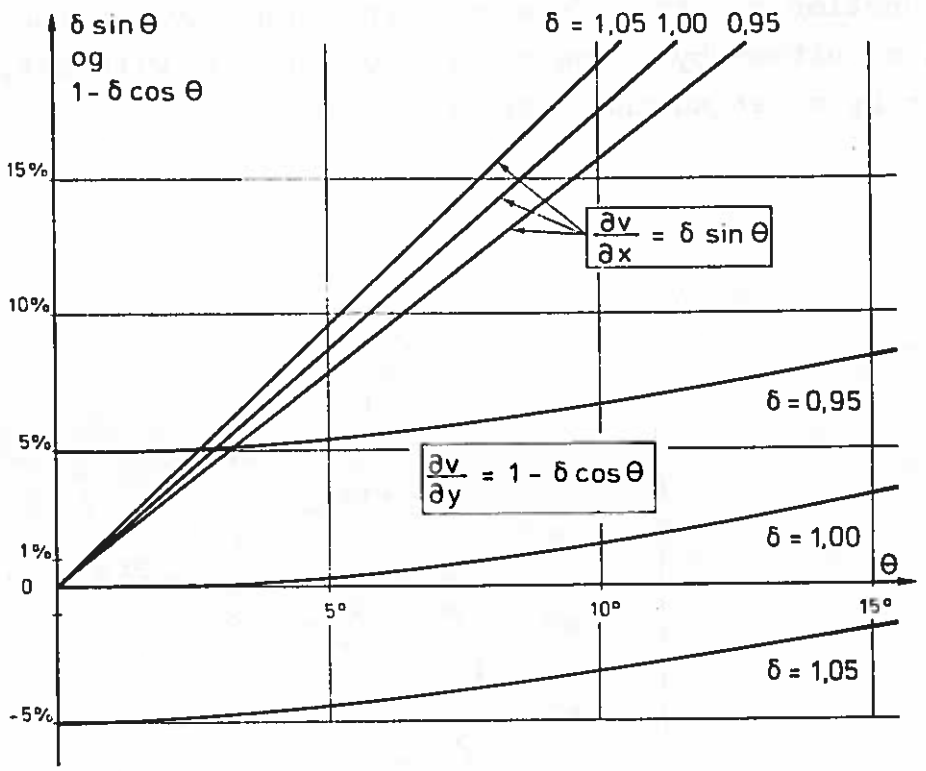

Figure 6.3-2

Dantu [58-1] drew attention to this possibility of drawing contour-lines for the derivatives of the displacement function, which is here called THE TANGENT METHOD, but examples of its application are only given in Theocaris [68-5].

In chapter 11 of Durelli and Parks [70-1] a similar method is given for calculating the rotation of the model grating lines. These authors consider the points along the moiré-lines at which the tangent is parallel to the reference grating lines, i.e.

$$\frac{dy}{dx} = \tan\theta \qquad (6.3\text{-}5)$$

Inserting this in (6.3-2), we get

$$\frac{dy}{dx} = \tan\theta \Rightarrow \frac{\frac{\partial v}{\partial x}}{1 - \frac{\partial v}{\partial y}} = \tan\theta \qquad (6.3\text{-}6)$$

When $\frac{\partial v}{\partial y} << 1$, a line through these points can be regarded as contour-line for $\frac{\partial v}{\partial x}$, and it is this approximation that Durelli and Parks utilize.

For moiré-line slopes that are not parallel with the axes, the following generally applies:

$$\frac{dy}{dx} = - \frac{\frac{\partial v}{\partial x} - \delta \sin\theta}{\frac{\partial v}{\partial y} - (1 - \delta \cos\theta)} \qquad (6.3\text{-}7)$$

Considering in particular the points on the curves at which

$$\frac{dy}{dx} = \frac{\delta \sin\theta}{\delta \cos\theta - 1} \qquad (6.3\text{-}8)$$

i.e. where the tangent is parallel to the moiré-lines prior to the deformation, we get from (6.3-2)

$$\frac{dy}{dx} = \frac{\delta \sin\theta}{\delta \cos\theta - 1} \Rightarrow dv = \frac{\partial v}{\partial x} dx + \frac{\partial v}{\partial x} dy = 0 \qquad (6.3\text{-}9)$$

This confirms the fact noted in section 6.2 to the effect that <u>the displacement function reaches its extreme values at the points at which the tangent is parallel to the moiré-lines before the deformation.</u>

In general, the derivatives of the grating displacement function cannot be determined separately solely on the basis of the slope of the moiré-line, the exception to this rule is the points with tangents parallel to the axes. On the other hand, relationships of the same type as (6.3-6) apply to all moiré-line slopes.

The special case of $\delta = 1 \wedge \theta = 0$ can be used to divide the moiré-pattern into areas within which the derivatives have constant signs. From (6.3-1) we get

$$\theta = 0 \wedge \delta = 1 \Rightarrow \frac{\partial v}{\partial x} dx + \frac{\partial v}{\partial y} dy = 0 \qquad (6.3\text{-}10)$$

from which we see that

and

for $\frac{dy}{dx} > 0$, $\frac{\partial v}{\partial x}$ and $\frac{\partial v}{\partial y}$ have opposite signs
for $\frac{dy}{dx} < 0$, $\frac{\partial v}{\partial x}$ and $\frac{\partial v}{\partial y}$ have the same sign

(6.3-11)

The zones are limited by curves for $\frac{\partial v}{\partial x} = 0$ and $\frac{\partial v}{\partial y} = 0$ (cf. figure 6.3-1). If the sign of one of the derivatives is known in one zone, the signs in other zones can be determined directly. The sign in one zone can, for example, be determined by rotating the reference grating and drawing one of the curves corresponding to (6.3-3 and 6.3-4). As the value of the derivative corresponding to one of these curves is determined by (6.3-3 and 6.3-4) the sign is also fixed.

When the curves for $\frac{\partial v}{\partial x} = 0$ and $\frac{\partial v}{\partial y} = 0$ are drawn, attention must be paid to the fact that the inclination of the moiré-line is indeterminate at the singular points (i.e. $\frac{\partial v}{\partial x} = \frac{\partial v}{\partial y} = 0$); furthermore, it is not certain that a moiré-fringe passes through the points at which the derivatives are equal to zero.

An example of this is shown in figure 6.3-3. Here, (b) shows the moiré-pattern corresponding to a displacement field (a) with $\frac{\partial v}{\partial x} = 0$, which results in a moiré-line inclination of zero. It is not immediately apparent from (b) that $\frac{\partial v}{\partial y}$ changes signs at A-A and B-B. Only when the reference grating has been rotated a small angle (c), do the "vertical" tangents at A-A and B-B reveal that here, too, $\frac{\partial v}{\partial y} = 0$.

The determination of the signs for the derivatives of the displacement function plays a decisive part in the determination of the variation in the moiré-line parameter. Even though the relations (6.3-11) are mentioned by Sciammarella and Durelli in both [61-1] and [63-2], these authors only propose guessing a sign for one of the derivatives on the basis of known boundary conditions. The method mentioned here, which combines Dantus's observations (6.3-3 and 6.3-4) and (6.3-11) was first arrived at in the preliminary work for this report and was mentioned at approximately the same time by Chiang in [69-3]. The method should render determination of the signs independent of an intuitive impression of the character of the deformation.

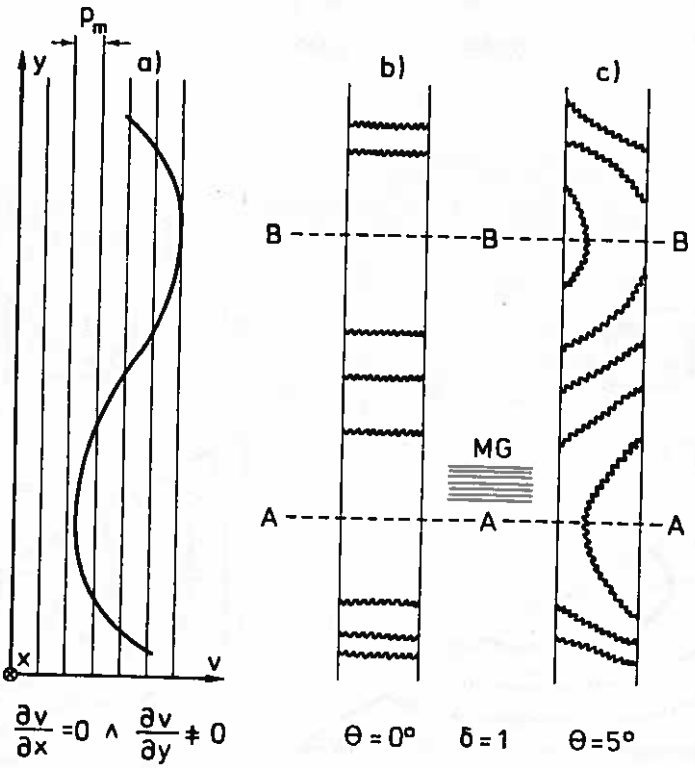

Displacement field with $\frac{\partial v}{\partial x} = 0$.

Figure 6.3-3

Example 6.3-1. Sign Determination I (The Tangent Method)

Figure 6.3-4 shows an example of this method. (a) shows the case where $\theta = 0 \wedge \delta = 1$, and the moiré-pattern can be divided into zones A-F. The reference grating is then rotated $\theta = 0.5^{o}$ (b), and it will be seen that $\frac{\partial v}{\partial x}$ is positive in zone B. $\frac{\partial y}{\partial x}$ is positive in zone B, so $\frac{\partial v}{\partial y}$ must be negative in this zone. The signs in the six zones are therefore as follows:

Zone	$\frac{\partial v}{\partial x}$	$\frac{\partial v}{\partial y}$
A	pos.	pos.
B	pos.	neg.
C	neg.	neg.
D	pos.	neg.
E	neg.	neg.
F	neg.	pos.

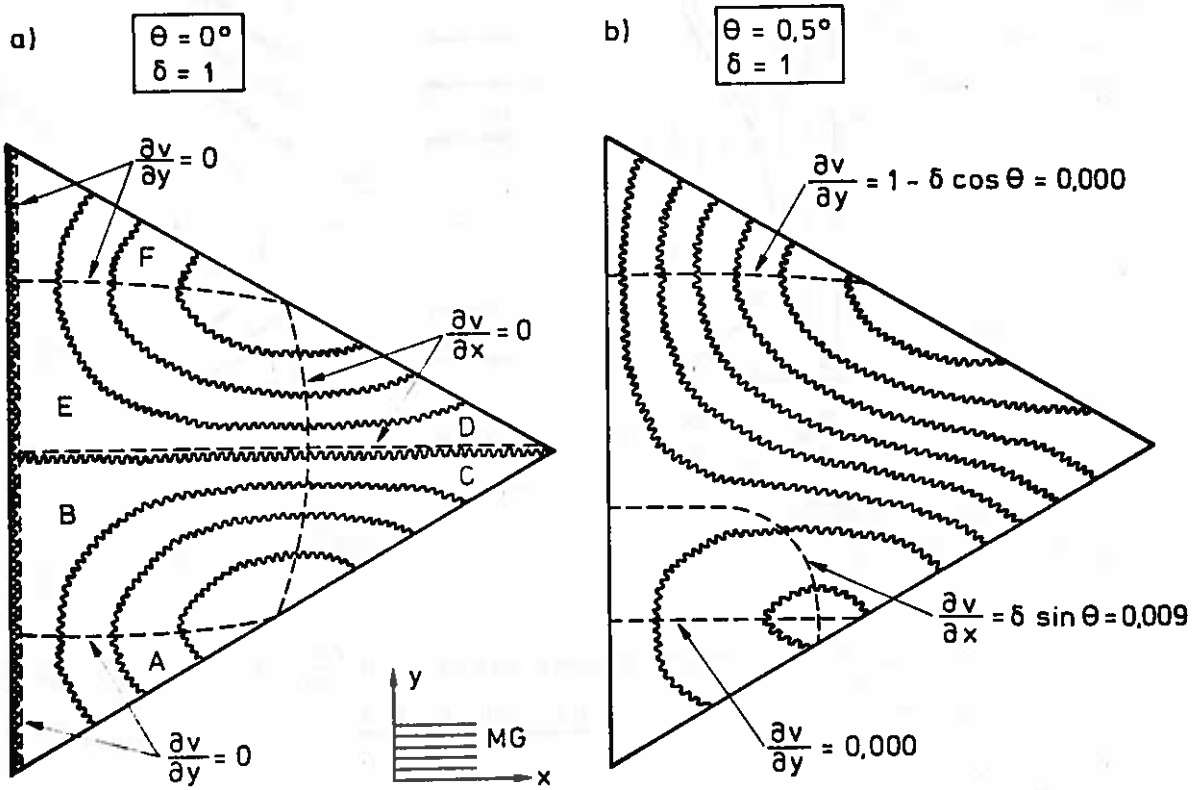

Figure 6.3-4

Example 6.3-2. Sign Determination II (Moiré-Line Inclination)

Another method of determining the signs for $\frac{\partial v}{\partial x}$ and $\frac{\partial v}{\partial y}$ is to consider the moiré-line inclination along the curves $\frac{\partial v}{\partial x} = 0$ and $\frac{\partial v}{\partial y} = 0$, when $\delta = 1 \wedge \theta \neq 0$, since we find from (6.3-7)

that:

Along the curve $\frac{\partial v}{\partial x} = 0$, the following applies

$$\theta > 0^{o} \wedge 0 > \frac{dy}{dx} > \frac{\sin\theta}{\cos\theta - 1} = \tan\left(\frac{\pi}{2} + \frac{\theta}{2}\right) \Rightarrow \frac{\partial v}{\partial y} < 0 \qquad (6.3\text{-}12)$$

which corresponds to the zone above B-B and below A-A in figure 6.3-3.

Analogously, along the curve $\frac{\partial v}{\partial y} = 0$:

$$\theta > 0^{o} \wedge 0 > \frac{dy}{dx} > \frac{\sin\theta}{\cos\theta - 1} = \tan\left(\frac{\pi}{2} + \frac{\theta}{2}\right) \Rightarrow \frac{\partial v}{\partial x} < 0 \qquad (6.3\text{-}13)$$

These relationships between fringe inclination and the signs for the derivatives of the displacement function are analogous to "The Rule of Mutual Rotation" given at the end of section 5.1.

6.4 Variation in Moiré-Line Parameter

The difference in parameter between two adjacent moiré-lines can either be 0 or 1, as, for reasons in continuity, bigger intervals than 1 cannot occur.

Between two points (x,y) and (x + Δx, y + Δy), the parameter difference Δn according to (6.2-1) is given by

$$\Delta n = \frac{1}{p_m} [\Delta v + \Delta y(\delta \cos\theta - 1) - \Delta x \, \delta \sin\theta] \qquad (6.4\text{-}1)$$

Along lines parallel to the axes (Δx = 0 and Δy = 0), we have

$$(\Delta n)_{\Delta x=0} = \frac{1}{p_m} [(\Delta v)_{\Delta x=0} + \Delta y(\delta \cos\theta - 1)] \qquad (6.4\text{-}2)$$

$$(\Delta n)_{\Delta y=0} = \frac{1}{p_m} [(\Delta v)_{\Delta y=0} - \Delta x \, \delta \sin\theta] \qquad (6.4\text{-}3)$$

For determination of Δn between two adjacent moiré-lines, it is sufficient to know the sign for the expressions in the brackets, since Δn can only assume values of -1, 0 or +1. If the expression in the brackets is positive, then Δn = +1, and

so on. It will be seen from (6.4-3), for example, that if $\Delta v < 0$ for $\Delta x > 0 \wedge \delta \sin\theta > 0$, then $(\Delta n)_{\Delta y=0} < 0$ and thus equal to -1.

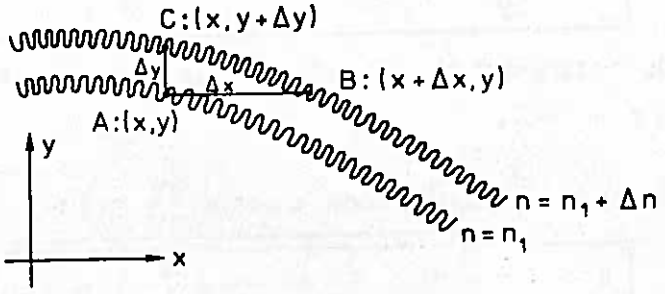

Figure 6.4-1

The increment $(\Delta v)_{\Delta y=0}$ in the value of the displacement function from A to B (see figure 6.4-1) along a line parallel to the x-axis can be written as

$$(\Delta v)_{\Delta y=0} = \int_{x}^{x+\Delta x} \frac{\partial v}{\partial x} dx$$

It will be seen from this that in zones in which $\frac{\partial v}{\partial x}$ is positive, $(\Delta v)_{\Delta y=0}$ is also positive. Correspondingly, it will be seen that the increment $(\Delta v)_{\Delta x=0}$ is positive if $\frac{\partial v}{\partial y}$ is positive, and negative if $\frac{\partial v}{\partial y}$ is negative. Within the zones in which the sign of the derivatives of the displacement function is constant, it is thus possible, for certain combinations of θ and δ, to state whether n increases or decreases in directions parallel to the axes. This is shown in figure 6.4-2.

As will be seen from the figure, it is only possible to determine the variation in n over the whole moiré-pattern for the case of $\delta = 1 \wedge \theta = 0$. For the other cases, the variation in n can only be determined in sub-zones of the moiré-pattern, but as the moiré-lines cross the boundaries of these sub-zones, it will usually be possible to determine the variation in n over the whole of the moiré-pattern on the basis of knowledge of the variation in the sub-zones.

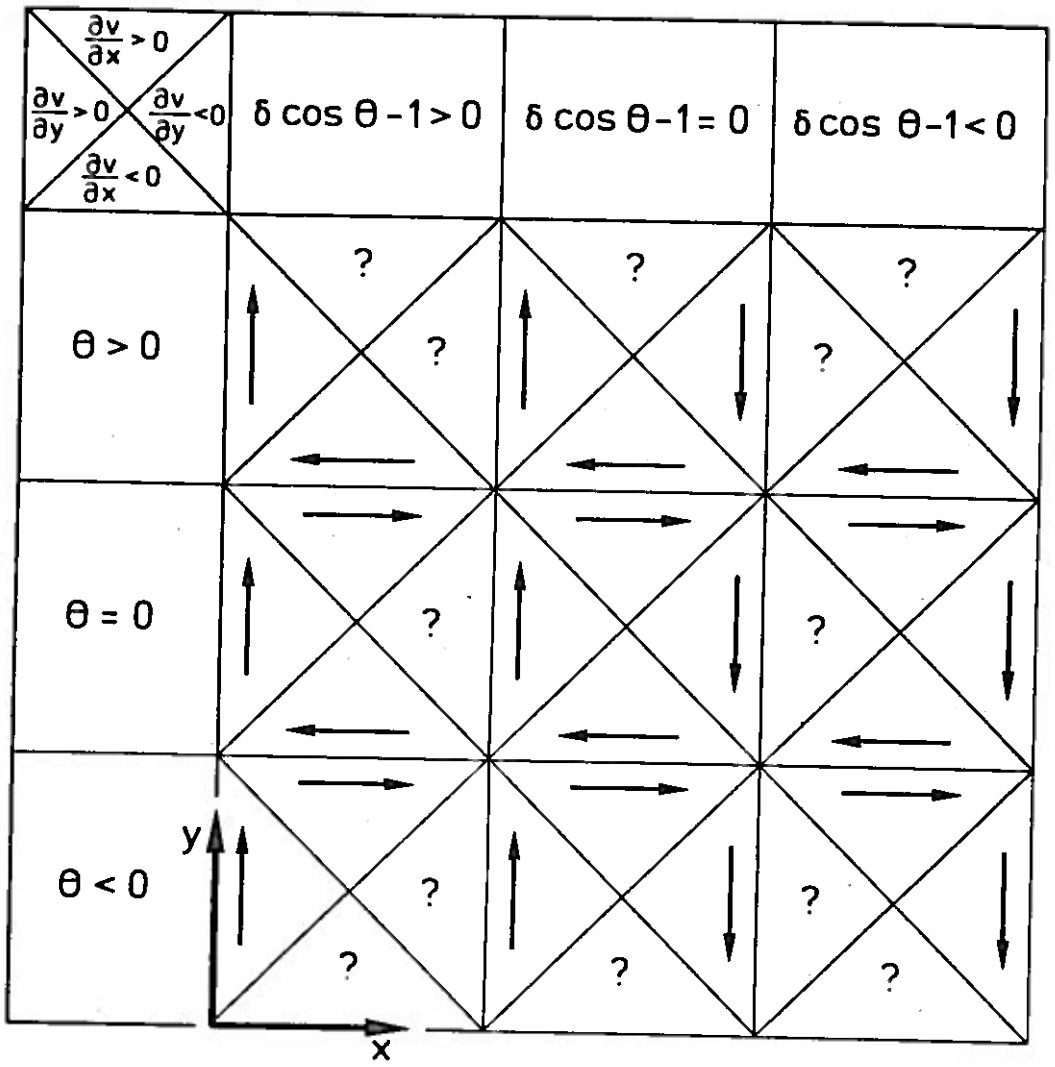

The arrows indicate the directions in which the moiré-line parameter n increases within zones in which the sign(s) of the derivatives of the displacement function are (is) constant.

Figure 6.4-2

An example of this is shown in figure 6.4-3, where the variation in the moiré-line parameter is determined for the moiré-pattern shown in figure 6.3-4.b. As shown in example 6.3-1: "Sign Determination I", the signs of the derivatives are as indicated in figure 6.4-3.a. From a comparison with figure 6.4-2 for $\delta \cos\theta - 1 < 0 \wedge \theta > 0$, we get the directions marked with arrows in figure 6.4-3.b with increasing parameter. Even though the variation in sub-zone A is indeterminate (unspecified), it will be seen that the variation for the entire moiré-pattern is determined.

In figure 6.4-3.b, the moiré-lines are numbered in accordance with the direction of the arrows, an arbitrary line being given the parameter n = 0.

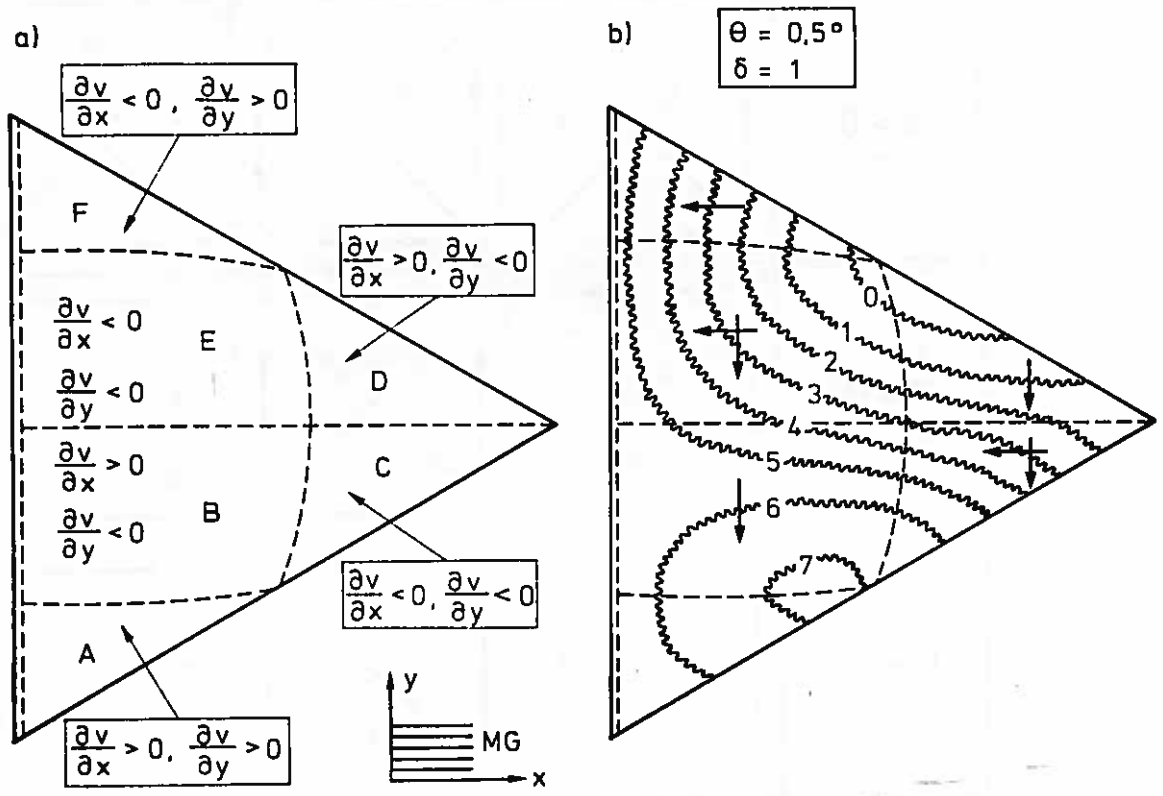

Variation in signs for the moiré-pattern shown in figure 6.3-4.b.

Figure 6.4-3

This zero-level can be selected at random as long as the variation of the displacement function within the moiré-pattern (cf. section 6.2) is investigated. What happens when a zero-level is selected is that the quantities A_r and A_m (see figure 4.2-1) are assigned certain values, but these quantities have no effect on the variation within the moiré-pattern.

6.5 Moiré-Line Density. "Mismatch". Geometrical Multiplication

It was mentioned in Section 4.1 that it was only possible with line gratings to determine the displacement for points located on the grating lines. When the displacement is to be determined

with a superposed reference grating and appurtenant moiré-pattern, the number of points is further reduced to comprise only those points on the deformed model grating lines that also lie on the moiré-lines. It is thus desirable for a given deformed model grating to get as high a moiré-line density as possible.

Efforts in this field have taken various directions. By utilizing the diffraction effect in the gratings it is possible to multiply the moiré-fringe in a moiré-pattern. This method, termed OPTICAL MULTIPLICATION in the following, is described in section 8.5. Another possibility is to develop on the same photograph the moiré-patterns for a number of cases in which the reference gratings is shifted a fraction of a pitch between each exposure. The method is termed GEOMETRICAL MULTIPLICATION and is described at the end of this section.

However, first, a third possibility, which lies in varying the angle θ and the relative pitch δ, will be discussed. Methods utilizing this possibility are termed "Mismatch Methods" in the English literature. Generally, the two possibilities are treated separately, variation of θ alone ($\theta \neq 0 \wedge \delta = 1$) being treated by the so-called "Rotational Mismatch" or "Angular Disparity" method, while variation of δ alone ($\theta = 0 \wedge \delta \neq 1$) is treated by the "Linear Mismatch" or "Linear Differential" method.

About a point A in the moiré-pattern (figure 8.5-1), the moiré-line density will vary as follows when either θ or δ is altered:

The number of moiré-lines between two points is generally greater than or equal to the parametric difference for the moiré-lines. This difference is given by (6.4-1).

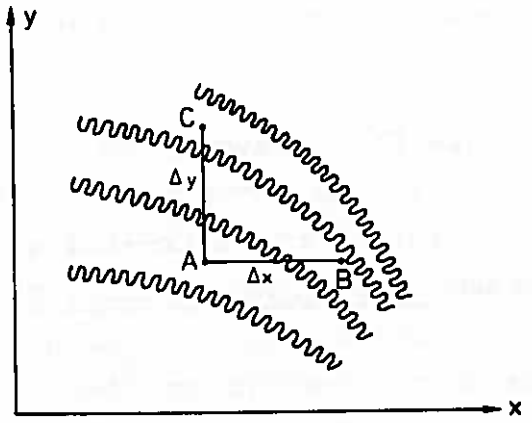

Figure 6.5-1

For $\delta = 1 \wedge \theta \neq 0$, (6.4-2 and 6.4-3) yield

$$\Delta n_{AB} = \frac{1}{p_m} [\Delta v_{AB} - \Delta x \sin\theta] \qquad (6.5\text{-}1)$$

$$\Delta n_{AC} = \frac{1}{p_m} [\Delta v_{AC} + \Delta y(\cos\theta - 1)] \qquad (6.5\text{-}2)$$

and for $\delta \neq 1 \wedge \theta = 0$

$$\Delta n_{AB} = \frac{1}{p_m} [\Delta v_{AB}] \qquad (6.5\text{-}3)$$

$$\Delta n_{AC} = \frac{1}{p_m} [\Delta v_{AC} + \Delta y(\delta - 1)] \qquad (6.5\text{-}4)$$

It will be seen that variation of θ alone will have a mainly incremental effect on the moiré-line density parallel to the model grating lines (the x-direction), while variation of δ alone will only alter the moiré-line density in the y-direction, i.e. perpendicular to the direction of the model grating lines.

θ =	0^o	1^o	2^o	5^o	10^o
1000 sinθ	0	18	35	87	174
1000(1-cosθ)	0	0	1	4	15

Table 6.5-1

The increase in number of moiré-lines by variation of θ.

δ-1	0	0,1 ‰	1 ‰	1 %	10 %
1000(δ-1)	0	0	1	10	100

Table 6.5-2

The increase in number of moiré-lines by variation of δ.

Tables 6.5-1 and 6.5-2 show the increase in number of moiré-lines by variation of θ from $\theta = 0^o$ and δ from $\delta = 1$, respectively, in zones in which $\Delta x = \Delta y = 1000\ p_m$. Finally, attention should be drawn to the fact that if the differences Δv_{AB} of Δv_{AC} in the displacement function have opposite signs in relation to the increment, the moiré-line density will not increase until the increment is greater than twice the difference in the displacement function.

An example of the change in a moiré-pattern by alteration of θ is shown in figure 6.5-2.

These two possibilities for increasing the moiré-line density were first discussed by Dantu [58-1]. Since then, the problem has mainly been treated by Tanaka and Nakashima [60-4], Chiang [65-4], Post [65-5] and Vafiadakis and Lamble [67-3].

Example 6.5-1. Sign Determination III. (Moiré-Fringe Density)

The third method of determining the signs for $\frac{\delta v}{\delta x}$ and $\frac{\delta v}{\delta y}$ is based on the variation in the moiré-fringe density during alteration of θ. The procedure is as follows:

Consider a zone in the moiré-pattern in which there are moiré-fringe inclinations that are not parallel

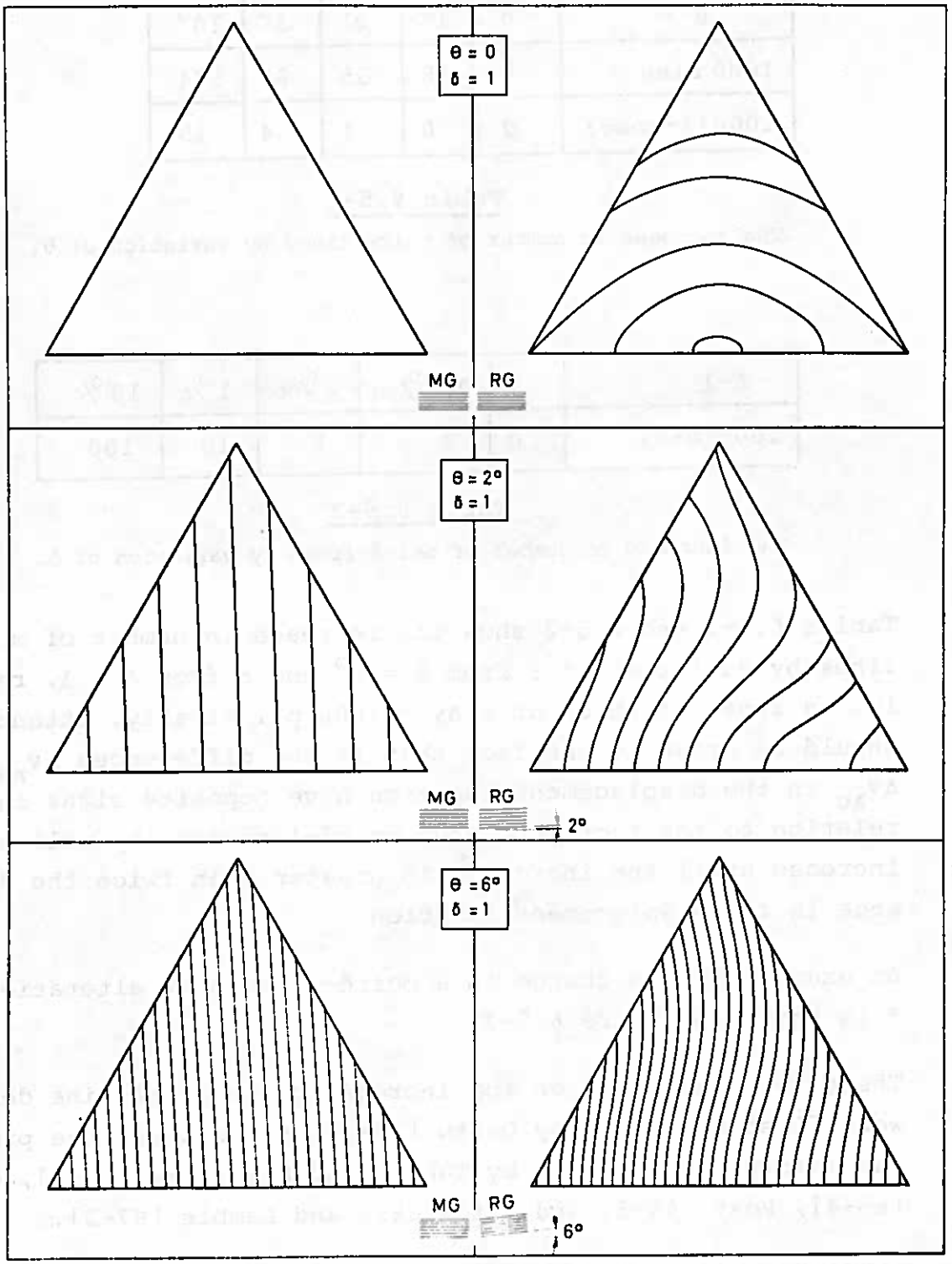

"Undeformed" moiré-pattern "Deformed" moiré-pattern

Variation in Moiré-Pattern with the angle θ.

Figure 6.5-2

to the axes in the state $\theta = 0^{o} \wedge \delta = 1$. Then rotate the reference grating to $\theta > 0$ and investigate whether the fringe density in the directions of the axes increases or decreases, since:

<u>If the fringe density increases in the directions of the axes during a small, positive rotation of the reference grating from $\theta = 0$, the moiré-line parameter will decrease in the corresponding directions, and vice versa if the fringe density decreases.</u>

This appears directly from (6.5-1 and 6.5-2), since the number of fringes $|\Delta n_x|$ for the length AB is

$$\theta = 0 \Rightarrow |\Delta n_x^o| = \frac{1}{p_m} |\Delta v_{AB}|$$

$$\theta > 0 \Rightarrow |\Delta n_x| = \frac{1}{p_m} |\Delta v_{AB} - \Delta x \sin\theta|$$

As long as θ is so small that the first term is numerically the greatest, the following is valid:

$$|\Delta n_x| = |\Delta n_x^o| \pm \frac{\Delta x}{p_m} \sin\theta \quad \begin{pmatrix} + \text{ if } \Delta v_{AB} < 0 \\ - \text{ if } \Delta v_{AB} > 0 \end{pmatrix}$$

i.e.

$$\boxed{\begin{aligned} |\Delta n_x| > |\Delta n_x^o| &\Leftrightarrow \Delta v_{AB} < 0 \\ |\Delta n_x| < |\Delta n_x^o| &\Leftrightarrow \Delta v_{AB} > 0 \end{aligned}} \qquad (6.5\text{-}5)$$

The method of increasing the moiré-line density termed <u>GEOMETRICAL MULTIPLICATION</u> or "<u>Grid-shift Technique</u>" was first described by Chiang, Parks and Durelli [68-10], and the latter two authors have again discussed the method in [68-11] and [70-1].

In brief, the geometrical multiplication method envisages the superposition, for example by double exposure, of several moiré-patterns that differ from each other in that the reference grating is each time shifted in fraction of the pitch perpendicular to its line orientation.

In the case $\theta = 0 \wedge \delta = 1$, the moiré-pattern is described by (6.1-1):

$$v\{x,y\} = n_1 p + A_r - A_m \qquad (6.5\text{-}6)$$

By shifting the reference grating $\frac{1}{2}p$ in the y-direction, we get a new pattern that can be described by

$$\begin{aligned} v\{x,y\} &= n_2 p + (A_r + \tfrac{1}{2}p) - A_m \\ &= (n_2 + \tfrac{1}{2})\, p + A_r - A_m \end{aligned} \qquad (6.5\text{-}7)$$

As it is the same displacement function that is described by both patterns, the following must be valid:

$$n_1 = n_2 + \frac{1}{2} \qquad (6.5\text{-}8)$$

If we superpose the two patterns, we can write the resultant pattern as

$$\boxed{v\{x,y\} = n\frac{p}{2} + A_r - A_m} \qquad (6.5\text{-}9)$$

n even corresponds to (6.5-6)
n uneven corresponds to (6.5-7)

It will thus be seen that the resulting pattern has half the difference in level or the double number of moiré-lines as the pattern (6.5-6). The pattern (6.5-6) has thereby been multiplied by the factor 2.

In the descriptions mentioned above, the maximum multiplication factor achieved is 3, and, due to experimental and other difficulties in connection with the reference grating displacement, the method seems inferior to that of optical multiplication, in addition to which, a considerably higher multiplication factor can be achieved with the latter (see section 8.5).

6.6 The Moiré-Surface. The Surface Slope Method

As mentioned earlier, the moiré-pattern can be regarded as the contour curve system for a surface. This surface is designated THE MOIRÉ-SURFACE $z = M\{x,y\}$ and is given by (4.2-7)

$$\boxed{z = M\{x,y\} = n\,p_m = v\{x,y\} + M_o\{x,y\}} \qquad (6.6\text{-}1)$$

where

$$M_o\{x,y\} = y(\delta\cos\theta - 1) - x\,\delta\sin\theta - A_r\,\delta\cos\theta + A_m \qquad (6.6\text{-}2)$$

is the moiré-surface prior to the deformation (4.2-6).

Figure 6.6-1 shows the moiré-surface corresponding to a moiré-pattern in the x,y-plane.

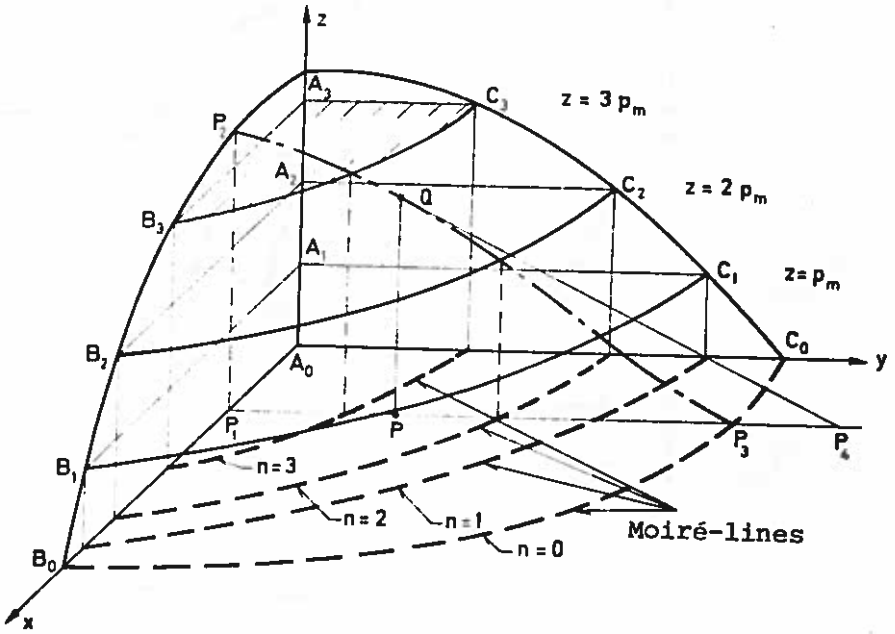

The moiré-surface $z = M\{x,y\}$

Figure 6.6-1

The derivatives of the displacement function can be determined on the basis of the inclinations of the moiré-surface in the directions of the axes (Surface Slope Method), since

$$\frac{\partial M}{\partial x} = \frac{\partial v}{\partial x} + \frac{\partial M_o}{\partial x} = \frac{\partial v}{\partial x} - \delta \sin\theta \qquad (6.6\text{-}3)$$

$$\frac{\partial M}{\partial y} = \frac{\partial v}{\partial y} + \frac{\partial M_o}{\partial y} = \frac{\partial v}{\partial x} + (\delta \cos\theta - 1) \qquad (6.6\text{-}4)$$

The method of determining the slope is explained in fig. 6.6-2 where, on the basis of the moiré-pattern, section curves in the moiré-surface in sections parallel to the axes are drawn up.

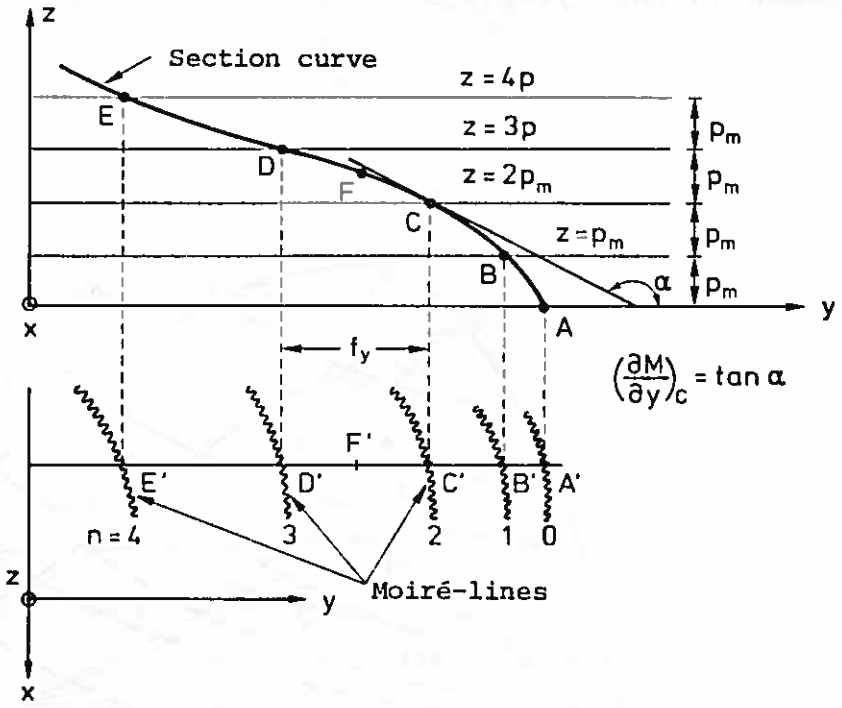

Determination of $\frac{\partial M}{\partial y}$

Figure 6.6-2

By measuring the inclination (slope) of the tangent at the individual points, the derivatives of the displacement function can be determined from (6.6-3 and 6.6-4), assuming that δ and θ are known. If this is not the case, they can be determined by measuring the slopes (inclinations) on the "undeformed" moiré-surface.

The accuracy of the method (see chapter 7) depends on, inter alia, the degree of correspondance between a drawn section curve and the real (true) section curve, and it will be seen that the denser the moiré-fringes, the better will be the section curves depicted.

The method is rather laborious as it entails drawing a large number of section curves, if the state of deformation must be determined throughout the moiré-pattern.

Another, somewhat speedier method with a slightly lower accuracy is to calculate the average (mean) slope at points halfway between two adjacent moiré-lines. In the case of the point F in fig. 6.6-2, the tangent slope can be written approximately as follows:

$$\left(\frac{\partial M}{\partial y}\right)_F \simeq \frac{\Delta M}{\Delta y} = \frac{p_m}{C'D'} = -\frac{p_m}{f_y} \qquad (6.6\text{-}5)$$

calculated with appropriate sign, where f_y is the local interfringe spacing in the y-direction.

The accuracy of the approximation depends on, inter alia, the interfringe spacing because, according to the mean average theorem in differential calculus, the true section curve will have the slope in question (6.6-5) at a point between C and D. The accuracy of the method can thus just as well be said to depent on the error of the determination of the point between C and D at which the section curve has the slope (6.6-5), and here, too, greater fringe density will also lead to increased accuracy.

A third method of determining the slope of the moiré-surface is to approximate the surface by a polynomial in x and y, which assumes values of the surface at a number of points, after which the slopes of the polynomial can be calculated and utilized as surface slopes. The method requires the formulation of a computer-programme, as described by Irons and Carter [67-15], Hinton and Irons [68-15] and Bossaert, Dechaene and Vinckier [68-12].

6.7 Super-Moiré. Moiré of Moiré. Second-Order Moiré.

Super-moiré,which is also known by the other two names, is yet another method of determining the derivatives of the displacement function. The method is a graphical differentiation method, and has been introduced in moiré-technique by Dantu, who has described it in [58-1] and [66-8]. Parks and Durelli have also discussed the method in [66-9].

Consider a contour-curve system (fig. 6.7-1.a) in the x,y-plane, given by

$$F\{x,y\} = n \tag{6.7-1}$$

A copy of the contour-curve system is shifted a distance Δx in the x-direction, and a second copy is shifted a distance $-\Delta x$, after which the two systems are superposed (fig. 6.7-1.b).

The function expressens for the two systems are:

$$G_1\{x,y\} = F\{x - \Delta x,\ y\} = n_1 \tag{6.7-2}$$

$$G_2\{x,y\} = F\{x + \Delta x,\ y\} = n_2 \tag{6.7-3}$$

If, now, curves are drawn through the points of intersection for the two contour-curve systems, in accordance with the parametric condition:

$$N = n_2 - n_1 \tag{6.7-4}$$

It will be seen that these curves are the contour curves for the derivatives of the contour function.

Inserting (6.7-2 and 6.7-3) in (6.7-4), we get

$$F\{x + \Delta x,\ y\} - F\{x - \Delta x,\ y\} = N$$

which can be written as follows after a expansion in Taylor-series for small values of Δx:

$$[F\{x,y\} + \Delta x \frac{\partial F}{\partial x}] - [F\{x,y\} - \Delta x \frac{\partial F}{\partial x}] \cong N$$

or

$$\boxed{\frac{\partial}{\partial x} F\{x,y\} \cong \frac{N}{2\,\Delta x}} \tag{6.7-5}$$

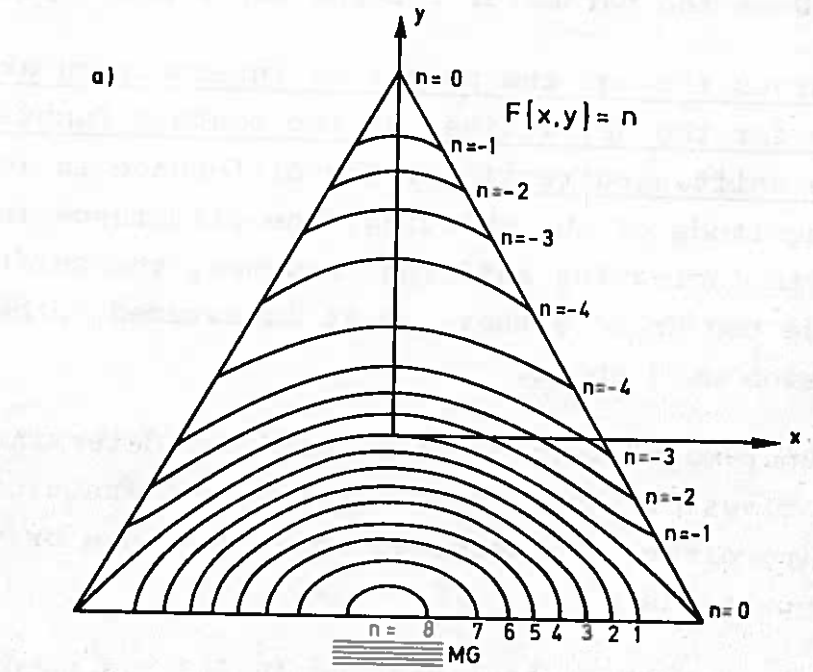
a)
y
x
n= 0
F(x,y)= n
n=-1
n=-2
n=-3
n=-4
n=-4
n=-3
n=-2
n=-1
n=0
n= 8 7 6 5 4 3 2 1
MG

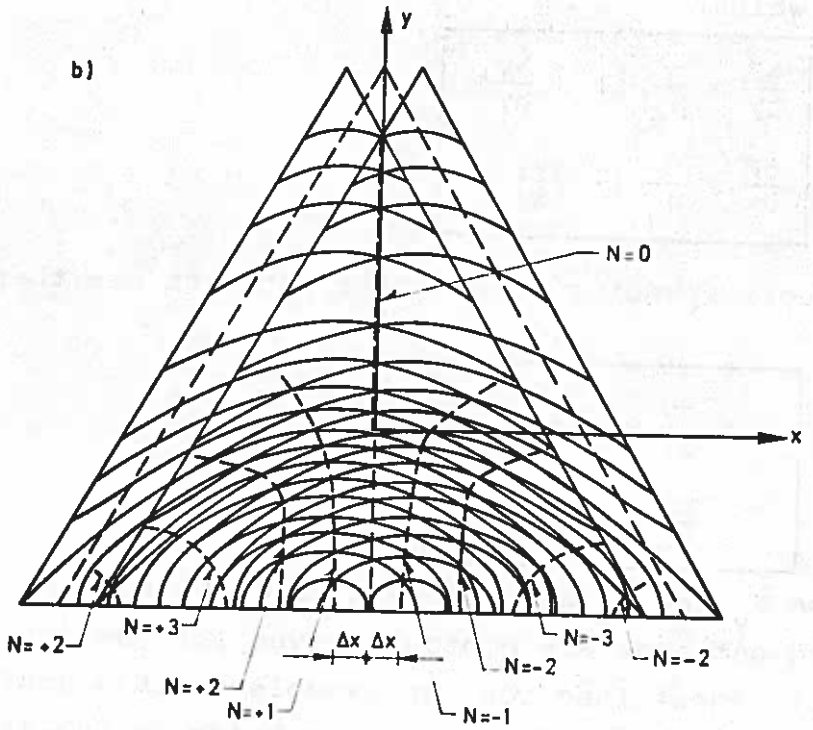
b)
y
x
N=0
N=+2
N=+3
N=+2
N=+1
Δx Δx
N=-1
N=-2
N=-3
N=-2

Figur 6.7-1

where N is the parameter for the super-moiré-pattern.

The curves through the points of intersection are thus contour curves for the derivatives of the contour function with respect to the shifting-directions. The difference in level depends on the magnitude of the shifting, the difference in level decreasing with increasing shifting. However, the shifting must not be made too great either, as it is assumed to be small in the expansion used above.

The super-moiré method can be used for determination of the derivatives of the grating displacement function by mutual shifting either two deformed model gratings or two "deformed" moiré-patterns.

When the deformed model grating (6.2-3) is used, we get

$$F\{x,y\} = \frac{1}{p_m} [y - v\{x,y\} - A_m]$$

from which

$$\frac{\partial F}{\partial y} = \frac{1}{p_m} [1 - \frac{\partial v}{\partial y}] \qquad (6.7\text{-}6)$$

$$\frac{\partial F}{\partial x} = \frac{1}{p_m} [- \frac{\partial v}{\partial x}] \qquad (6.7\text{-}7)$$

The corresponding super-moiré patterns are then contour curves for

$$1 - \frac{\partial v}{\partial y} \cong \frac{N_y}{2\,\Delta y} p_m \qquad (6.7\text{-}8)$$

$$\frac{\partial v}{\partial x} \cong \frac{N_x}{2\,\Delta x} p_m \qquad (6.7\text{-}9)$$

where N_y and N_x are integers. It will be seen that both super-moiré patterns are contour curves for the derivatives of the displacement function. An example of this application of the super-moiré method is given by Heise in [67-16], in which he uses it on Ligtenberg's reflection moiré-method.

The most recent contribution is that of Sciammarella and Chang [71-6], who have developed a method in which the grating shifting is effected optically. This method is also discussed in section 8.7.

When the super-moiré method is used on the "deformed" moiré-pattern, (6.6-1) yields

$$F\{x,y\} = \frac{1}{p_m} M\{x,y\}$$

and the super-moiré patterns become contour curves for (6.6-3 and 6.6-4):

$$\frac{\partial v}{\partial x} - \delta \sin\theta \cong \frac{N_x}{2\,\Delta y} p_m \qquad (6.7\text{-}10)$$

$$\frac{\partial v}{\partial y} - (1 - \delta \cos\theta) \cong \frac{N_y}{2\,\Delta y} p_m \qquad (6.7\text{-}11)$$

In other words, in this case, too, the super-moiré patterns are contour curves for the derivatives of the displacement function.

De Haas and Loof [66-7] were the first to use this method on reflection-moiré, and at the same time, they introduced the optical filtering technique (section 8.6.1) for filtering off the grating lines in the moiré pattern. During the shifting, these would otherwise result in the appearance of secondary moiré-fringes, which complicate interpretation of the super-moiré pattern. Since then, Beranek in particular [67-17],[68-13] and [68-14], has described applications of the super-moiré method for determination the curvature of plates by means of Ligtenberg's reflection-moiré method.

6.8 For How Great Displacements and Displacement Gradients is the Theory Valid ?

The analysis of the "deformed" moiré-pattern in chapter 6 is mainly based on two assumptions. Firstly, it must be possible to observe the moiré-pattern, and secondly, it must be determined by the parametric condition (4.2-4). The requirements to be made to the magnitudes of the displacement function and its derivatives in the x,y-directions can be determined by a comparison with the "undeformed" moiré-pattern. For this, the requirements are fulfilled if the relative pitch δ and the angle θ between the grating lines lie within the limiting curve shown in fig. 5.1-5.

The following analogous requirements can be formulated: The ratio δ^* between the pitch in the deformed model grating and the reference grating pitch p_r and the angle θ^* between the deformed model grating lines and reference grating lines shall fulfil, at every point of the "deformed" moiré-pattern, the same requirements as δ and θ in the "undeformed" moiré-pattern (fig. 5.1-5).

As the density of the moiré-pattern depends on the magnitudes of the derivatives of the displacement function and not on its absolute value, the requirements underlined above only define limits for the magnitudes of the derivatives. These limitations can be found by considering a homogeneously deformed model grating.

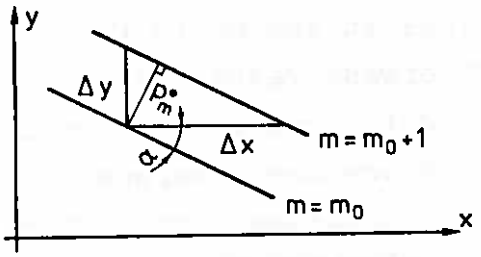

Homogeneously deformed model grating

Figure 6.8-1

Fig. 6.8-1 shows a pair of homogeneously deformed model grating lines characterized by the pitch p^*_m and the angle α. The parametric description of the model grating is given by (4.2-3):

$$y = v\{x,y\} + m\,p_m + A_m \qquad (6.8\text{-}1)$$

which, rewritten and differentiated, yields

$$\frac{\partial v}{\partial x} = -\frac{\partial m}{\partial x}\,p_m = -\frac{p_m}{\Delta x} \qquad (6.8\text{-}2)$$

and

$$\frac{\partial v}{\partial y} = 1 - \frac{\partial m}{\partial y}\,p_m = 1 - \frac{p_m}{\Delta y} \qquad (6.8\text{-}3)$$

where Δx and Δy are the interfringe spacings measured in the directions of the axes. Expressing these by p_m^* and α, and inserting them in (6.8-2 and 6.8-3), we get

$$\frac{\partial v}{\partial x} = - \frac{p_m}{p_m^*} \sin\alpha \qquad (6.8\text{-}4)$$

$$\frac{\partial v}{\partial y} = 1 - \frac{p_m}{p_m^*} \cos\alpha \qquad (6.8\text{-}5)$$

In order to take the angle θ^* into account in the expressions for the derivatives, it is necessary to differentiate between the various δ,θ-cases.

When $\underline{\delta = 1 \wedge \theta = 0}$, $\theta^* = \alpha$ and $p_m = p_r$, i.e.

$$\left.\begin{array}{l} \delta = 1 \\ \theta = 0 \end{array}\right\} \Rightarrow \left\{\begin{array}{l} \dfrac{\partial v}{\partial x} = - \dfrac{\sin\theta^*}{\delta^*} \\ \dfrac{\partial v}{\partial y} = 1 - \dfrac{\cos\theta^*}{\delta^*} \end{array}\right. \qquad \begin{array}{l} (6.8\text{-}6) \\ (6.8\text{-}7) \end{array}$$

where $\delta^* = \dfrac{p_m^*}{p_r}$.

Inserting in (6.8-6 and 6.8-7) the values for δ^* and θ^* corresponding to the limiting curve in fig. 5.1-5, we get the possible combinations of the two derivatives shown in fig. 6.8-2.

<u>If δ and θ can be varied</u> arbitrarily, it will not be the magnitudes of the derivatives that are limited, but their variation within the moiré-pattern, since, with $\alpha = \theta^* - \theta$, the general expressions corresponding to (6.8-6 and 6.8-7) are

$$\frac{\partial v}{\partial x} = - \frac{\delta}{\delta^*} \sin\{\theta^* - \theta\} \qquad (6.8\text{-}8)$$

$$\frac{\partial v}{\partial y} = 1 - \frac{\delta}{\delta^*} \cos\{\theta^* - \theta\} \qquad (6.8\text{-}9)$$

It will be seen that the two derivatives vary about the values $\delta \sin\theta$ and $1 - \delta \cos\theta$, while θ^* and δ^* vary in permissible combinations. The variations about these two values are of the same order of magnitude as the variation about (0,0) in fig. 6.8-2.

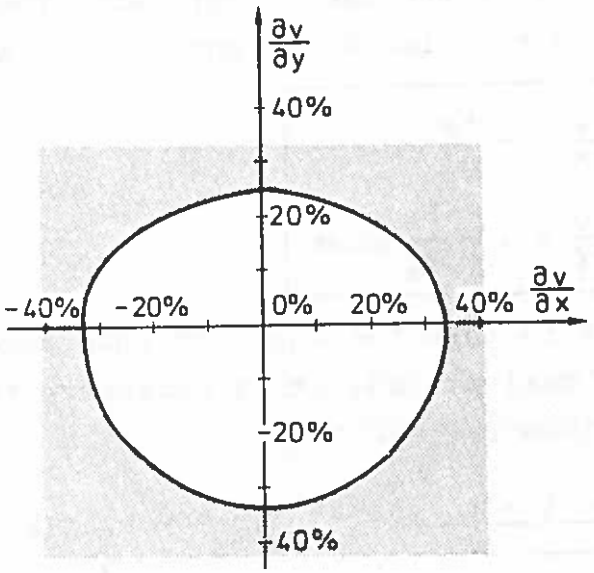

Limiting curve for possible combinations of $\frac{\partial v}{\partial x}$ and $\frac{\partial v}{\partial y}$ when $\delta = 1 \wedge \theta = 0$.

Figure 6.8-2

As will appear from the above, a displacement field in which the derivatives of the displacement function do not vary more than shown in fig. 6.8-2 can be determined using a moiré-pattern in agreement with the theory discussed in this chapter.

7. ACCURACY IN DETERMINATION OF DEFORMATION

One of the most important questions arising in connexion with a measuring method is that of determining its accuracy and resolving power. Nonetheless, in only a few of the papers on moiré-methods is this question touched upon. The main contributions on the subject are provided by Guild [56-1], page 100-144, Crisp [57-1], Dantu [58-1] and [66-8], Söderquist [66-10], Theocaris [69-1] and Durelli and Parks [70-1].

In the division applied here, i.e. into moiré pattern theory and moiré-method theory, the contributions to the error in the measurements fall into two groups, only one of which will be discussed here. The assumptions for the following are:

a) that there is a photographic copy of a moiré pattern,

b) that the error in connexion with the moiré-method theory (relationship between model grating displacement and deformation of specimen) is neglected,

c) that the error in the determination of the relative pitch (6.2-5) is insignificant,

d) that both the reference grating and the undeformed model grating are perfect line gratings,

e) that the parametric distribution of the moiré-lines is known (e.g. determined as specified in section 6.3).

However, assumption c) need not be rigorously fulfilled, since the "undeformed" model grating can be a line grating with a certain initial deformation. Nevertheless, this initial deformation must be determined before the real deformation occurs and be subtracted from the measured deformation. As regards assumption e), this need not be complied with when the "tangent method" is used.

On the basis of these assumptions, the measuring accuracy will now be calculated for determination of the grating displacement function and its derivative by means of the three methods: the tangent method, the surface slope and the super-moiré method.

7.1 Accuracy of Determination of Displacement

The determination of the variation of the displacement function within a moiré pattern is described in section 6.2, and the possibility is discussed of specifying, in certain cases, the absolute value of the displacement function. As this function varies from one method the another, we will here consider only the accuracy with which the relative variation of the displacement function can be determined.

The variation Δv is given by (6.2-1):

$$\Delta v = \Delta n\, p_m - \Delta y(\delta \cos\theta - 1) + \Delta x\, \delta \sin\theta \qquad (7.1\text{-}1)$$

and the absolute error $s\{\Delta v\}$ is then given by the law of accumulation of error:

$$s\{\Delta v\}^2 = [\frac{\partial v}{\partial n} s\{\Delta n\}]^2 + [\frac{\partial v}{\partial y} s\{\Delta y\}]^2 + [\frac{\partial v}{\partial x} s\{\Delta x\}]^2 + [\frac{\partial v}{\partial \theta} s\{\theta\}] \qquad (7.1\text{-}2)$$

$$\boxed{s\{\Delta v\}^2 = [p_m\, s\{\Delta n\}]^2 + [(\delta \cos\theta - 1)\, s\{\Delta y\}]^2 + [\delta \sin\theta\, s\{\Delta x\}]^2 + [(\Delta y\, \delta \sin\theta + \Delta x\, \delta \cos\theta) s\{\theta\}]^2} \qquad (7.1\text{-}3)$$

It will be seen that the first three terms are independent of the distance between the two points under consideration and can be regarded as constants for the pattern. The last term, on the other hand, depends on both the distance between the points and the direction, and will be seen to be equal to zero in the special case,

$$\frac{\Delta y}{\Delta x} = -\cot\theta$$

i.e. in the direction perpendicular to the referencegrating lines.

If the error in the parameter determination at a point can be regarded as independent of the fringe density, then $s\{n\}$ is constant, and the error in the determination of the variation

in the displacement will be seen to be minimum for $\theta = 0 \wedge \delta = 1$. Determination of the parameter n at a point is carried out by interpolating between two moiré-fringes and it is, therefore, assumed that it can be done with the same accuracy as determination of the fringe-centreline. This accuracy (cf. section 5.2) is normally 10% of the fringe spacing (1% when optical methods are used), so s{n} is put equal to 10%, which gives

$$s\{\Delta n\} = \sqrt{2}\, s\{n\} = 14\% \qquad (7.1\text{-}4)$$

The error s{Δv} in the determination of the difference in displacement is therefore, at minimum,

$$\boxed{s\{\Delta v\} = 0{,}14\, p_m} \qquad (7.1\text{-}5)$$

and increases if $\theta \neq 0$ and $\delta \neq 1$ are used.

7.2 Accuracy in the Tangent Method

This method is described in section 6.3, and the following relation (6.2-3 and 6.2-4) are shown to be valid at points on the moiré-curves at which there are tangents parallel to the coordinate-axes:

$$\frac{dy}{dx} = 0 \Rightarrow \frac{\delta v}{\delta x} = \delta \sin\theta \qquad (7.2\text{-}1)$$

$$\frac{dx}{dy} = 0 \Rightarrow \frac{\delta v}{\delta y} = 1 - \delta \cos\theta \qquad (7.2\text{-}2)$$

The error in this connexion depends on the extent to which it can be decided whether the tangent to the moiré-curve is parallel to an axis (φ-error) and on error on the determination of the angle θ (θ-error).

φ-error can be determined from (6.3-2) in that, for tangents that are not parallel to the axes, we have

$$\boxed{\frac{\delta v}{\delta x} = \delta \sin\theta - \frac{dy}{dx}\left[\frac{\delta v}{\delta y} + \delta \cos\theta - 1\right]} \qquad (7.2\text{-}3)$$

$$\boxed{\frac{\delta v}{\delta y} = 1 - \delta \cos\theta - \frac{dx}{dy}\left[\frac{\delta v}{\delta x} - \delta \sin\theta\right]} \qquad (7.2\text{-}4)$$

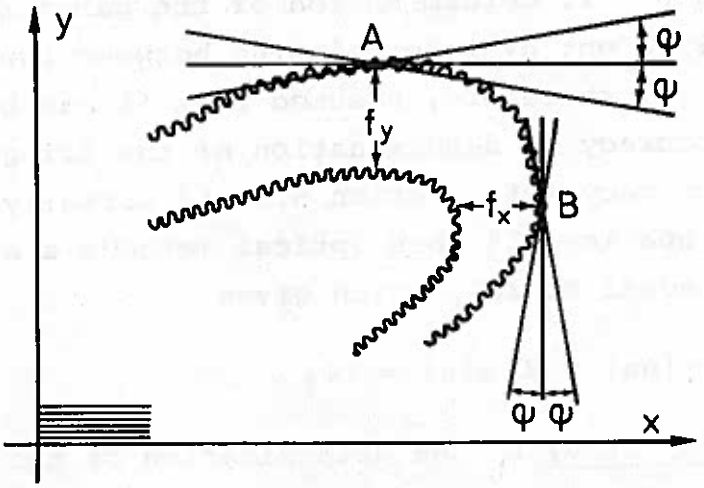

Figure 7.2-1

A comparison with (7.2-1 and 7.2-2) will show that the last term in (7.2-3 and 7.2-4) expresses the φ-errors if the derivatives are determined from (7.2-1 and 7.2-2) in the points where tha tangents are not parallel to the axes. In other words,

$$\varphi\text{-error on } \frac{\partial v}{\partial x} : -\frac{dy}{dx}\left[\frac{\partial v}{\partial y} + \delta\cos\theta - 1\right] \qquad (7.2\text{-}5)$$

$$\varphi\text{-error on } \frac{\partial v}{\partial y} : -\frac{dx}{dy}\left[\frac{\partial v}{\partial x} - \delta\sin\theta\right] \qquad (7.2\text{-}6)$$

If the tangent slopes can be determined to be parallel to the coordinate axes with the error $\varphi << 1$

$$\frac{dy}{dx} = 0 \pm s\{\tan\varphi\} \simeq \pm s\{\varphi\} \qquad (7.2\text{-}7)$$

$$\frac{dx}{dy} = 0 \pm s\{\tan\varphi\} \simeq \pm s\{\varphi\} \qquad (7.2\text{-}8)$$

In the following the angle φ is assumed to be of order of magnitude 2^o, i.e.

$$s\{\varphi\} = 2^o \simeq 0.04 \text{ radians} \qquad (7.2\text{-}9)$$

The variation in the φ-errors on $\frac{\partial v}{\partial x}$ and $\frac{\partial v}{\partial y}$ are shown in fig. 7.2-2 and 7.2-3.

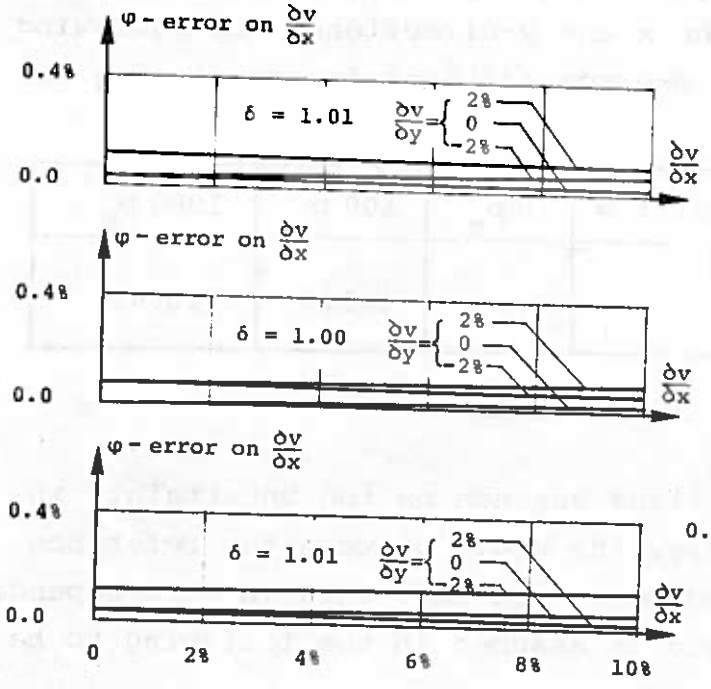

Figure 7.2-2

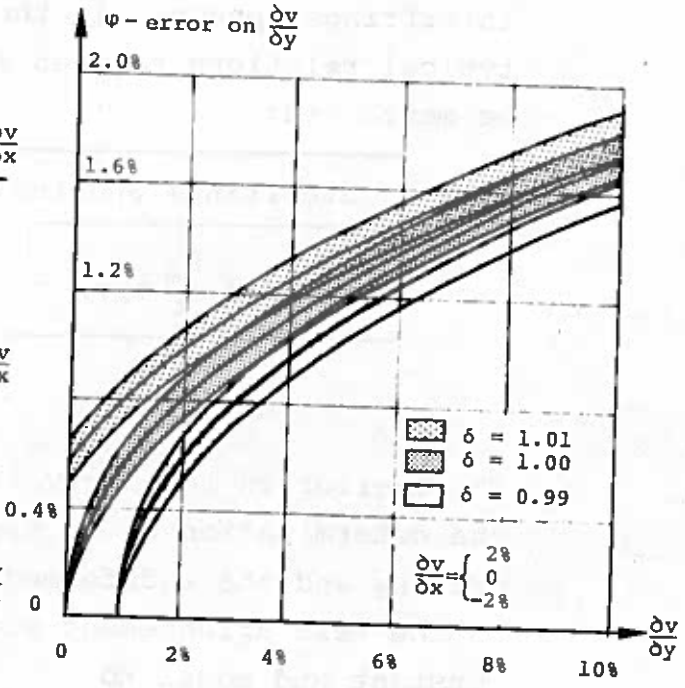

Figure 7.2-3

The φ-error can also be determined directly by measurement on the moiré-pattern, the expressions in the square brackets in (7.2-5 and 7.2-6) being approximated by means of (6.2-2 and 6.2-3) by:

$$\left|\frac{\partial v}{\partial y} + \delta\cos\theta - 1\right| \simeq \left|\frac{\Delta v}{\Delta y} + \delta\cos\theta - 1\right| = \left|\frac{\Delta n}{\Delta y}\right| p_m = \frac{p_m}{f_y} \qquad (7.2\text{-}10)$$

$$\left|\frac{\partial v}{\partial x} - \delta\sin\theta\right| \simeq \left|\frac{\Delta v}{\Delta y} - \delta\sin\theta\right| = \left|\frac{\Delta n}{\Delta x}\right| p_m = \frac{p_m}{f_x} \qquad (7.2\text{-}11)$$

where f_y and f_x are the local interfringe spacings measured in the x and y-directions (cf. fig. 7.2-1). The absolute error can thus also be written as

$$\varphi\text{-error on } \frac{\partial v}{\partial x} : \frac{p_m}{f_y} s\{\varphi\} \qquad (7.2\text{-}12)$$

$$\varphi\text{-error on } \frac{\partial v}{\partial y} : \frac{p_m}{f_x} s\{\varphi\} \qquad (7.2\text{-}13)$$

The φ-errors can thus be determined directly by measuring the interfringe spacings in the x and y-directions. The following typical relations between φ-error and interfringe spacing can be mentioned:

Interfringe Spacing: f =	10 p_m	100 p_m	1000 p_m
φ-error: $\frac{p_m}{f} s\{\varphi\}$ =	0,4%	0,04%	0,004%

Table 7.2-1

The θ-error on the derivatives depends on the uncertainty in the determination of θ, i.e. the angle between the reference grating and the undeformed model grating. This in turn depends on the test arrangement and is assumed in the following to be constant and equal to

$$s\{\theta\} = \frac{1^o}{2} \simeq 0.01 \text{ radian} \qquad (7.2\text{-}14)$$

The absolute θ-error is then obtained from (7.2-1 and 7.2-2):

$$\theta\text{-error on } \frac{\partial v}{\partial x} = \left|\frac{\partial}{\partial \theta}\left\{\frac{\partial v}{\partial x}\right\}\right| s\{\theta\} = \delta \cos\theta \, s\{\theta\} \qquad (7.2\text{-}15)$$

$$\theta\text{-error on } \frac{\partial v}{\partial x} = \left|\frac{\partial}{\partial \theta}\left\{\frac{\partial v}{\partial y}\right\}\right| s\{\theta\} = \delta \left|\sin\theta\right| s\{\theta\} \qquad (7.2\text{-}16)$$

These are depicted in fig. 7.2-4 and 7.2-5.

In accordance with the law of accumulation of error, the total error in the tangent method is:

$$\text{Total error} = \sqrt{(\varphi\text{-error})^2 + (\theta\text{-error})^2}$$

These are shown in fig. 7.2-6 and 7.2-7 for various values of δ and $\frac{\partial v}{\partial x}$ and $\frac{\partial v}{\partial y}$.

With the assumptions made regarding the errors on the tangent slope φ (7.2-9) and the angle θ (7.2-14), it will be seen that the errors are generally too high in relation to the 10% relative error normally considered an acceptable accuracy for a measuring method.

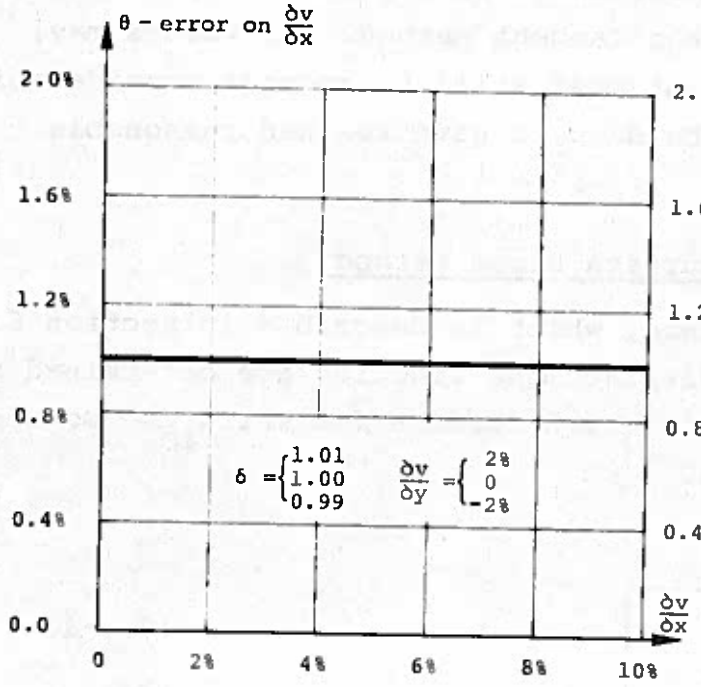

Figure 7.2-4

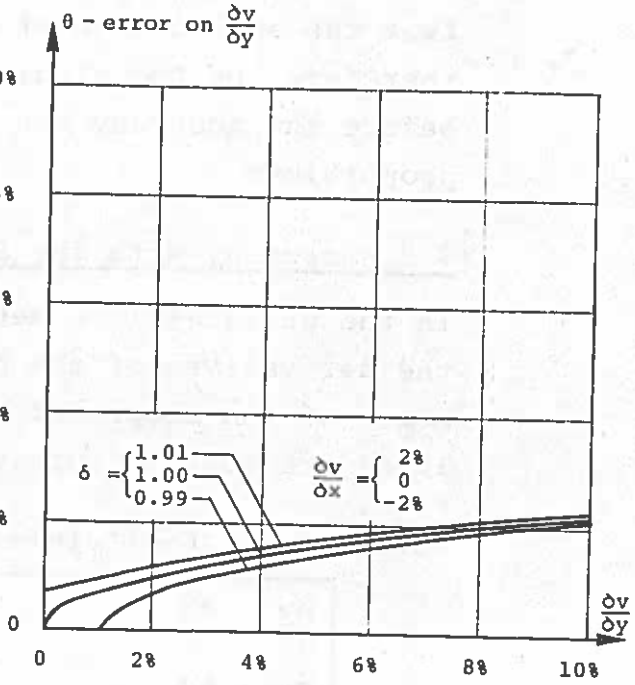

Figure 7.2-5

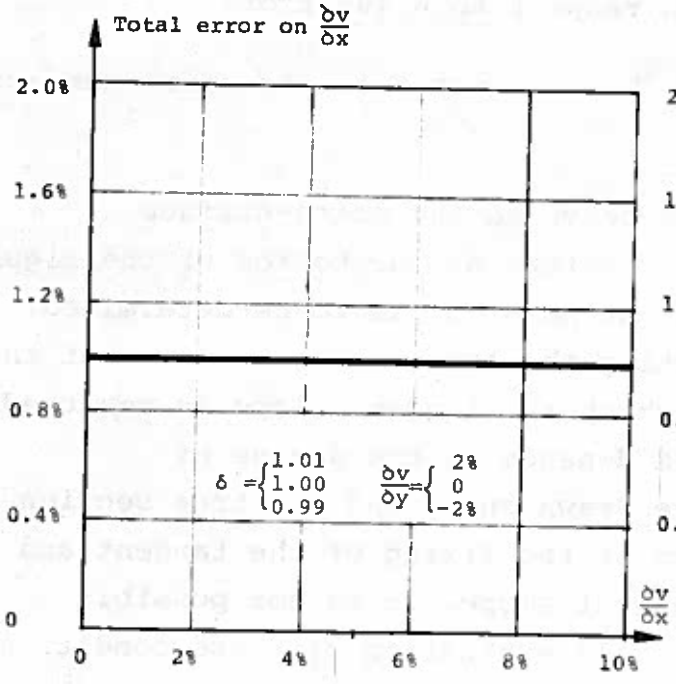

Figure 7.2-6

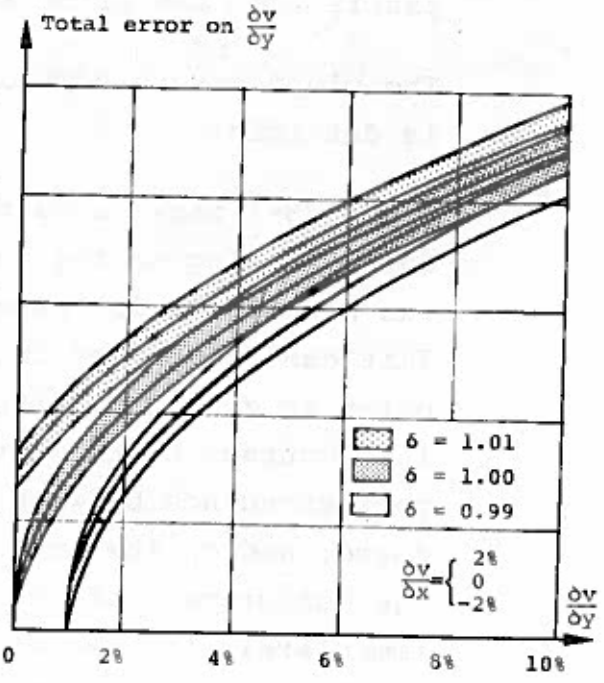

Figure 7.2-7

The orders of magnitude is s{φ} and s{θ} are fixed on a rough estimate, which is not based on any great experience from the application of the tangent method. The values may, therefore, be too high, but must still be reduced considerably before the accuracy can be said to have reached reasonable proportions.

7.3 Accuracy with the Surface-Slope Method

In the surface-slope method, which is described in section 6.6, the derivatives of the displacement function are determined by means of the slopes of the moiré-surface for which the moiré-lines are contour curves.

(6.6-3 and 6.6-4) yield:

$$\frac{\partial v}{\partial x} = \frac{\partial M}{\partial x} + \delta \sin\theta \qquad (7.3\text{-}1)$$

$$\frac{\partial v}{\partial y} = \frac{\partial M}{\partial y} + 1 - \delta \cos\theta \qquad (7.3\text{-}2)$$

where M{x,y} is the equation of the moiré-surface.

The uncertainty in this method consists partly of the error in the determination of the surface slopes (slope-error) and partly from the error with respect to θ (θ-error).

The slope errors depend on how the slope of the moiré-surface is determined.

Fig. 7.3-1 shows a section curve to the moiré-surface corresponding to the moiré-pattern at the bottom of the figure. The slope $\frac{\partial M}{\partial y}$, for example at point B, is to be determined. This can be done by inserting the tangent to the curve at the point in question, after which the tangent slope is measured. The accuracy of the method depends on the degree of correspondence between the drawn curve and the true section curve, and on the accuracy of the fixing of the tangent and the measurement of the tangent slope. It is not possible immediately to give an overall evaluation of these conditions if there is no analytical expression of the section curve with which the results of the measurements can be compared.

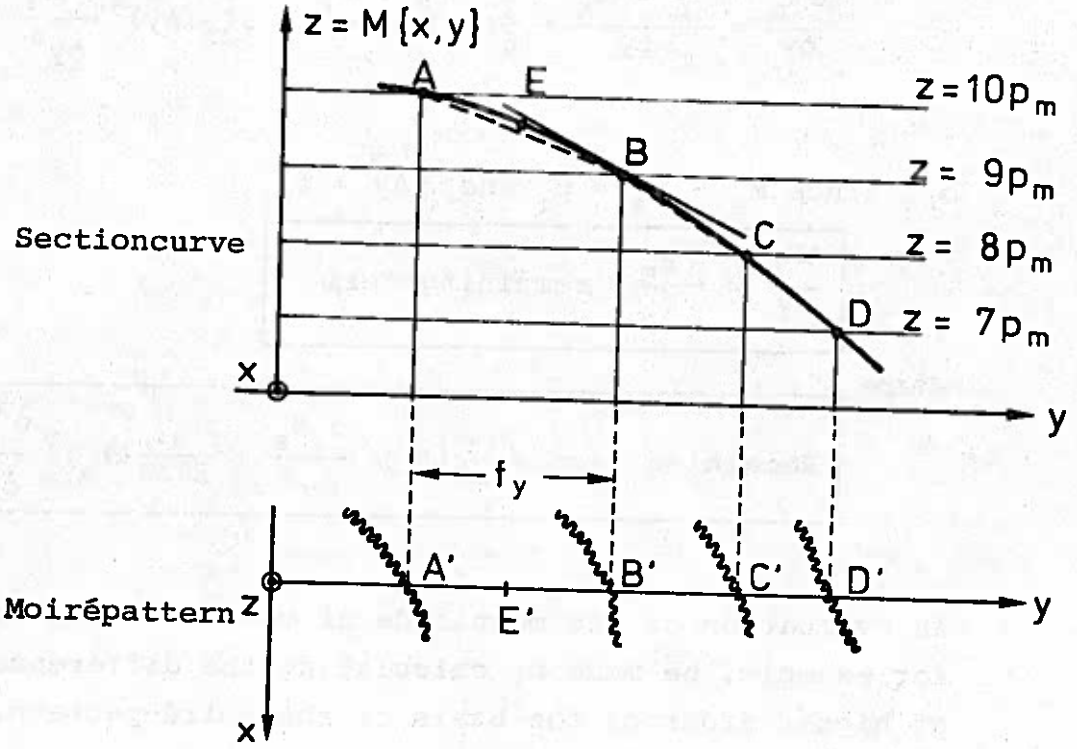

Figure 7.3-1

However, there is no doubt that the accuracy is greater than in the approximation method to follow.

The approximation lies in the assumption that the tangent slope at a point (E) halfway between two moiré-line points (A and B) is equal to the slope to be secant AB, i.e.

$$\left|\frac{\partial M}{\partial y}\right|_E \simeq \left|\frac{\Delta M}{\Delta y}\right| = \frac{p_m}{f_y} \qquad (7.3\text{-}3)$$

The error in this approximation can be evaluated on the basis of a Taylor expansion of the surface function M{x,y}. If we put A'E' = E'B' = Δy, then

$$M_E = M\{x,y\}$$

$$M_A = M\{x, y-\Delta y\} = M_E - \Delta y \frac{\partial M_E}{\partial y} + \frac{1}{2}(\Delta y)^2 \frac{\partial^2 M_E}{\partial y^2} - \frac{1}{6}(\Delta y)^3 \frac{\partial^3 M_E}{\partial y^3} + \ldots.$$

$$M_B = M\{x, y+\Delta y\} = M_E + \Delta y \frac{\partial M_E}{\partial y} + \frac{1}{2}(\Delta y)^2 \frac{\partial^2 M_E}{\partial y^2} + \frac{1}{6}(\Delta y)^3 \frac{\partial^2 M_E}{\partial y^3} + \ldots.$$

which yields

$$\frac{\partial M_E}{\partial y} = \frac{M_B - M_A}{2\,\Delta y} + \frac{1}{6}(\Delta y)^2 \frac{\partial^3 M_E}{\partial y^3} + \frac{1}{120}(\Delta y)^4 \frac{\partial^5 M_E}{\partial y^5} + \ldots. \tag{7.3-4}$$

or, since $M_B - M_A = p_m$ and $2\,\Delta y = f_y$,

$$\boxed{\frac{\partial M_E}{\partial y} = -\frac{p_m}{f_y} + \text{remaining term}} \tag{7.3-5}$$

where

$$\boxed{\text{Remaining term} = \frac{1}{24}(f_y)^2 \frac{\partial^3 M_E}{\partial y^3} + \frac{1}{1920}(f_y)^5 \frac{\partial^5 M_E}{\partial y^5} + \ldots.} \tag{7.3-6}$$

An evaluation of the magnitude of the remaining term can, for example, be made by calculating the difference quotients of higher order on the basis of the moiré-pattern.

As an example, consider fig. 7.3-2, where the difference quotient of third order for the length BC can be proved to be

$$\boxed{\begin{aligned}\frac{\partial^3 M}{\partial y^3} \simeq \frac{\Delta^3 M}{\Delta y^3} &= \frac{p_m}{(f_y)^3} \frac{\dfrac{1-\alpha_1}{\alpha_1(1+\alpha_1)} + \dfrac{1-\alpha_2}{\alpha_2(1+\alpha_2)}}{1+\alpha_1+\alpha_2} \\ &= \frac{p_m}{(f_y)^3} S\{\alpha_1,\alpha_2\}\end{aligned}} \tag{7.3-7}$$

The first term in the remaining term (7.3-6) is thus

$$\frac{1}{24}\frac{p_m}{f_y} S\{\alpha_1,\alpha_2\} \tag{7.3-8}$$

and the factor $S\{\alpha_1,\alpha_2\}$ takes the values given in table 7.3-1.

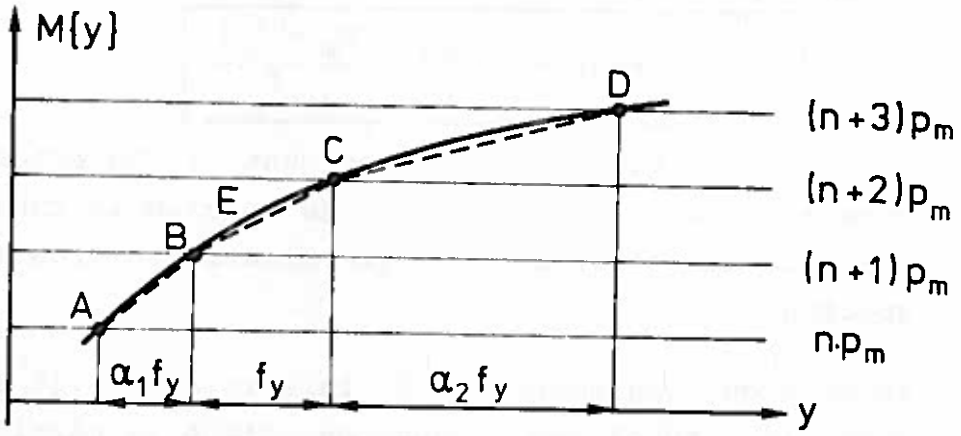

Figure 7.3-2

α_2 \ α_1	0,5	0,8	1,0	1,2	1,5	2,0	3,0
0,5	0,67	0,35	0,27	0,22	0,18	0,17	0,13
0,8	0,35	0,06	0,05	0,02	0,00	-0,01	-0,01
1,0	0,27	0,05	0,00	-0,03	-0,04	-0,04	-0,03
1,2	0,22	0,02	-0,03	-0,04	-0,06	-0,06	-0,05
1,5	0,18	0,00	-0,04	-0,06	-0,07	-0,07	-0,06
2,0	0,17	-0,01	-0,04	-0,06	-0,07	-0,07	-0,06
3,0	0,13	-0,01	-0,03	-0,05	-0,06	-0,06	-0,05

The factor $S\{\alpha_1,\alpha_2\}$ (7.3-7)

Table 7.3-1

If the adjacent interfringe spacing $\alpha_1 f_y$ and $\alpha_2 f_y$ is greater than half the interfringe spacing on the measuring length BC, the first term in the remaining term will not exceed 3% of the approximated value (7.3-3).

The slope-error can thus largely be put equal to the uncertainty in the determination of the difference quotient

of the first order, and can be written:

$$\text{Slope-error} = s\{\frac{p_m}{f_y}\} = \frac{p_m}{f_y}\frac{s\{f_y\}}{f_y} \qquad (7.3\text{-}9)$$

The relative slope-error on account of the error on the determination of the interfringe spacing is thus equal to the relative error on the determination of the interfringe spacing.

As mentioned in section 5.2, this is about 14% if the determination of the fringe-centreline is carried out with the naked eye, but is reduced to about 2% if it is done by means of a photocell, i.e.

$$\text{Relative slope-error on } \frac{\delta M}{\delta y} : 2\% - 14\% \qquad (7.3\text{-}10)$$

The θ-error in the surface slope method will be seen, from a comparison of (7.2-1 and 7.2-2) and (7.3-1 and 7.3-2), to be the same (7.2-15 and 7.2-16) as in the tangent method. Thus,

$$\theta\text{-error on } \frac{\delta v}{\delta x} = \delta \cos\theta \, s\{\theta\} \qquad (7.3\text{-}11)$$

$$\theta\text{-error on } \frac{\delta v}{\delta y} = \delta \left|\sin\theta\right| s\{\theta\} \qquad (7.3\text{-}12)$$

However, unlike the tangent method, it is possible in certain cases with the surface-slope method to reduce the magnitude of these uncertainties considerably. The cases in question are those in which, prior to deformation, an undeformed moiré-pattern is formed, with the same θ and δ as the deformed moiré-pattern. The fact is that in these cases, $\delta \sin\theta$ and $1 - \delta \cos\theta$ are equal to the slopes in the x- and y-directions to the moiré-surface corresponding to the undeformed state. As this surface is plane, the slopes can be determined as the mean value over several interfringe spacings. Measuring over n interfringe spacings, we find the relative error, analogously with (7.3-9), to be

$$\frac{1}{n} \cdot \frac{s\{f\}}{f} \qquad (7.3\text{-}13)$$

If, for example, n = 20, the relative θ-errors (cf. 7.3-10) will be of the order or magnitude of 0.1% to 0.7%.

If the above-mentioned prodecure cannot be used, the absolute θ-error with s{θ} = 1% (7.2-14) will be

$$\boxed{\begin{aligned} &\theta\text{-error on } \frac{\delta v}{\delta x} \simeq 1\% \\ &\theta\text{-error on } \frac{\delta v}{\delta y} = \begin{cases} < 0.04\% & \text{for } |\theta| < 2^{o} \\ < 0.1\% & \text{for } |\theta| < 5^{o} \\ < 0.2\% & \text{for } |\theta| < 10^{o} \end{cases} \end{aligned}} \qquad (7.3\text{-}15)$$

Thus, the method generally gives a considerable error for $\frac{\delta v}{\delta x}$, while in the case of $\frac{\delta v}{\delta y}$, it can be kept down by using θ = 0.

In some methods, an attempt is made to eliminate the uncertainty on $\frac{\delta v}{\delta x}$ by measuring other quantities, which, in the special cases, give the possibility of calculating $\frac{\delta v}{\delta x}$. (See, e.g. Post [65-5] and Chiang [70-11]). However, as an exception, the "double-exposure technique" can be mentioned in cases in which there is no rotation of the reference grating. In that case, the error on θ can be made equal to zero, and there will then be no θ-error on $\frac{\delta v}{\delta x}$.

For cases in which the θ-errors can be eliminated, it will be seen that the uncertainty of the surface-slope method is equal to the slope-error (7.3-9). The optimum result obtainable is thus

$$\boxed{\text{relative uncertainty} = 2\%} \qquad (7.3\text{-}16)$$

when a photocell is used for determination of the fringe-centreline and when δ is chosen such that $\frac{\delta M}{\delta y}$ and 1 - δ have the same sign.

7.4 Accuracy in Super-Moiré Method

The super-moiré method is described in section 6.7, and for the cases in which the "deformed" moiré-patterns are shifted,

the following applies:

$$\frac{\delta v}{\delta x} \cong \frac{N_x p_m}{2 \Delta x} + \delta \sin\theta \qquad (7.4\text{-}1)$$

$$\frac{\delta v}{\delta y} \cong \frac{N_y p_m}{2 \Delta y} + 1 - \delta \cos\theta \qquad (7.4\text{-}2)$$

These expressions are entirely analogous to (7.3-1 and 7.3-2), due, in reality, to the fact that the differentiation process is the same.

The approximation (7.3-3) is analogous to (6.7-5), and the error in the latter can be investigated in the same way as in section 7.3. If the θ-error is optimized with $\theta = 0$, the error in the super-moiré method originates from the error on the displacements $2\Delta x$ and $2\Delta y$. If this is estimated to be of the relative magnitude of 1%, we get, analogously to (7.3-9) and 7.3-16), a

$$\text{relative error} = 1\% \qquad (7.4\text{-}3)$$

assuming, here too, that $\frac{N_y}{\Delta y}$ and $1 - \delta$ have the same sign.

If, for example, n = 20, the relative θ-errors (cf. 7.3-10) will be of the order or magnitude of 0.1% to 0.7%.

If the above-mentioned prodecure cannot be used, the absolute θ-error with s{θ} = 1% (7.2-14) will be

$$\boxed{\begin{aligned} &\theta\text{-error on } \frac{\partial v}{\partial x} \simeq 1\% \\ &\theta\text{-error on } \frac{\partial v}{\partial y} = \begin{cases} < 0.04\% & \text{for } |\theta| < 2^{o} \\ < 0.1\% & \text{for } |\theta| < 5^{o} \\ < 0.2\% & \text{for } |\theta| < 10^{o} \end{cases} \end{aligned}} \qquad (7.3\text{-}15)$$

Thus, the method generally gives a considerable error for $\frac{\partial v}{\partial x}$, while in the case of $\frac{\partial v}{\partial y}$, it can be kept down by using θ = 0.

In some methods, an attempt is made to eliminate the uncertainty on $\frac{\partial v}{\partial x}$ by measuring other quantities, which, in the special cases, give the possibility of calculating $\frac{\partial v}{\partial x}$. (See, e.g. Post [65-5] and Chiang [70-11]). However, as an exception, the "double-exposure technique" can be mentioned in cases in which there is no rotation of the reference grating. In that case, the error on θ can be made equal to zero, and there will then be no θ-error on $\frac{\partial v}{\partial x}$.

For cases in which the θ-errors can be eliminated, it will be seen that the uncertainty of the surface-slope method is equal to the slope-error (7.3-9). The optimum result obtainable is thus

$$\boxed{\text{relative uncertainty} = 2\%} \qquad (7.3\text{-}16)$$

when a photocell is used for determination of the fringe-centreline and when δ is chosen such that $\frac{\partial M}{\partial y}$ and 1 - δ have the same sign.

7.4 Accuracy in Super-Moiré Method

The super-moiré method is described in section 6.7, and for the cases in which the "deformed" moiré-patterns are shifted,

the following applies:

$$\frac{\partial v}{\partial x} \cong \frac{N_x p_m}{2\Delta x} + \delta \sin\theta \qquad (7.4\text{-}1)$$

$$\frac{\partial v}{\partial y} \cong \frac{N_y p_m}{2\Delta y} + 1 - \delta \cos\theta \qquad (7.4\text{-}2)$$

These expressions are entirely analogous to (7.3-1 and 7.3-2), due, in reality, to the fact that the differentiation process is the same.

The approximation (7.3-3) is analogous to (6.7-5), and the error in the latter can be investigated in the same way as in section 7.3. If the θ-error is optimized with $\theta = 0$, the error in the super-moiré method originates from the error on the displacements $2\Delta x$ and $2\Delta y$. If this is estimated to be of the relative magnitude of 1%, we get, analogously to (7.3-9) and 7.3-16), a

$$\text{relative error} = 1\% \qquad (7.4\text{-}3)$$

assuming, here too, that $\frac{N_y}{\Delta y}$ and $1 - \delta$ have the same sign.

8. OPTICAL METHODS IN MOIRÉ-PATTERN ANALYSIS

The analysis of the moiré-pattern in the previous chapters has been based on the geometry of the moiré-lines without taking into consideration the variation in light intensity between these.

When this factor is taken into account, further information can be extracted from a moiré-pattern, and it was investigations of this by Sciammarella, Ross and Sturgeon [65-2] that started the development that has so far led to the concepts interpolation, optical filtering and optical multiplication of moiré-patterns. Guild was really the first to undertake the theoretical derivation of the interference between two crossed diffraction gratings in his book [56-1], but an actual utilization of the theory for deformation measurements does not seem to have occurred before [65-2].

The theory on which the explanation of the concepts mentioned is based is grounded in physical optics, which differs from geometrical optics mainly in the fact that it takes into consideration the wave-nature of light. In the following, theoretical derivations are omitted for the sake of clearness. Instead, the theoretical treatment is given in Appendix B.

8.1 The Optical Arrangement

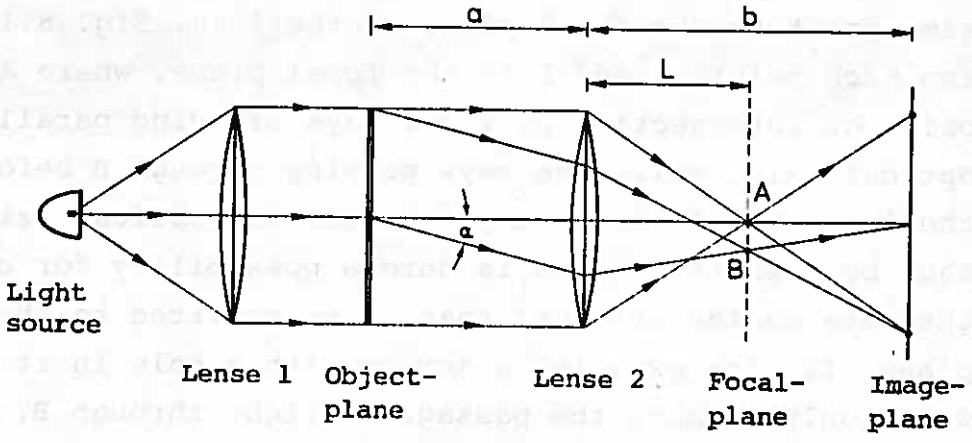

The Optical Arrangement

Figure 8.1-1

The principle of the optical arrangement, which all the methods to be described here can make use of, appears from fig. 8.1-1. A monochromatic, point light source is placed at the focal point of a converging lens (1), which changes the radiation of the light to a parallel beam. A photographic negative with the moiré-pattern is placed at right-angles to the direction of radiation of this beam. Part of the light will pass through the negative and will be collected by the second converging lens (2) on the image plane, where it will form a picture of the moiré-pattern, which is only a partially true copy of the original.

If all the light emitted by the original moiré-pattern passed lens (2) and continued unimpeded towards the image plane, the picture would be a true copy of the original. However, the light from the original is emitted in all directions, and part of it therefore fails to pass through lens (2). Furthermore, various types of apertures may be placed between the lens (2) and the image plane, which further limit the quantity of light reaching the image plane. As shown in Appendix B, it is possible, under certain idealized assumptions, to specify which parts of the light from the original reach the image plane.

We know from geometrical optics that parallel light rays passing through a converging lens intersect each other at the same point in the focal plane of the lens. Fig. 8.1-1 shows two such points A and B in the focal plane, where A is the point of intersection of light rays arriving parallel to the optical axis, while the rays passing through B before reaching the lens (2), form the angle α with the optical axis. It will thus be seen that there is here a possibility for controlling the data on the original that is transmitted to the image plane. If, for example, a screen with a hole in it (a filter), which only permits the passage of light through B, is placed in the focal plane, only the part of the light from the original that is emitted in the direction α will reach the image plane.

It has proved possible to calculate by means of Fourier analysis the information on the original picture contained in light rays in the direction α. This will be discussed in brief in the following, where we will study the distribution of light intensity on the focal plane. This distribution is also known as the diffraction pattern.

8.2 The Diffraction Pattern of a Line Grating and the Optical Filtering of its Image

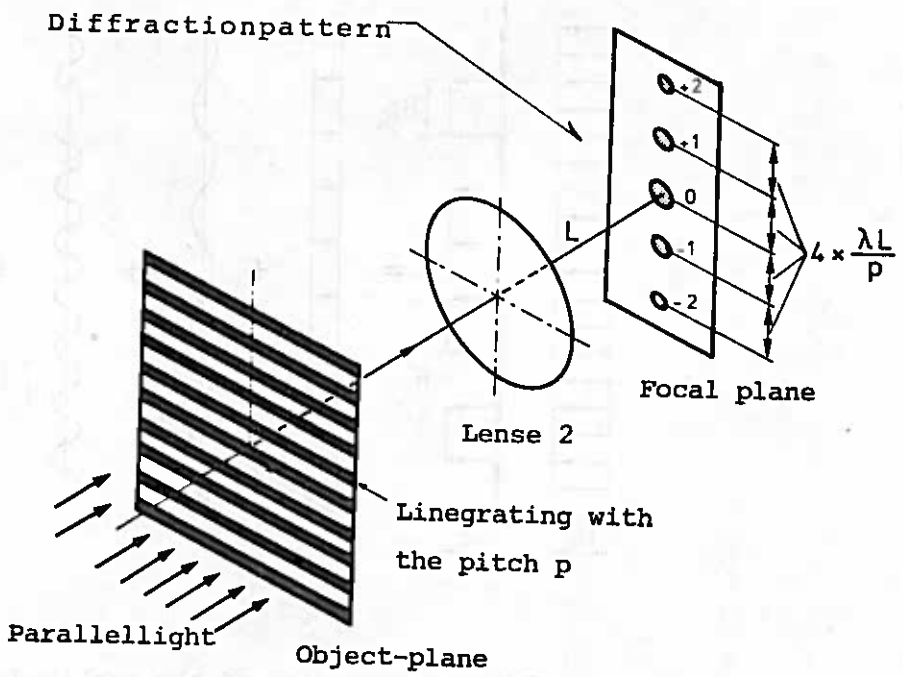

Diffraction Pattern for a Line Grating

Figure 8.2-1

If a transmission line grating with the pitch p is placed in the object plane in fig. 8.2-1, a number of dots will be formed on a screen in the focal plane, as shown in fig. 8.2-1. These dots lie on a line perpendicular to the direction of the grating lines and are symmetrical about the optical axis. The central dot is denoted the diffraction order zero, and its two adjacent diffraction orders +1 and -1, etc., their spacing being as shown in the figure.

The relationship between the diffraction orders and the distribution of the light intensity in the object plane proves to be as follows.

The light intensity I at a point is proportional to the square U^2 on the light-wave amplitude U at the point (cf. Appendix B). Fig. 8.2-2 shows (a) the arriving plane light-wave with constant amplitude U_o, which distributes itself (b) as a step function after passing the grating.

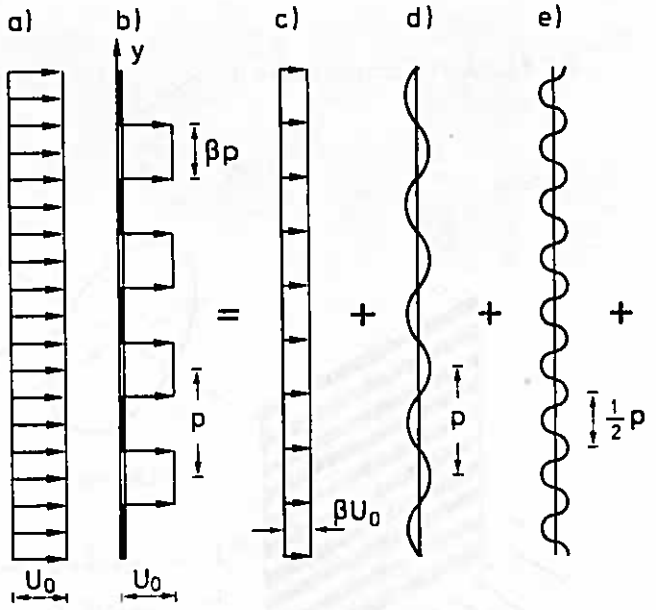

Fourier Expansion of the Amplitude

Figure 8.2-2

This can be expanded by Fourier analysis (cf. Appendix B (4.1)), as

$$U = U_o\, g\{x,y\} = U_o\, \beta\, [1 + c_1 \cos\{\frac{2\pi}{p} y\} + c_2 \cos\{2\,\frac{2\pi}{p} y\} + ..] \qquad (8.2\text{-}1)$$

where

$$c_n = 2\,\frac{\sin\{n\pi\beta\}}{n\pi\beta} \qquad (8.2\text{-}2)$$

The contribution of the first three terms is shown in fig. 8.2-2, c, d and e. g{x,y} denotes the grating transmission function and expresses the ratio between departing and arriving amplitude.

Each term in this expansion can be said to have a unique connexion with the individual diffraction orders as follows: a light-wave from the object plane with an amplitude distribution as the first term U_o in (8.2-1) wil give a distribution of light intensity in the focal plane equal to the central diffraction order of the line grating, while an amplitude distribution equal to the second term will give two dots equal to No. +1 and No. -1, and the third term, two dots equal to No. +2 and No. -2 etc.

This relationship can also be expressed by means of the complex expansion in series of the transmission function. Applying Euler's formula,

$$\cos\alpha = \frac{1}{2}[e^{i\alpha} + e^{-i\alpha}] = \frac{1}{2}[\exp\{i\alpha\} + \exp\{-i\alpha\}]$$

(8.2-1) can also be written

$$U = \frac{1}{2} U_o \beta \sum_{N=-\infty}^{N=\infty} c_N \exp\{iN\frac{2\pi}{p}y\} \qquad (8.2\text{-}3)$$

where $c_N = c_{-N} = c_{|N|}$.

The relationship can then be expressed by the fact that the Nth diffraction order originates from the Nth term in (8.2-3).

Or: A complex amplitude distribution on $\exp\{iN\frac{2\pi}{p}y\}$ gives rise to a diffraction dot at the distance $N\frac{\lambda L}{p}$ from the optical axis.

The diffraction pattern thus provides the possibility of selecting suitable terms in the expansion (8.2-3) in such a way that only a part of the terms contributes to the formation of the picture of the line grating. This is designated OPTICAL FILTERING, examples of which are shown in fig. 8.2-3. Here, a magnification of 1:1 is assumed, which is obtained by placing the object plane and the focal plane in fig. 8.1-1 in such a way that the distances a = b = 2L, where L is the focal length of lens 2. Fig. 8.2-3, left, shows an area of the line grating in the object plane, while on the right, it shows the area on the image plane on which it is reproduced.

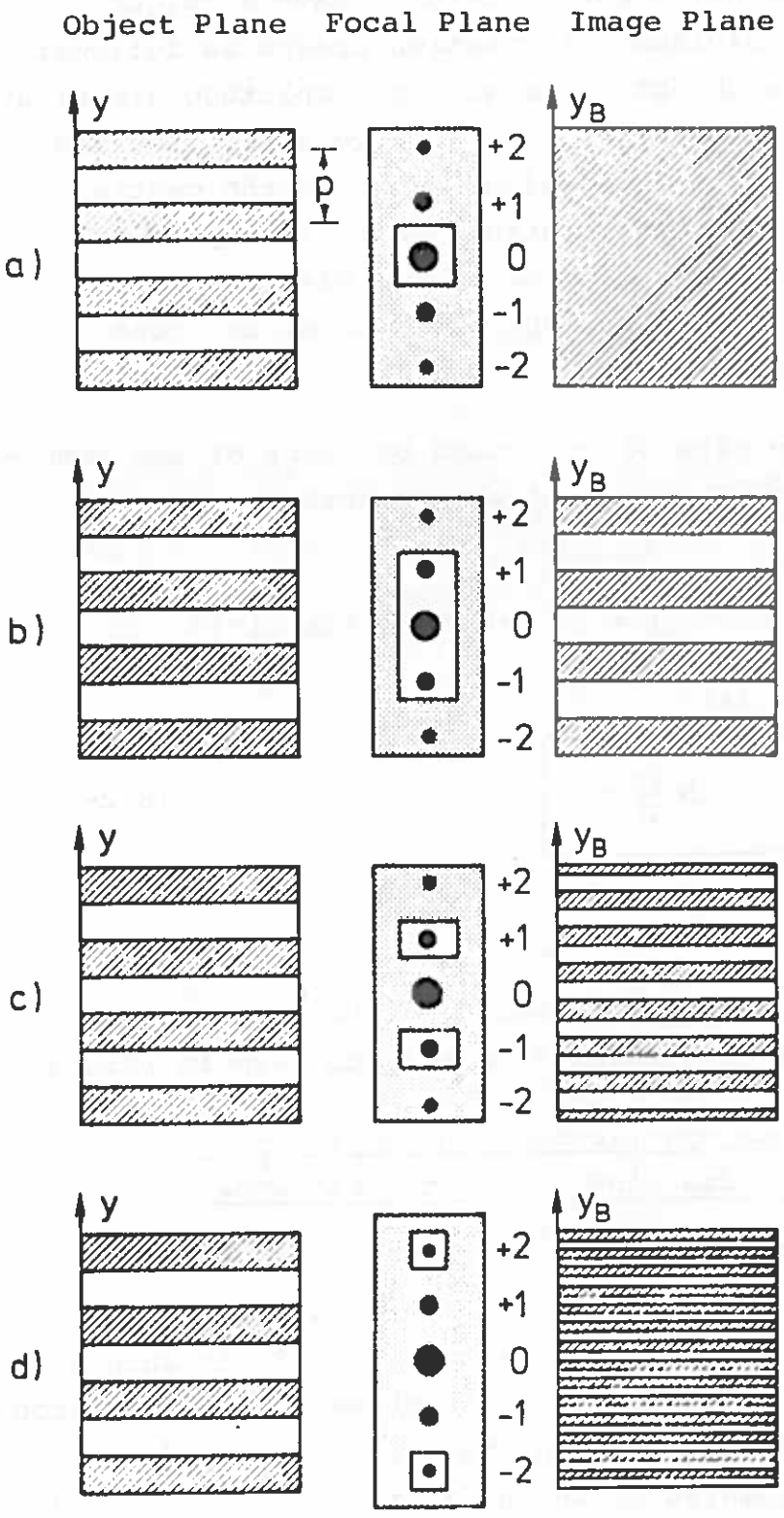

Optical Filtering of Picture of a Line Grating

Figure 8.2-3

The distribution of light intensity I in the image plane depends on the diffraction orders that are allowed to pass the focal plane. If a filter that only permits the passage of the central diffraction order (fig. 8.2-3a) is arranged in the focal plane, the light intensity will correspond to the first term in (8.2-1) and will thus be constant over the whole image plane.

In the calculation of the distribution of the light intensity when the amplitude U is complex, the following applies:

$$I = U\,U^K \qquad (8.2\text{-}4)$$

where U^K is the complex conjugate to U. As

$$I_N = U_N\,U_N^K = C\exp\{iN\frac{2\pi y}{p}\}\exp\{-iN\frac{2\pi y}{p}\} = C$$

this means that every diffraction order that passes the filter alone produces a uniformly illuminated image plane.

If the filter permits the passage of the orders -1, 0 and +1, we get a periodic distribution (fig. 8.2-3b), with the period p as in the original grating in the object plane. If the filter also excludes the central dot, so that only +1 and -1 pass (fig. 8.2-3c), we get a periodic distribution with the half period in relation to the previous case. In general, <u>if the filter only permits the passage of the diffraction orders +N and -N, the period of the picture will be $\frac{1}{2N}$ p, whereby a grating is obtained with a line-density that is 2N times that of the original grating</u>.

This <u>OPTICAL MULTIPLICATION</u> of the line-density has an upper bound, which depends particularly on two factors. Firstly, the part of the optical signal that passes through a symmetrical pair of diffraction orders generally decreases heavily with increasing orders. However, this can be compensated to som extent by using gratings with a small relative space width (ß), since this factor determines how heavily the intensity decreases with increasing order (cf. B.4-3 with relevant text). Further, it is sometimes advantageous to use phase gratings instead of

the amplitude gratings treated here. The latter factor is discussed by Post in this context in [67-8],[68-6] and [68-7].

The second factor setting an upper bound to the multiplication factor is the geometry of the optical arrangement. As described in Appendix B (B.4-6), the diffraction order N corresponds to the light emitted in a certain direction from the object plane. The higher the order, the greater will be the angle of the path of the ray with the optical axis of the arrangement, and from a certain order N_{max} (B.5-3), the light from higher orders will pas right outside the lens.

In the above-mentioned articles, Post mentions 30 as the maximum multiplication factor obtained, and this was achieved using phase gratings. Sciammarella and Lurowist, on the other hand, only reach a factor 5 with amplitude gratings in [67-9].

In order to get an idea of the order og magnitude of the optical arrangement used in grating multiplication, Sciammarella [69-6] uses a lens with a focal length L = 150 cm. With a light source with the wavelength $\lambda = 6000$ Å $= 6000 \cdot 10^{-8}$ cm and a line grating with 20 ℓ/mm, the distance between the diffraction dots in the focal plane is

$$\frac{\lambda L}{p} = 1.5 \text{ cm.}$$

A diameter of 2R = 25 cm is specified for the lens, which means that the maximum diffraction order N_{max}, that manages to pass through the lens is ((B.5-3) with r << R),

$$N_{max} \simeq \frac{R}{2L} \frac{p}{\lambda} \simeq 4$$

However, this value can be increased considerably by altering the distance from object plane to lens, whereas the distance 1.5 cm between the diffraction dots remains unaltered by such manipulation.

Multiplication of a single line grating is utilized by Boone and van Beeck in [70-10], where, by projecting the model grating on the reference grating, they carry out partly a

magnification and partly a multiplication of the model grating, so that approximately the same nominal pitch is obtained in the two superposed gratings. The principle is used in cases in which the model and reference gratings do not have the same initial pitch.

8.3 Diffraction Pattern for a Moiré-Pattern and its Optical Filtering

Two crossed line gratings assumed to lie in the same plane, e.g. on a photographic negative, are now placed in the object plane. The two line gratings MG and RG, which form an "undeformed" moiré-pattern in the object plane, are assumed to have the following parametric descriptions:

$$\text{MG} : \quad y = m\,p_m \tag{8.3-1}$$

$$\text{RG} : \quad y = r\,\frac{p}{\cos\theta} + x\tan\theta \tag{8.3-2}$$

or

$$\text{RG} : \quad y^* = r\,p_r \tag{8.3-3}$$

where an alternative coordinate system is used:

$$x^* = x\cos\theta + y\sin\theta \tag{8.3-4}$$

$$y^* = -x\sin\theta + y\cos\theta \tag{8.3-5}$$

and where p_m and p_r are the pitches and θ the angle between the grating lines (cf. (4.2-1 and 4.2-2)).

The relevant diffraction pattern is indicated in fig. 8.3-1a. The mutual positions of the dots are shown in fig. 8.3-1b, and they are provided with "dot coordinates" [M,R]. M specifies the diffraction order in the diffraction pattern of the grating MG to which the dot corresponds, and analogously for R. Thus, the points [0,-4],[0,-3],.....[0,0],.....[0,+4] correspond to the diffraction pattern that would be formed by the line grating RG if this were not superposed with the other grating in the object plane.

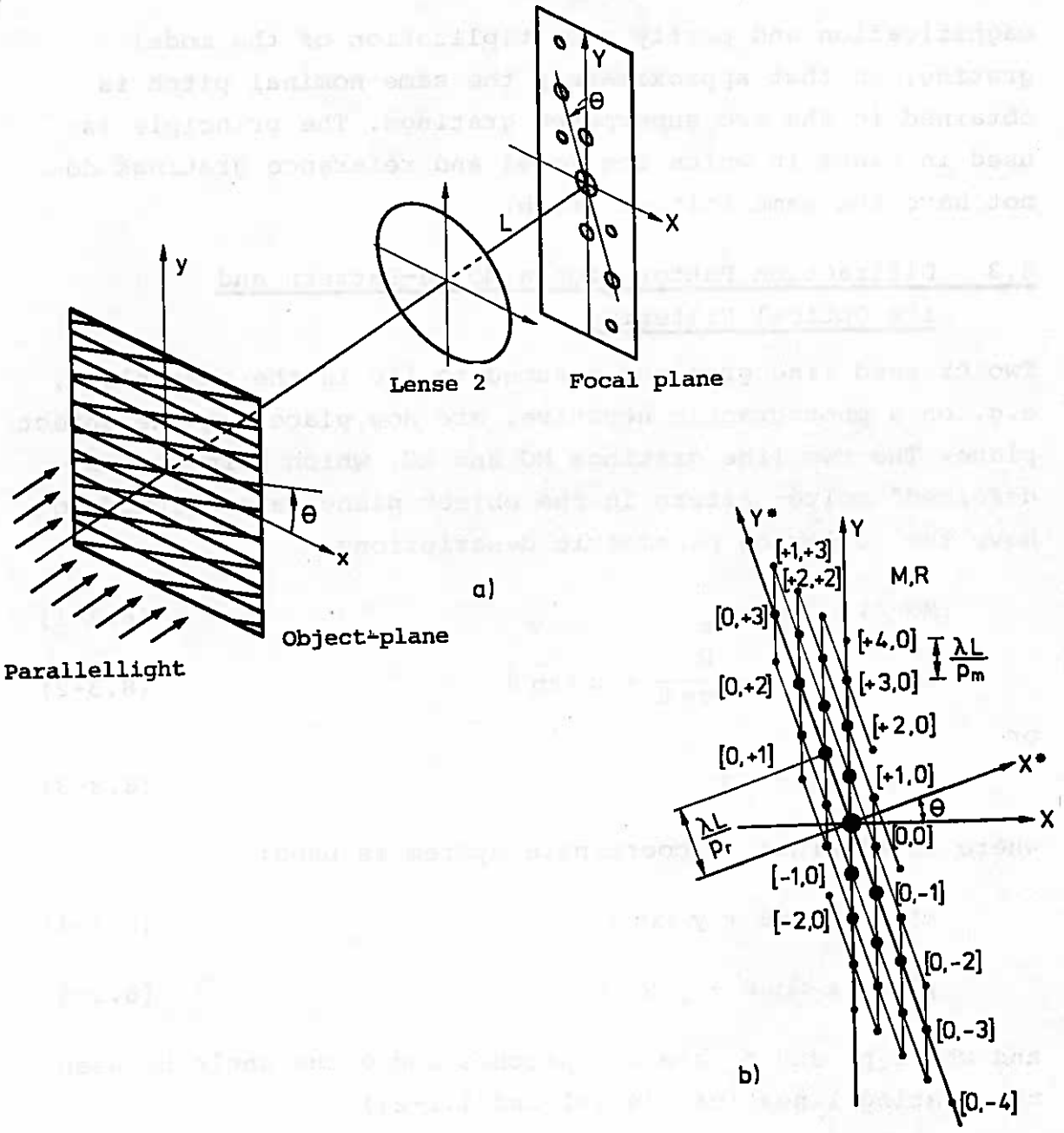

Diffraction pattern for two crossed line gratings.

Figure 8.3-1

As in the case of the line gratings, there is a unique relationship between the individual diffraction dots and the Fourier expansion of the amplitude distribution in the object plane.

This can be written

$$U\{x,y\} = U_o\, g_m\{x,y\}\, g_r\{x,y\} \qquad (8.3\text{-}6)$$

where $g_m\{x,y\}$ and $g_r\{x,y\}$ are the transmission functions of the two gratings. Assuming that the two gratings have the same β-value, these are

$$g_m\{x,y\} = \beta\,[1 + c_1 \cos\{2\pi m\} + c_2 \cos\{4\pi m\} + \ldots] \quad (8.3\text{-}7)$$

and

$$g_r\{x,y\} = \beta\,[1 + c_1 \cos\{2\pi r\} + c_2 \cos\{4\pi r\} + \ldots] \quad (8.3\text{-}8)$$

where (8.2-1) is related to (8.3-1 and 8.3-3).

The amplitude distribution (8.3-6) thus assumes the form,

$$\begin{aligned} U\{x,y\} &= U_o \beta^2 [1 + c_1 \cos\{2\pi m\} + c_1 \cos\{2\pi r\} \\ &\quad + (c_1)^2 \cos\{2\pi m\} \cos\{2\pi r\} + \ldots] \\ &= U_o \beta^2 [1 + c_1 \cos\{2\pi m\} + c_1 \cos\{2\pi r\} \\ &\quad + \tfrac{1}{2} (c_1)^2 [\cos\{2\pi(r+m)\} + \cos\{2\pi(r-m)\}] + \ldots \end{aligned} \quad (8.3\text{-}9)$$

where only the contributions from the first two terms in each of (8.3-7 and 8.3-8) are calculated. The contributions of the individual terms to the diffraction dots are as follows:

Term	Diffraction Orders
1	[0,0]
$c_1 \cos\{2\pi m\}$	[+1,0] and [-1,0]
$c_1 \cos\{2\pi r\}$	[0,+1] and [0,-1]
$\frac{1}{2} (c_1)^2 \cos\{2\pi(r+m)\}$	[+1,+1] and [-1,-1]
$\frac{1}{2} (c_1)^2 \cos\{2\pi(r-m)\}$	[-1,+1] and [+1,-1]

Table 8.3-1

A filtering of the diffraction pattern of the moiré-pattern can be carried out in the same way as for that of the line grating. A number of cases are shown in fig. 8.3-2.

The Diffraction Pattern after Filtering	The Image after Filtering	Distribution of Intensity

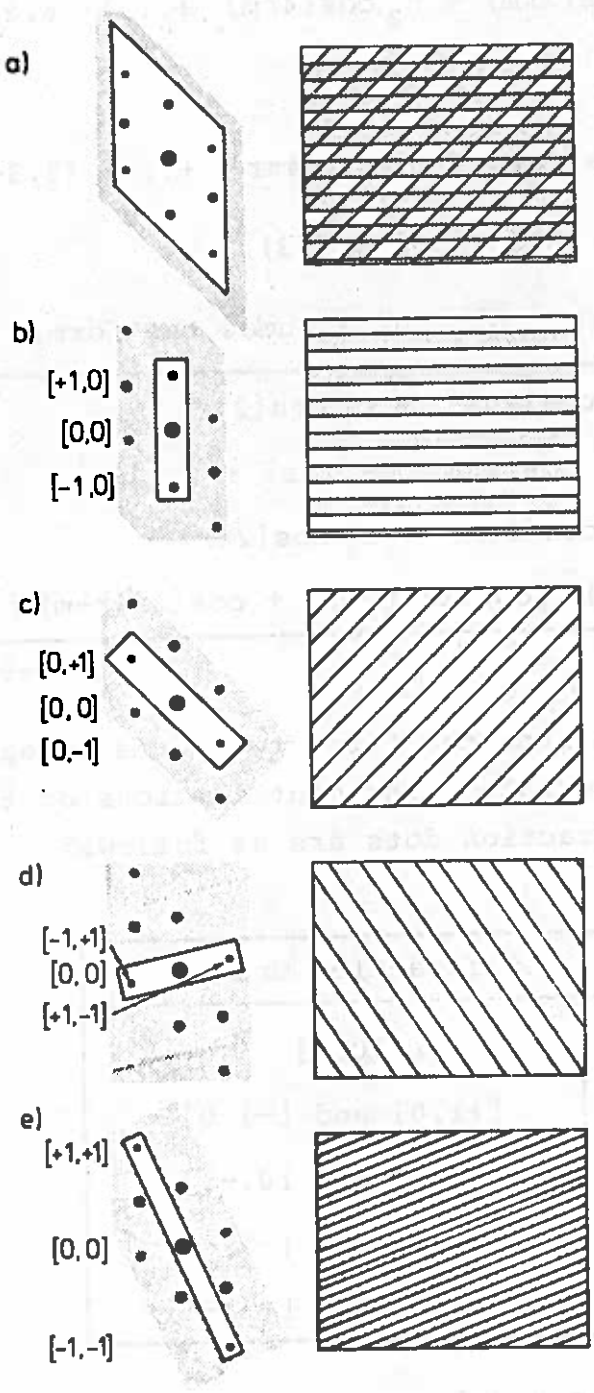

$$I=I_o\,[1+2\,c_1\cos\{2\pi m\}+2\,c_1\cos\{2\pi r\}+(c_1)^2\cos\{2\pi(r-m)\}+(c_1)^2\cos\{2\pi(r+m)\}+(c_1)^2\cos^2\{2\pi m\}+\ldots\ldots\ldots]$$

$$I=I_o\,[1+2\,c_1\cos\{2\pi m\}+(c_1)^2\cos^2\{2\pi m\}]$$

$$I=I_o\,[1+2\,c_1\cos\{2\pi r\}+(c_1)^2\cos^2\{2\pi r\}]$$

$$I=I_o\,[1+(c_1)^2\cos\{2\pi(r-m)\}+\tfrac{1}{4}(c_1)^4\cos^2\{2\pi(r-m)\}]$$

$$I=I_o\,[1+(c_1)^2\cos\{2\pi(r+m)\}+\tfrac{1}{4}(c_1)^2\cos^2\{2\pi(r+m)\}]$$

Optical Filtering of Moiré-Pattern

Figure 8.3-2

Case a shows the filtered picture when the nine most significant (central) diffraction orders pass through. The picture retains the structure of the original, but gets a uniformly varying distribution of the intensity as against the steps between bar and space in the original.

In cases b and c, the filtering only gives the two gratings separately and is analogous to fig. 8.2-3b. It is thus possible to separate two superposed gratings. Applications of this will be treated later.

Finally, d and e show distributions of the intensity that vary periodically with the quantities r-m and r+m, which are precisely the subtractive and the additive moiré-patterns (cf. (3.1-6 and 3.1-7)) formed by the two superposed gratings. With filtering, it has been possible to get rid of the original grating lines so that only the moiré-fringes remain.

The various applications arising from filtering are discussed in greater detail in the following.

8.4 Interpolation by Means of Measurements of Light Intensity

In the study of the diffraction pattern of two crossed line gratings both were assumed to be undeformed. An extension of the theory to the case in which one of the gratings is deformed can be carried out, with a certain approximation, as follows. The approximation lies in the assumption that the state of deformation can be regarded as homogeneous within the area under consideration.

The treatment here is limited to a moiré-pattern in which the two gratings are identical and congruent prior to deformation. In this case (cf. example 6.1-1), the moiré-pattern is contour-curve system for the displacement function, i.e.

$$v\{x,y\} = n\,p \qquad (8.4\text{-}1)$$

In order to be able to determine the value of the displacement function between the moiré-lines, it is now assumed that the deformed grating is homogenous locally between two moiré-

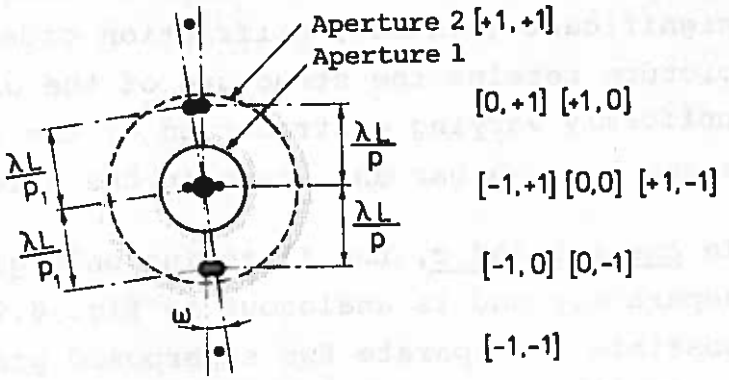

Diffraction Pattern for Two Almost Identical Line Gratings with Approximately Parallel Grating Lines

Figure 8.4-1

lines. The deformed grating can thus be ascribed a pitch p_1 with the grating lines rotated a small angle ω in relation to the orientation in the undeformed state. The reference grating with the pitch p remains in this state, and for small deformations, $p_1 = p(1 + \varepsilon)$, where $|\varepsilon| << 1$.

Two superposed line gratings with the pitches p and $p(1 + \varepsilon)$ and with a mutual angle $\omega << 1$ will form the diffraction pattern shown in fig. 8.4-1, where some of the dots will almost coincide. If the optical arrangement has an aperture in the focal plane which only permits the passage of light about the central dot (aperture 1 in the figure), the distribution of intensity of the picture will correspond to case d in fig. 8.3-2 and can be written

$$I = I_o \left[1 + (c_1)^2 \cos\{2\pi n\} + \frac{1}{4}(c_1)^4 \cos^2\{2\pi n\}\right] \qquad (8.4\text{-}2)$$

This can be approximated to

$$I = I_o + I_1 \cos\{2\pi n\} \qquad (8.4\text{-}3)$$

where

$$I_1 = I_o (c_1)^2 [1 + \frac{1}{4} (c_1)^2]$$

Hence, the relationship between the light intensity and the displacement can be written

$$v\{x,y\} = \frac{p}{2\pi} \arccos\{\frac{I - I_o}{I_1}\} \qquad (8.4\text{-}4)$$

The approximation from (8.4-2) to (8.4-3) is shown in fig. 8.4-2. The deviation between the two curves depends on the factor c_1, which in turn depends on the relative space width β (cf. fig. B.5-3), but will not be discussed in detail here, since it is only the principle involved that is to be illustrated.

If (8.4-3) is assumed to have sufficient validity, it will be seen from (8.4-4) that it is possible to interpolate between the moiré-lines by measuring the variation in the light intensity.

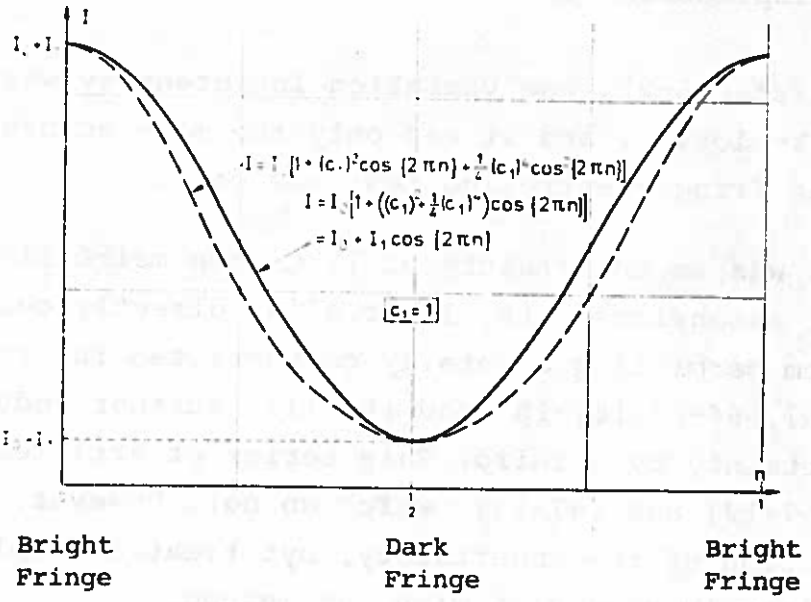

Variation in Light Intensity between the Moiré-Fringes

Figure 8.4-2

Sciammarella has been the leading force in the development of an interpolation technique on the basis of measurement of the light intensity. However, his original starting part was based on another optical filtering technique than that discussed here, which assumes coherent light. The filtering technique used by Sciammarella in [65-2] has been described by Françon [63-6], amongst others, and consists, in brief, of a calculation of the filtering effect of a lens in simple picture formation. For periodic objects such as line gratings, higher order terms in a Fourier expansion can be filtered off, and Sciammarella reaches bis "Basic Optical Law for the Moiré-Displacement-Field" in precisely the form of (8.4-3 and 8.4-4).

The main features of the interpolation technique are as follows. Along a line in the moiré-pattern, where the displacement function is to be determined, the relative variation in the light intensity is measured by means of a photo-cell. On this basis, the mean intensity I_o is determined together with the maximum and minimum points. By drawing sine curves through a couple of maximum points and the intermediate minimum point the interpolation can be carried out, and the variation in the displacement function determined.

At first [65-2], the variation in intensity was recorded on an X-Y-plotter, and it was only the more accurate determination of the fringe-centreline that was used.

There was an uncertainty of 1% on the moiré-line spacing. Later extensions with, inter alia, directly connected digital system permitting a totally computerized interpolation process [66-5],[66-6],[67-10] and [67-11], further reduces the uncertainty by a third. This series of articles is concluded by [67-12] and [67-13], which do not, however, report further reduction of the uncertainty, byt treat a couple of special problems in connexion with the method.

Sciammarella's interpolation method based on measurement of the variation in light intensity in a moiré-pattern is not widely used. This is due partly to the requirement to instruments and partly the rather complicated procedure. Finally, the appearance of the optical multiplication technique, which can increase the sensitivity in a simpler way, has, to some extent, rendered the complicated interpolation procedure superfluous. However, it is worth noting that it is presumably the clarification of the moiré-theory resulting from Sciammarella's work that has formed the basis for, inter alia, the optical multiplication technique.

An alternative interpolation procedure without the use of a filtering technique has been described by Theocaris in [69-1], pages 85-111, and in [69-7]. Instead of drawing a sine curve through the extreme points, Theocaris measures the density directly on the photographic negative of the moiré-pattern. This is done automatically, and the result appears as contour-curves over the density of the negative. The method is stated to have a resolving power of less than $\frac{1}{20}$ of the moiré-line spacing.

8.5 Optical Multiplication of a Moiré-Pattern

In section 8.2 the possibility of carrying out an optical multiplication of a line grating was mentioned, and here we shall now take a look at the possibility of doing the same thing with a couple of crossed line gratings (a moiré-pattern).

Consider again the case of two almost identical, undeformed line gratings with a small mutual angle ω. With the arrangement shown in fig. 8.1-1, the resultant diffraction pattern is as shown in fig. 8.5-1.

The diffraction dots are collected in groups, in which $M + R$ = constant, where M and R are the diffraction orders for the two gratings.

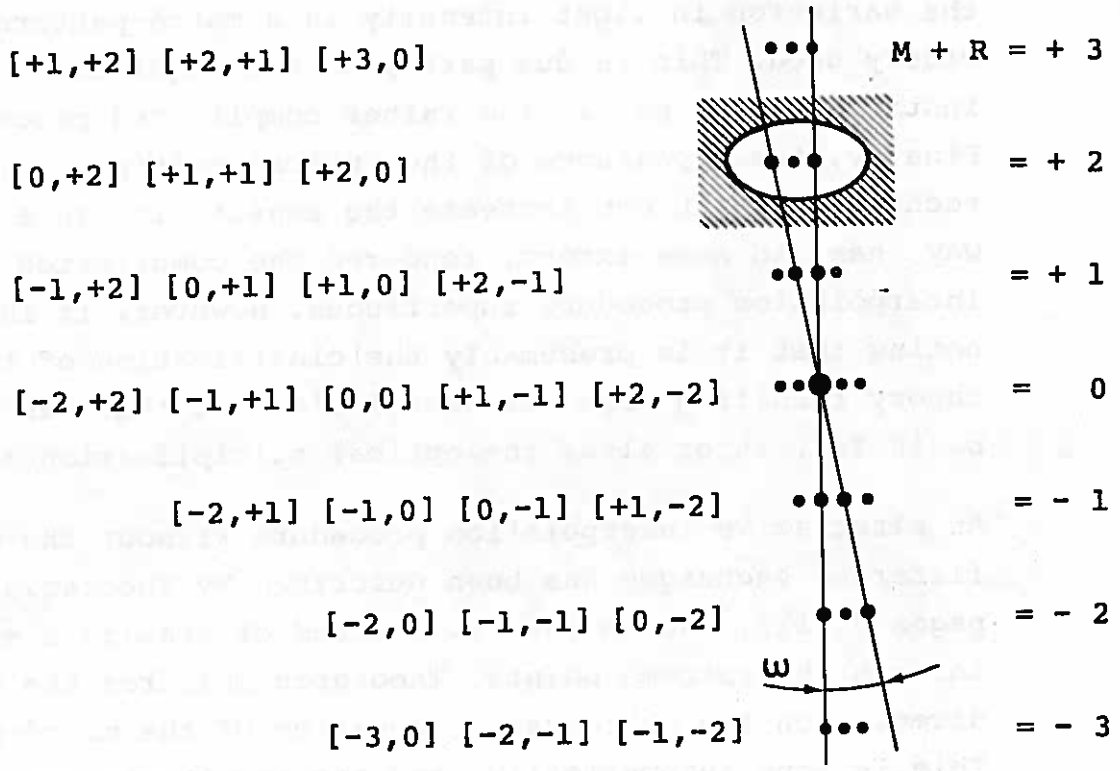

Diffraction Pattern with "Dot Coordinates" [M,R]

Figure 8.5-1

If the filter only permits the passage of such a group, a periodic distribution of the light intensity will appear in the image plane, with the same fringe orientation as in the subtractive moiré-pattern and with a $|M + R|$ times greater fringe density. For $M + R = 0$, however, the multiplication factor is equal to 1. This possibility of multiplication is given by Durelli and Parks in [70-1], pages 50-54, but is only possible for certain values of β.

In, for example, the group with $M + R = +3$, the central dots are:

[-1,4],[0,3],[+1,2],[2,1],[3,0],[4,-1]

Each dot [M,R]'s contribution to the amplitude distribution in the image plane, dU is analogous to (8.2-3), given by

$$\boxed{dU = \tfrac{1}{4}(\beta)^2 U_o c_M c_R \exp\{i\,2\pi\,(Mm + Rr)\}} \qquad (8.5\text{-}1)$$

and if only the dots from [0,3] to [3,0] are considered, the amplitude distribution will be:

$$U = \tfrac{1}{4}\beta^2 U_o [c_o c_3 (\exp\{i\,6\pi\,m\} + \exp\{i\,6\pi\,r\}) + c_1 c_2 (\exp\{i\,2\pi\,(2\,m+r)\} + \exp\{i\,2\pi\,(m+2\,r)\})]$$

As the light intensity I is given by

$$\boxed{I = U U^k} \qquad (8.5\text{-}3)$$

where U^k is the complex conjugate to U, we get, after some calculation,

$$I = (\tfrac{1}{4}\beta^2 U_o)^2\, 2 \Big[(c_o c_3)^2 + (c_1 c_2)^2 + [(c_1 c_2)^2 + 2\,c_o c_1 c_2 c_3] \cos\{2\pi n\} + 2\,c_o c_1 c_2 c_3 \cos\{4\pi n\} + (c_o c_3)^2 \cos\{6\pi n\} \Big] \qquad (8.5\text{-}4)$$

where $\underline{n = r - m}$ is the parameter used previously for the subtractive moiré-pattern. The intensity function will be seen to be the sum of three periodic functions with the periods n, $\frac{1}{2}$n and $\frac{1}{3}$n, and only in the case in which the coefficient of the last term is dominant will a moiré-pattern appear that is multiplied by the factor M + R = 3. This applies, for instance, to gratings with $\beta \simeq \frac{1}{2}$, since $\beta = \frac{1}{2} \Rightarrow c_2 = 0$ (8.2-2), and the distribution of the intensity will then be

$$\boxed{I = (\tfrac{1}{4}\beta^2 U_o)^2\, 2\,(c_o c_3)^2\,[1 + \cos\{6\pi n\}]} \qquad (8.5\text{-}5)$$

The arrangement shown in fig. 8.1-1 can thus be used for optical multiplication in cases in which a single factor is dominant. Post discusses applications of the principle in [67-8],[68-6],[68-7], and[71-2], but he mainly uses transmission-phase gratings of the "Blazed grating" type, where there is a special possibility of making a single

direction dominant. Post reaches a multiplication factor of up to 30, but also makes use of the possibility of applying the principle to two gratings with a pitch ratio of

$$\frac{p_r}{p_m} = H + \varepsilon$$

where H is an integer and $\varepsilon << 1$.

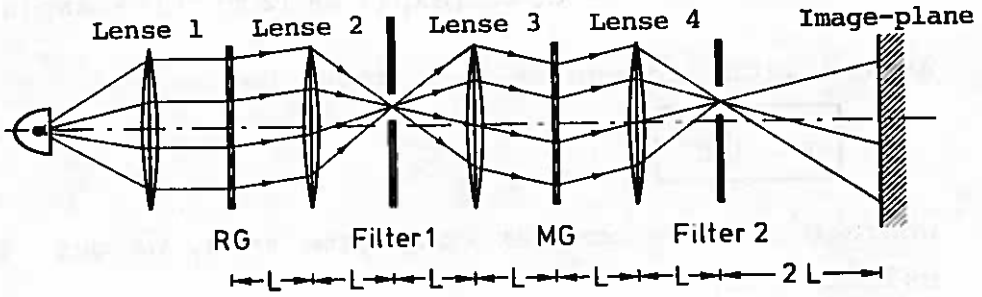

Figure 8.5-2

Another arrangement, shown in fig. 8.5-2, makes the above-mentioned dominance partly superfluous. It has been described by Sciammarella and Lurowist in [67-9] and has also been used by Luxmoore [68-8].

In comparison with the arrangement in fig. 8.1-1, that in 8.5-2 has two extra lenses and a filter. Furthermore, the two gratings RG and MG are separated, which facilitates selection of diffraction orders in multiplication filtering.

What happens before the lens (3) is the same as happened with the line grating in section 8.2.

If the first grating (RG) has the transmission function

$$g_r\{x,y\} = \frac{1}{2}\beta \sum_{N=-\infty}^{N=\infty} c_N \exp\{iN2\pi r\} \qquad (8.5\text{-}6)$$

and if the filter (1) only lets the order R pass, the following complex amplitude distribution will arrive at the second grating (MG):

$$U_1 = \frac{1}{2}\beta\, U_o\, c_R \exp\{iR2\pi r\} \tag{8.5-7}$$

If the second grating (MG) has the transmission function,

$$g_m\{x,y\} = \frac{1}{2}\beta \sum_{N=-\infty}^{N=\infty} c_N \exp\{iN2\pi m\} \tag{8.5-8}$$

the amplitude distribution departing from this grating will be

$$U_2 = U_1\, g_m = \frac{1}{4}\beta^2\, U_o \sum_{N=-\infty}^{N=\infty} c_N\, c_R \exp\{\, i2\pi(Nm+Rr)\,\} \tag{8.5-9}$$

After passing the lens (4), this distribution will give rise to diffraction dots in the plane of the second filter, with the same locations as .....[-2,R], [-1,R], [0,R], [+1,R],... [M,R],... in fig. 8.3-1b or fig. 8.5-1.

If the two gratings are practically identical with a small mutual angle only one of the dots in each group in fig. 8.5-1 will be formed in this way. Sciammarella and Lurowist's multiplication method now consists in letting two selected orders pass through in first filter, e.g. R = 0 and R = R_o. These will give two dots in each group. In the case of the group $M_o = M + R = R_o$, it will be the dots:

$$[M_o,0] = [R_o,0] \text{ and } [0,R_o]$$

If the filter (2) only lets this group pass, the amplitude distribution in the image plane will be

$$\begin{aligned} U_3 &= \frac{1}{4}\beta^2\, U_o\, [c_{R_o}\, c_o \exp\{i2\pi R_o m\} \\ &\qquad + c_o\, c_{R_o} \exp\{i2\pi R_o r\}] \\ &= \frac{1}{4}\beta^2\, U_o\, c_o\, c_{R_o}\, [\exp\{i2\pi R_o m\} + \exp\{i2\pi R_o r\}] \end{aligned} \tag{8.5-10}$$

The distribution of the light intensity will then be

$$I = U_3\, U_3^K = (\tfrac{1}{4}\beta^2\, U_o\, c_o\, c_{R_o})^2\, 2\,[1 + \cos\{2\pi R_o(r - m)\}] \tag{8.5-11}$$

The variation is periodic and has the same orientation as the subtractive moiré-pattern that the two gratings would normally form if they were superposed in the same plane. However, a multiplication by the factor R_o has been achieved. As mentioned earlier, Sciammarella and Lurowist managed to produce patterns multiplied up to five times when they used transmission amplitude gratings.

In a later article [69-6], Sciammarella describes a modified procedure that can multiply the pattern up to 20 times. In the new method, the procedure described in section 8.2 for multiplication of a single line grating is used first. By allowing the orders +R and -R to pass the filter in the image plane, the following distribution of the intensity is obtained:

$$I_r = (\beta U_o c_R)^2 \cos^2\{2\pi Rr\} \qquad (8.5\text{-}12)$$

This is exposed on a negative. The grating is then deformed and the procedure repeated. The second distribution of the intensity is

$$I_m = (\beta U_o c_R)^2 \cos^2\{2\pi Rm\} \qquad (8.5\text{-}13)$$

The double exposed negative now has a distribution of the intensity

$$I = I_r + I_m \qquad (8.5\text{-}14)$$

When the negative is correctly exposed, its transmission function is proportional to the distribution of the intensity (8.5-14), and if the negative is placed in the object plane in the arrangement shown in fig. 8.1-1, the following dots will form in the diffraction plane:

[2R,2R]
[2R,0], [0,2R]
[2R, -2R], [0,0], [-2R,2R]
[-2R,0], [0,-2R]
[-2R,2R]

If, for example, [0,2R] and [2R,0] are allowed to pass the filter, we get in the image plane the subtractive moiré-pattern multiplied 2R times.

As mentioned, 2R = 20 has been achieved, and an important reason for this is stated to be the use of a transmission phase grating, which is easy to produce.

8.6 Other Applications of Optical Filtering Technique

As a supplement to the study of the optical filtering technique, a couple of other applications of the method will be mentioned in brief.

8.6-1 The Schlieren-Method

The Schlieren-method is generally a contrast-improving method (Born and Wolf [65-24] p.425) for coherently illuminated, transparent specimens. The method consists in filtering-off all diffraction orders on one side of the central dot. It is therefore incorrect to call the method described by de Haas and Loof [66-7] by this name.

de Haas and Loof use an arrangement like that shown in fig. 8.1-1, with a poor contrast moiré-pattern negative in the image plane, and allow the group M + R = +1 to pass the filter (cf. fig. 8.5-1). They achieve a richly contrasted subtractive moiré-pattern corresponding to a multiplication factor of 1. In complete analogy with the calculations (8.5-1) - (8.5-5), the dots passing the filter are

$$\ldots\ldots, [-1,2], [0,1], [1,0], [2,-1], [3,-2], [4,-3], \ldots$$

In the case $\beta = \frac{1}{2}$ (grating bars and space of equal width), $c_2 = c_4 = c_6 = c_8 = 0$, i.e. the only dots that form in the group M + R = 1 are

$$[0,1] \text{ and } [1,0]$$

and they give an intensity distribution,

$$I = I_o [1 + \cos\{2\pi n\}]$$

with maximum visibility (equal to 1).

de Haas and Loof use the filtered moiré-pattern for second-order moiré (cf. section 6.7) and manage to filter off the original grating lines that would otherwise have produced extra moiré-fringes beside the second-order moiré-fringes.

8.6-2 Separation of Moiré-Patterns of Cross-Gratings

In some moiré applications (see, for example, Post [65-5]), one negative contains two moiré-patterns corresponding to four superposed line gratings or two cross-gratings. In the case of two orthogonal line gratings (fig. 2.1-2), with almost parallel pairs of lines, optical filtering in the arrangement shown in fig. 8.1-1 will result in the formation in the diffraction plane of a diffraction pattern composed of two patterns of the type and orientation shown in fig. 8.5-1, at right-angles to each other.

The use of a slit-aperture, which, for example, only allows the diffraction dots corresponding to one of the orientations through, results in only one of the moiré-patterns being formed in the image plane. Applications of this principle are described by Chiang in [69-5] and by Clark, Durelli and Parks in [71-4] and [71-5].

8.6-3 Addition and Subtraction of Two Crossed Gratings

In connexion with fig. 8.3-2, it was shown that it was possible to form both the additive and the subtractive moiré-pattern between two superposed line gratings when these formed a not too small mutual angle. This has been described in the above-mentioned [71-4] and [71-5], where it is used to produce contour-curves for the rotation and the shear strain term in the two-dimensional strain tensor by the direct-moiré method.

8.7 Other Applications of the Diffraction Effect of the Gratings

In the space behind a diffraction object (line grating, moiré-pattern or similar), plane waves radiate in a number of characteristic directions. An investigation of the inter-

ference between these waves shows that at certain distances, the amplitude distribution from the diffraction plane is recreated.

The conditions have been described and utilized by Sciammarella et alios in [68-9], [70-6] and [71-6], by Durelli and Parks in [70-1], pages 52-62, and by Ebbeni and Rezette in [70-7], [70-8] and [70-9]. Only a couple of the applications of a more general character will be discussed in the following.

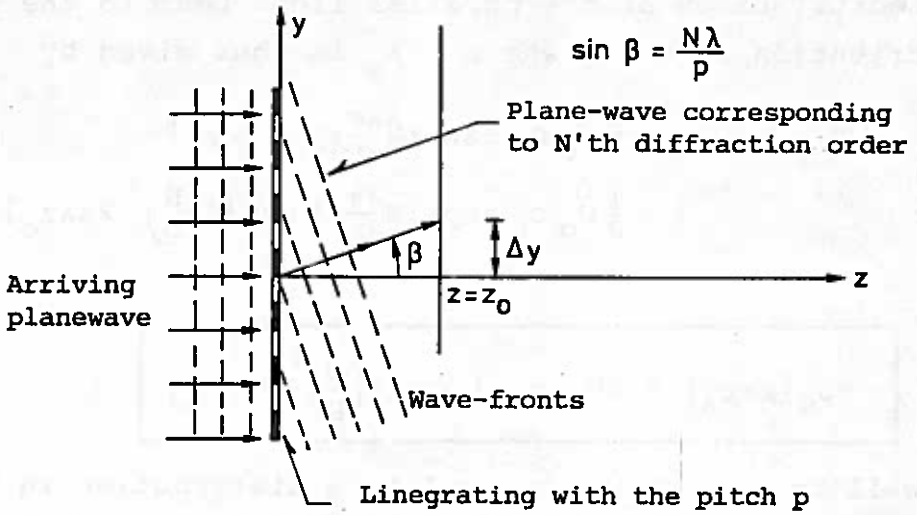

Figure 8.7-1

Fig. 8.7-1 shows a line grating illuminated by a coherent and monochromatic parallel light-beam perpendicular to the grating plane. After passing the grating, the light separates into a number of parallel light-beams, which radiate in directions corresponding to the individual diffraction orders. The figure shows one of these, corresponding to the diffraction order N. The direction of radiation for this is given by the angle β, for which

$$\sin \beta = N \frac{\lambda}{p} \qquad (8.7\text{-}1)$$

where p is the pitch of the line grating and λ the length of the light wave. The appurtenant proportion of the amplitude distribution in the grating plane is given by (8.3-2):

$$dU_N\{z=0\} = \frac{1}{2}\beta\, U_o\, c_N \exp\{iN\frac{2\pi}{p}y\} \qquad (8.7\text{-}2)$$

This distribution shifts (as the waves gradually radiate) in the y-direction a distance

$$\Delta y = z \tan\beta \simeq z \sin\beta = z\, N\frac{\lambda}{p}$$

$$\text{for } \beta << 1 \qquad (8.7\text{-}3)$$

The contribution of the parallel light-beam to the amplitude distribution in the plane $z = z_o$ is thus given by

$$dU_N\{z=z_o\} = \frac{1}{2} U_o\, c_N \exp\{iN\frac{2\pi}{p}(y + \Delta y)\}$$

$$= \frac{1}{2} U_o\, c_N \exp\{iN\frac{2\pi}{p}y\} \exp\{i\left(\frac{N}{p}\right)^2 2\pi\lambda z_o\}$$

or

$$\boxed{dU_N\{z=z_o\} = dU_N\{z=0\} \exp\{i\left(\frac{N}{p}\right)^2 2\pi\lambda z_o\}} \qquad (8.7\text{-}4)$$

It will be seen that the amplitude distribution in the $z = z_o$ plane is identical to that in the $z = 0$ plane every time the last factor is equal to 1, i.e.

$$\exp\{i\left(\frac{N}{p}\right)^2 2\pi\lambda z_o\} = 1$$

$$\Leftrightarrow \left(\frac{N}{p}\right)^2 2\,\pi\,\lambda\, z_o = n\, 2\,\pi$$

$$\Leftrightarrow \boxed{z_o = \frac{n}{\lambda}\left(\frac{p}{N}\right)^2} \qquad (8.7\text{-}5)$$

where n is a positive integer. In the particular case of $N = 0$ (mean amplitude), (8.7-5) does not, of course, apply, but as it is a parallel light beam that radiates in the z-direction, there is no shift in the distribution in the y-direction.

Considering the distance,

$$\boxed{z_o = \frac{p^2}{\lambda}} \qquad (8.7\text{-}6)$$

it will be seen to be the first distance in which the amplitude distribution for N = ± 1 is equal to that in the grating plane. Further, it will be seen that (8.7-5) is also satisfied for all higher orders. The individual terms are shifted a distance $\Delta y = Np$ at this distance.

This means that the amplitude distribution for all orders at this distance is the same as in the grating plane. The amplitude distribution of the grating plane (8.2-3) is thus recreated at distances behind the grating that are multiples of (8.7-6). Thus, if another grating is placed at the same distance behind a monochromatically and coherently illuminated grating, a moiré-pattern will appear that is identical to the pattern that would be formed by the two gratings if they lay in the same plane.

The orders of magnitudes of these distances for $\lambda = 6000\text{Å} = 6 \cdot 10^{-4}$ mm are as follows at line densities of 1, 10 and 20 ℓ/mm:

1 ℓ/mm	$z_o = 1{,}67$ m
10 ℓ/mm	$z_o = 1{,}67$ cm
20 ℓ/mm	$z_o = 0{,}42$ cm

Consider now the space behind a moiré-pattern formed by two superposed, parallel line gratings with the pitches p_m and p_r ($p_m > p_r$). Here, the following conditions apply.

The expressions corresponding to (8.7-1) - (8.7-5) become (denoting the individual diffraction orders of the two gratings M and R):

$$\sin\beta = \lambda\left(\frac{M}{p_m} + \frac{R}{p_r}\right) \qquad (8.7\text{-}7)$$

$$dU_{M,R}\{z=0\} = \frac{1}{4}\beta^2 U_o c_M c_R \exp\{i2\pi\left(\frac{M}{p_m} + \frac{R}{p_r}\right)y\} \qquad (8.7\text{-}8)$$

$$dU_{M,R}\{z=z_o\} = dU_{M,R}\{z=0\} \exp\{i\left(\frac{M}{p_m} + \frac{R}{p_r}\right)^2 2\pi\lambda z_o\} \qquad (8.7\text{-}9)$$

The requirements to the distance z_o in order to get the same amplitude distribution in the $z = z_o$ plane as in the grating

plane is analogous to (8.7-5):

$$\boxed{z_o = \frac{n}{\lambda}\left(\frac{1}{\frac{R}{p_r} + \frac{M}{p_m}}\right)^2} \qquad (8.7\text{-}10)$$

According to Ebbeni and Rezette, at the distance

$$\boxed{z = \frac{n}{\lambda}\frac{p_r p_m}{\varepsilon}} \qquad (8.7\text{-}11)$$

where

$$\varepsilon = \frac{p_m - p_r}{p_r} << 1 \qquad (8.7\text{-}12)$$

there will be a light intensity distribution corresponding to the moiré-pattern. The specified distance (8.7-11) is generally stated to be only an approximate value, and it is only correct in cases in which the reciprocal value of the relative difference in pitch ε (8.7-12) is an integer, i.e.

$$\boxed{\frac{1}{\varepsilon} = H} \qquad (8.7\text{-}13)$$

where H is an integer.

The requirement to be satisfied is that the last factor (8.7-9) must be equal to 1. This leads to the condition

$$A = \left(\frac{M}{p_m} + \frac{R}{p_r}\right)^2 \lambda z_o = \text{integer for all R and M.}$$

Inserting z_o from (8.7-11), we get

$$A = \left(\frac{M}{p_m} + \frac{R}{p_r}\right)^2 \frac{p_r p_m}{\varepsilon} n = \frac{(Mp_r + Rp_m)^2}{p_m p_r \varepsilon} n$$

$$= \frac{p_r}{p_m}\left[M + R\frac{p_m}{p_r}\right]^2 \frac{n}{\varepsilon}$$

Assuming that (8.7-13) is satisfied, then

$$\frac{p_m}{p_r} = 1 + \varepsilon = 1 + \frac{1}{H} = \frac{1 + H}{H}$$

and A can thus be written

$$A = \frac{H}{1 + H}\left[M + R\frac{1 + H}{H}\right]^2 n H \qquad (8.7\text{-}14)$$

As n is an arbitrary integer, it will be seen that $n = (1 + H)H^2$ at any rate ensures that A is an integer when (8.7-13) is satisfied.

Ebbeni and Rezette used the described appearance of the intensity distribution of the moiré-pattern to determine the relative pitch difference or changes in this in two different ways.

In the first, "Méthode de variation de distance", the negative with the moiré-pattern is placed at right-angles to a coherent and monochromatic light beam. Then, the distance z behind the negative at which the light intensity distribution of the moiré-pattern is recreated with the greatest contrast is sought on a screen. This z corresponds to (8.7-11), and ε can then be determined if one pitch, e.g. p_r is known. In the second, "Méthode spectroscopique", a parallel light beam with white light is used instead. If the screen is placed at a distance z_1 from the negative, (8.7-11) will be satisfied for one of the light-wave lengths of which the white light is composed. To determine this wavelength, a spectroscope is used because the wave length in question dominates in the spectrum. In [70-7], it is stated that the method can be used to determine ε with a resolving power of 10^{-5} and that it can only be used in areas of moiré-pattern in which the deformation is homogeneous.

Sciammarella and Chang, in [71-6], use the displacement of the amplitude distribution perpendicular to the direction of the grating lines for second-order moiré (cf. section 6.7). They place a negative with a deformed line grating at right-angles to the coherent and monochromatic parallel light beam, and catch (expose) on another negative the light intensity distribution at the characteristic distance z_o (8.7-6) for the undeformed line grating.

It can be proved [71-6] that when the magnitude of the deformation is subjected to certain restrictions, the light intensity distribution exposed on the negative will be proportional to the distribution that would appear if the individual terms in the amplitude distribution of the deformed model grating (analogous, but not identical, to (8.2-3)) were shifted the distance

$$\Delta y = N p$$

in the y-direction.

If optical filtering is then carried out, in which only the orders $\pm N$ are allowed to pass, a contour-curve picture of the derivatives of the grating displacement function in the y-direction will appear, thus:

$$\boxed{\frac{\partial v}{\partial y} = \frac{H}{2N^2}} \qquad H = 0, \pm 1, \pm 2, \ldots \qquad (8.7\text{-}15)$$

This corresponds to two deformed model gratings multiplied N times being mutually shifted a distance $\Delta y = Np$, and the method is thus a combination of multiplication and second-order moiré.

Instead of the displaced amplitude distributions being exposed at equal to z_o (8.7-6), it can be done at distances that are multiples of this. If we denote this multiple M, then the shift will be

$$\Delta y = M N p$$

and, for the final contour-curve picture of the derivatives of the displacement functions,

$$\boxed{\frac{\partial v}{\partial y} = \frac{H}{2N^2 M}} \qquad (8.7\text{-}16)$$

In [71-6] Sciammarella and Chang show examples corresponding to M = 10 and N = 4, which corresponds to a difference in level in (8.7-16) of 0.00313. For the derivatives in the x-direction, i.e. the direction of the grating lines, the shifting cannot be done by means of the diffractive action of the grating, but must be purely mechanical, as described in section 6.7. On the other hand, optical filtering of this can also be carried out so that the possibility of multiplication is utilized too.

APPENDIX A: REFERENCES

[48-1] Weller, R. & Shepard, B.M.
"DISPLACEMENT MEASUREMENT BY MECHANICAL INTERFEROMETRY"
Proceedings of the S.E.S.A.
Vol. 6, No. 1, pp. 35-58, (1948)

[51-1] Sneddon, I.N.
"FOURIER TRANSFORMS"
New York 1951

[52-1] Kaczer, J. & Kroupa, F.
"THE DETERMINATION OF STRAINS BY MECHANICAL INTERFERENCE"
Czechoslovak Journal of Physics
Vol. 1, pp. 80-85 (1952)

[52-2] Ligtenberg, F.K.
"OVER EEN METHODE, OM DOOR EEN EENVOUDIG EXPERIMENT DE MOMENTEN IN STIJVE PLATEN TE BEPALEN"
De Ingenieur
Vol. 64, pp. 0.42-0.50 (1952)

[54-2] Dantu, P.
"RECHERCES DIVERSES D'EXTENSOMÉTRIE ET DE DÉTERMINATION DES CONTRAINTES"
Analyse des Contraintes. Mémoire des G.A.M.A.C.
Vol. 2, No. 2, pp. 3-14 (1954)

[55-1] Ligtenberg, F.K.
"THE MOIRÉ METHOD. A NEW EXPERIMENTAL METHOD FOR THE DETERMINATION OF MOMENTS IN SMALL SLAB MODELS"
Proceedings of the S.E.S.A.
Vol. 12, No. 2, pp. 83-98 (1955)

[56-1] Guild, J.
"THE INTERFERENCE SYSTEMS OF CROSSED DIFFRACTION GRATINGS. THEORY OF MOIRÉ FRINGES"
Oxford 1956

[56-2] Mesmer, G.
"THE INTERFERENCE SCREEN METHOD FOR ISOPACHIC PATTERNS"
Proceedings of the S.E.S.A.
Vol. 13, No. 2, pp. 21-26 (1956)

[57-1] Crisp, J.D.C.
"THE MEASUREMENT OF PLANE STRAINS BY A PHOTOSCREEN METHOD"
Proceedings of the S.E.S.A.
Vol. 15, No. 1, pp. 65-76 (1957)

[57-2] Linge, J.R.
"MECHANICAL INTERFERENCE IN THE MEASUREMENT OF STRAIN "
Aircraft Engineering
Vol. 29, No. 337, pp. 70-74 (1957)

[58-1] Dantu, P.
"UTILISATION DES RÉSEAUX POUR L'ÉTUDE DES DÉFORMATIONS"
Annales de l'Institut technique du Batiment et des Travaux Publics
Vol. 11, No. 121, pp. 78-98 (1958)

[59-1] Bradley, W.A.
"LATERALLY LOADED THIN FLAT PLATES"
Proceedings of the A.S.C.E.
Journal of Eng.Mech.Div.
Vol. 85, No. EM4, pp. 77-107 (1959)

[60-1] Pirard, A.
"CONSIDERATIONS SUR LA MÉTHODE DU MOIRÉ EN PHOTOELASTICITÉ"
Revue Universelle des Mines, 9. Serie
Vol. 16, No. 4, pp. 1-24 (1960)

[60-2] Morse, S., Durelli, A.J. & Sciammarella, C.A.
"GEOMETRY OF MOIRÉ FRINGES IN STRAIN ANALYSIS"
Proceedings of the A.S.C.E.
Journal of Eng.Mech.Div.
Vol. 86, No. EM4, pp. 105-126 (1960)

[60-3] Vinckier, A. & Dechaene, R.
"USE OF THE MOIRÉ EFFECT TO MEASURE PLASTIC STRAIN"
Journal of Basic Engineering
Transactions of the A.S.M.E.
Vol. 82, Series D.No. 2, pp. 426-434 (1960)

[60-4] Tanaka, K. & Nakashima, M.
"STRAIN MEASUREMENT BY PHOTOGRATING"
Proceedings of the Third Japan Congress on Testing Materials
pp. 161-163, Kyoto 1960

[60-5] Guild, J.
"DIFFRACTION GRATINGS AS MEASURING SCALES"
London 1960

[60-6] Burch, J.M.
"PHOTOGRAPHIC PRODUCTION OF SCALES FOR MOIRÉ FRINGE APPLICATIONS"
Optics in Metrologi. Edited by P. Mollet
pp. 361-368 (1960)

[61-1] Sciammarella, C.A. & Durelli, A.J.
"MOIRÉ FRINGES AS A MEANS OF ANALYSING STRAINS"
Proceedings of the A.S.C.E.
Journal of the Eng.Mech.Div.
Vol. 87, No. EM1, pp. 51-74 (1961)

[61-1.a]Morse, S.
"DISCUSSION OF [61-1]"
Transactions of the A.S.C.E.
Vol. 126, part 1, pp. 601-603 (1962)

[62-1] Dew, G.D.
"MULTI-SECTIONAL GRATINGS FOR LINEAR MEASUREMENT"
Journal of Scientific Instruments
Vol. 39, pp. 141-144 (1962)

[63-1] Košťák, B.
"MOIRÉ APPEARING WITH LARGE STRAINS OF FUNDAMENTAL LINE WARPS"
Acta Technica ČSAV
Vol. 8, pp. 57-580 (1963)

[63-2] Durelli, A.J., Sciammarella, C.A. & Parks, V.J.
"INTERPRETATION OF MOIRÉ PATTERNS"
Proceedings of the A.S.C.E.
Journal of Eng.Mech.Div.
Vol. 89, No. EM2 part 1, pp. 71-88 (1963)

[63-3] Shepherd, A.T.
"RECENT DEVELOPMENTS IN MOIRÉ FRINGE MEASURING SYSTEMS FOR MACHINE TOOL CONTROL"
International Journal of Machine Tool Design & Research.
Vol. 3, pp. 47-59 (1963/64)

[63-4] Wong, G.S.K. & Koenigsberger, F.
"THE EFFECT OF SOME ALIGNMENTS ERRORS ON THE ACCURACY OF A DIFFRACTION-GRATING MEASURING SYSTEM"
Ibid. [63-3] pp. 139-158

[63-5] Wong, G.S.K.
"AN INTERPOLATION ARRANGEMENT TO IMPROVE THE SENSITIVITY OF A DIFFRACTION-GRATING MEASURING SYSTEM"
Ibid. [63-3] pp. 211-217

[63-6] Françon, M.
"MODERN APPLICATIONS OF PHYSICAL OPTICS"
London 1963

[64-1] Bjerge, T.
"OPTICS" (lecturebook in Danish)
Copenhagen 1964

[64-2] Oster, G.,Wassermann, M. & Zwerling, C.
"THEORETICAL INTERPRETATION OF MOIRÉ-PATTERNS"
Journal of the Optical Society of America
Vol. 54, No. 2, pp. 169-175 (1964)

[64-3] Oster, G.
"REPRESENTATION AND SOLUTION OF OPTICAL PROBLEMS BY MOIRÉ-PATTERNS"
Proceedings of the Symposium on QUASI-OPTICS
New York (1964) pp. 59-69

[64-4] Parks, V.J. & Durelli, A.J.
"VARIOUS FORMS OF THE STRAIN-DISPLACEMENT RELATIONS APPLIED TO EXPERIMENTAL STRAIN ANALYSIS"
Experimental Mechanics
Vol. 4, No. 2, pp. 37-47 (1964)

[64-5] McIlraith, A.H.
"A MOIRÉ FRINGE INTERPOLATOR OF HIGH RESOLUTION"
Journal of Scientific Instruments
Vol. 41, pp. 34-37 (1964)

[65-1] Theocaris, P.S. & Kuo, H.-H.
"THE MOIRÉ METHOD OF ZONAL AND LINE GRATINGS"
Experimental Mechanics
Vol. 5, No. 8, pp. 267-272 (1965)

[65-2] Sciammarella, C.A., Ross, B.E. & Sturgeon, D.
"BASIC OPTICAL LAW IN THE INTERPRETATION OF MOIRÉ PATTERNS APPLIED TO THE ANALYSIS OF STRAINS",
Part 1 & 2
Experimental Mechanics
Vol. 5, Nos.5 and 6, pp. 154-166 (1965)

[65-3] Zandman, F., Holister, G.S., & Brcic, V.
"THE INFLUENCE OF GRID GEOMETRY ON MOIRÉ FRINGE PROPERTIES"
Journal of Strain Analysis
Vol. 1, No. 1, pp. 1-10

[65-4] Chiang, F.P.
"A METHOD TO INCREASE THE ACCURACY OF MOIRÉ METHOD"
Proceedings of the A.S.C.E.
Journal of Eng.Mech.Div.
Vol. 91, No. EM1, pp. 137-149 (1965)

[65-4.a]Middleton, E.
DISCUSSION OF [65-4]
Ibid. Vol. 91, No. EM5, pp. 227-232

[65-5] Post, D.
"THE MOIRÉ GRID-ANALYZER METHOD FOR STRAIN ANALYSIS"
Experimental Mechanics
Vol. 5, No. 11, pp. 368-377 (1965)

[65-5.a]Parks, V.J.
DISCUSSION OF [65-5]
Experimental Mechanics
Vol. 6, No. 5, pp. 287-288 (1966)

[65-6] Diruy, M.
"EXTENSOMETRE DE HAUTE SENSIBILITÉ POUR MEASURES SUR GRANDE BASE"
RILEM-Bulletin No. 26, pp. 96-100 (1965)

[65-7] Sim, P.J.
"A CONSTANT GAP MOIRÉ FRINGE READING HEAD"
Journal of Scientific Instruments
Vol. 42, pp. 156-157 (1965)

[65-8] Born, M. & Wolf, E.
"PRINCIPLES OF OPTICS"
Oxford 1965

[65-9] Rieder, G. & Ritter, R.
"KRÜMMUNGSMESSUNG AN BELASTETEN PLATTEN NACH DEM LIGTENBERGSCHEN MOIRÉ-VERFAHREN"
Forschung im Ingenieurwesen
Vol. 31, No. 2, pp. 33-44 (1965)

[66-1] Košťák, B. & Popp, K.
"MOIRÉ STRAIN GAUGES"
Strain
Vol. 2, No. 2, pp. 5-16 (1966)

[66-2] Holister, G.S., Jones, W.E.M. & Luxmoore, A.R.
"A MOIRÉ EXTENSOMETER"
Strain
Vol. 2, No. 4, pp. 27-33 (1966)

[66-3] McIlraith, A.H. & Scott, A.D.C.
"A DYNAMIC MOIRÉ FRINGE INTERPOLATOR"
Journal of Scientific Instruments
Vol. 43, No. 8, pp. 585-587 (1966)

[66-4] Russel, A.
"AN ABSOLUTE DIGITAL MEASURING SYSTEM USING OPTICAL GRATING AND SHAFT ENCODER"
N.E.L. Report No. 233
National Engineering Laboratory (July 1966)

[66-5] Ross, B.E.
"OBJECTIVE EXPERIMENTAL STRESS ANALYSIS USING THE MOIRÉ METHOD"
Developments in Theoretical and Applied Mechanics
Vol. 3, pp. 397-418 (1967)

[66-6] Sciammarella, C.A. & Sturgeon, D.
"SUBSTANTIAL IMPROVEMENTS IN THE PROCESSING OF MOIRE DATA BY OPTICAL AND DIGITAL FILTERING"
V.D.I.-Berichte No. 102, pp. 71-74 (1966)

[66-7] de Haas, H.M. & Loof, H.W.
"AN OPTICAL METHOD TO FACILITAETE THE INTERPRETATION OF MOIRÉ PICTURES"
V.D.I.-Berichte No. 102, pp. 65-70 (1966)

[66-8] Dantu, P.
"MOIRÉ DU DEUXIEME ORDRE - MÉTHODE PERMETTANT D'OBTENIR DIRECTEMENT LES LIGNES D'ÉGALE DILATATION LINÉIQUE"
Revue Francaise de Mechanique
Jan. - Mar. 1966 No. 17, pp. 55-62

[66-9] Parks, V.J. & Durelli, A.J.
"MOIRÉ PATTERNS OF PARTIAL DERIVATIVES OF DISPLACEMENT COMPONENT"
Journal of Applied Mechanics
Transactions of the A.S.M.E.
Vol. 33, Series E, No. 4, pp. 901-906 (1966)

[66-10] Söderquist, B.
"MEASUREMENT OF BIAXIAL CREEP STRAINS USING THE MOIRÉ METHOD"
Acta Polytechnica Scandinavica
Physics including Nucleonics Series No. 43 (Ph 43)
Stockholm (1966)

[67-1] Post, D.
"SHARPENING AND MULTIPLICATION OF MOIRÉ FRINGES"
Experimental Mechanics
Vol. 7, No. 4, pp. 154-159 (1967)

[67-2] Durelli, A.J. & Parks, V.J.
"MOIRÉ FRINGES AS PARAMETRIC CURVES"
Experimental Mechanics
Vol. 7, No. 3, pp. 97-104 (1967)

[67-3] Vafiadakis, A.P. & Lamble, J.H.
"THE APPLICATION OF MOIRÉ ROTATIONAL MISMATCH TECHNIQUE TO STRAIN ANALYSIS"
Journal of Strain Analysis
Vol. 2, No. 2, pp. 99-108 (1967)

[67-4] Fidler, R. & Nurse, P.
"FURTHER DEVELOPMENTS IN THE MOIRÉ TECHNIQUE OF STRAIN ANALYSIS"
Laboratory Report No. RD/L/R 1479
C.E.R.L. (Central Electricity Research Laboratories)
Leatherhead, Surrey (1967)

[67-5] Oster, G.
"HOLOGRAPHY AS A MOIRÉ PHENOMENON"
Proceedings of the Symposium on MODERN OPTICS
New York (1967), pp. 541-551.

[67-6] Vafiadakis, A.P.
"TWO MOIRÉ INSTRUMENTS"
Journal of Scientific Instruments
Vol. 44, No. 12, pp. 1008-1010 (1967)

[67-7] Hsu, H.P.
"OUTLINE OF FOURIER ANALYSIS"
Associated Educational Services Corp.
New York 1967

[67-8] Post, D.
"ANALYSIS OF MOIRÉ FRINGE MULTIPLICATION PHENOMENA"
Applied Optics
Vol. 6, No. 11, pp. 1938-1942 (1967)

[67-9] Sciammarella, C.A. & Lurowist, N.
"MULTIPLICATION AND INTERPOLATION OF MOIRÉ FRINGE ORDERS BY PURELY OPTICAL TECHNIQUES"
Journal of Applied Mechanics
Transactions of the A.S.M.E.
Vol. 34, Series E, No. 2, pp. 425-430 (1967)

[67-10] Sciammarella, C.A.
"TECHNIQUES OF FRINGE INTERPOLATION IN MOIRÉ PATTERNS"
Experimental Mechanics
Vol. 7, No. 11, pp. 19A-30A (1967)

[67-11] Sciammarella, C.A. & Sturgeon, D.L.
"DIGITAL-FILTERING TECHNIQUES APPLIED TO THE INTERPOLATION OF MOIRÉ-FRINGES DATA"
Experimental Mechanics
Vol. 7, No. 11, pp. 468-475 (1967)

[67-12] Sturgeon, D.L.
"ANALYSIS AND SYNTHESIS OF A MOIRÉ PHOTO-OPTICAL SYSTEM"
Experimental Mechanics
Vol. 7, No. 8, pp. 346-352

[67-13] Sciammarella, C.A. & Doddington
"EFFECT OF PHOTOGRAPHIC-FILM NONLINEARITIES ON PROCESSING OF MOIRÉ-FRINGE DATA"
Experimental Mechanics
Vol. 7, No. 9, pp. 398-402 (1967)

[67-14] Sampson, R.C. & Campbell, D.M.
"THE GRID-SHIFT TECHNIQUE FOR MOIRÉ ANALYSIS OF STRAIN IN SOLID PROPELLANTS"
Experimental Mechanics
Vol. 7, No. 11, pp. 449-457 (1967)

[67-15] Irons, B.M. & Carter, M.
"A COMPUTER PROGRAMME TO INTERPRET LARGE STRAINS"
Strain
Vol. 3, No. 1, pp. 16-17 (1967)

[67-16] Heise, U.
"A MOIRÉ-METHOD FOR MEASURING PLATE CURVATURE"
Experimental Mechanics
Vol. 7, No. 1, pp. 47-48 (1967)

[67-16.a] Theocaris, P.S.
"DISCUSSION OF [67-16]"
Ibid. Vol. 8, No. 9, pp. 431-432 (1968)

[67-17] Beranek, W.J.
"HET RECHTSTREEKS WAPENEN VAN PLATTEN AAN DE HAND VAN MOIRÉFOTO'S"
Cement
Vol. 19, No. 6, pp. 203-209 (1967)

[68-1] de Lamotte, F.
"EXPLOITATION DES FRANGES D'INTERFERENCE DITES "D'ÉTALE EPAISSEUR" EN PHOTOELASTICITÉ"
Bulletin de la Société Royale des Sciences de Liege
Vol. 27, No. 1-2, pp. 64-75 (1968)

[68-2] Košťák, B.
"GENERAL INTERPRETATION OF MOIRÉ PATTERNS IN STRAIN ANALYSIS"
Journal of Strain Analysis
Vol. 3, No. 2, pp. 90-95 (1968)

[68-3] Holister, G.S. & Luxmoor, A.R.
"THE PRODUCTION OF HIGH-DENSITY MOIRÉ GRIDS"
Experimental Mechanics
Vol. 8, No. 5, pp. 210-216 (1968)

[68-3.a]Chiang, F.-P.
DISCUSSION OF [68-3]
Experimental Mechanics
Vol. 9, No. 6, pp. 286-288 (1969)

[68-4] Oster, G.
"MOIRÉ PATTERNS IN PHYSICS"
Endeavour
Vol. 27, No. 101, pp. 60-64 (1968)

[68-5] Theocaris, P.S.
"DIRECT TRACING OF ISOENTATICS BY MOIRÉ PATTERNS"
Materialprüfung
Vol. 10, No. 5, pp. 155-158

[68-6] Post, D.
"NEW OPTICAL METHODS OF MOIRÉ FRINGE MULTIPLICATION"
Experimental Mechanics
Vol. 8, No. 2, pp. 63-68 (1968)

[68-7] Post, D.
"MOIRÉ FRINGE MULTIPLICATION WITH NON-HOMOGENEOUS STRAIN FIELDS"
J.B.C.S.A. Conference, Recent Advances in Stress Analysis, pp. 6.16-6.18
Royal Aeronautical Society (1969)

[68-8] Luxmoore, A.R.
"APPLICATIONS OF THE TELECENTRIC PRINCIPLES IN OPTICAL STRAIN MEASUREMENTS"
Ibid [68-7], pp. 5.19-5.23

[68-9] Sciammarella, C.A. & Davies, D.
"GAP EFFECT IN MOIRÉ FRINGES OBSERVED WITH COHERENT MONOCHROMATIC COLLIMATED LIGHT"
Experimental Mechanics
Vol. 8, No. 10, pp. 459-466 (1968)

[68-10] Chiang, F.-P., Parks, V.J. & Durelli, A.J.
"MOIRÉ-FRINGE INTERPOLATION AND MULTIPLICATION BY FRINGE SHIFTING"
Experimental Mechanics
Vol. 8, No. 12, pp. 554-560 (1968)

[68-11] Parks, V.J.
"MOIRÉ ANALYSIS OF MOTION"
Ph.D. Dissertation
The Catholic University of America (1968)

[68-12] Bossaert, W., Dechaene, R. & Vinckier, A.
"COMPUTATION OF FINITE STRAINS FROM MOIRÉ DISPLACEMENT PATTERNS"
Journal of Strain Analysis
Vol. 3, No. 1, pp. 65-75 (1968)

[68-13] Beranek, W.J.
"RAPID INTERPRETATION OF MOIRÉ PHOTOGRAPHS"
Experimental Mechanics
Vol. 8, No. 6, pp. 249-256

[68-14] Beranek, W.J.
"MOIRÉMETHODE VOOR PLATEN"
De Ingenieur
Vol. 80, No. 23, pp. 0.65-0.78 (1968)

[68-15] Hinton, E. & Irons, B.
"LEAST SQUARES SMOOTHING OF EXPERIMENTAL DATA USING FINITE ELEMENT"
Strain
Vol. 4, No. 3, pp. 24-27 (1968)

[68-16] Pelzer-Bawin, G.
"SUR UNE PARTICULARITÉ PHOTOGRAPHIQUE DANS LA DOMAINE DU MOIRÉ"
Bulletin de la Société Royale des Sciences de Liege
Vol. 37, No. 3-4, pp. 182-185 (1968)

[69-1] Theocaris, P.S.
"MOIRÉ FRINGES IN STRAIN ANALYSIS"
Pergamon Press, Oxford (1969)

[69-2] Martin, L.P. & Ju, F.D.
"THE MOIRÉ METHOD FOR MEASURING LARGE PLANE DEFORMATIONS: GENERAL THEORY AND APPLICATION TO HOMOGENEOUS DEFORMATION"
Journal of Applied Mechanics
Transactions of the A.S.M.E.
Vol. 36, Series E, No. 3, pp. 385-391 (1969)

[69-3] Chiang, F.-P.
"DETERMINATION OF SIGNS IN MOIRÉ METHOD"
Proceedings of the A.S.C.E.
Journal of Eng.Mech.Div.
Vol. 95, No. EM6, pp. 1379-1391 (1969)

[69-3.a]Parks, V.J.
DISCUSSION OF [69-3]
Ibid. Vol. 96, No. EM4, pp. 503-505 (1969)

[69-4] Košťák, B.
"A NEW DEVICE FOR IN-SITU MOVEMENT DETECTION AND MEASUREMENT"
Experimental Mechanics
Vol. 9, No. 8, pp. 374-379 (1969)

[69-5] Chiang, F.-P.
"TECHNIQUES OF OPTICAL SPATIAL FILTERING APPLIED TO THE PROCESSING OF MOIRÉ-FRINGE PATTERNS"
Experimental Mechanics
Vol. 9, No. 11, pp. 523-526 (1969)

[69-6] Sciammarella, C.A.
"MOIRÉ-FRINGE MULTIPLICATIONS BY MEANS OF FILTERING AND A WAVE-FRONT RECONSTRUCTION PROCESS"
Experimental Mechanics
Vol. 9, No. 4, pp. 179-185 (1969)

[69-7] Theocaris, R.S.
"THE FORMATION, RETRIEVAL AND MULTIPLICATION OF THE MOIRÉ SIGNAL"
Materialprüfung
Vol. 11, No. 1, pp. 11-19 (1969)

[70-1] Durelli, A.J. & Parks, V.J.
"MOIRÉ ANALYSIS OF STRAIN"
Prentice-Hall, New Jersey (1970)

[70-2] Borchersen, E.
"THE MOIRÉ METHOD FOR MEASURING DEFORMATIONS"
Lecturenote No. F 16 (in Danish)
Structural Research Laboratory (1970)
Technical University of Denmark

[70-3] Martin, L.P. & Ju, F.D.
"THE MOIRÉ METHOD FOR MEASURING LARGE-PLANE NONHOMOGENEOUS DEFORMATIONS"
Experimental Mechanics
Vol. 10, No. 12, pp. 521-528 (1970)

[70-4] Danh, T.X. & Taylor, F.M.
"THE MOIRÉ-GRID ANALYZER METHOD FOR THE ANALYSIS OF FINITE STRAIN"
Experimental Mechanics
Vol. 10, No. 10, pp. 415-420 (1970)

[70-5] Dykes, B.C.
"ANALYSIS OF DISPLACEMENTS IN LARGE PLATES BY THE GRID-SHADOW MOIRÉ TECHNIQUE"
Experimental Stress Analysis and its Influence on Design
Proc. of the 4th Int.Conf. on Stress Analysis
Cambridge, April 1970, pp. 125-134

[70-6] Sciammarella, C.A., di Chirico, G. & Chang, T.-Y.
"MOIRÉ-HOLOGRAFIC TECHNIQUE FOR THREE-DIMENSIONAL STRESS ANALYSIS"
Journal of Applied Mechanics
Transactions of the A.S.M.E.
Vol. 37, Series E, No. 1, pp. 180-185 (1970)

[70-7] Ebbeni, J. & Rezette, Y.
"NOUVEAUX DEVELOPPEMENTS DE LA METHODE DES MOIRÉS APPLIQUEE A L'ETUDE DES STRUCTURES"
Ibid. [70-5], pp. 207-216 (1970)

[70-8] Ebbeni, J.
"NOUVEAUX ASPECTS DU PHÉNOMENE DE MOIRÉ"
Nouv. Rev. d'Optique appliquée
Vol. 1, No. 5, pp. 333-342
Vol. 1, No. 6, pp. 353-358 (1970)

[70-9] Rezette, Y.
"DIRECT MEASURE OF STRAIN BY AN EXTENSION OF MOIRÉ"
Strain
Vol. 6, No. 2, pp. 55-61 (1970)

[70-10] Boone, P. & van Beeck, W.
"MOIRÉ FRINGE MULTIPLICATION WITH SPATIALLY FILTERING PROJECTION SYSTEM"
Strain
Vol. 6, No. 1, pp. 14-21 (1970)

[70-11] Chiang, F.-P.
"MOIRÉ-ROSETTE METHOD FOR STRAIN ANALYSIS"
Proceedings of the A.S.C.E.
Journal of Eng.Mech.Div.
Vol. 96, No. EM6, pp. 1285-1289 (1970)

[70-12] Meadows. D.M., Johnson, W.O. & Allen, J.B.
"GENERATION OF SURFACE CONTOURS BY MOIRÉ PATTERNS"
Applied Optics
Vol. 9, No. 4, pp. 942-947 (1970)

[71-1] Borchersen, E.
"THE MOIRÉ METHOD FOR MEASURING DISPLACEMENTS AND DEFORMATIONS" (in Danish)
Lecturenote No. F 29
Structural Research Laboratory (1971)
Technical University of Denmark

[71-2] Post, D. & MacLaughlin, T.F.
"STRAIN ANALYSIS BY MOIRÉ-FRINGE MULTIPLICATION"
Experimental Mechanics
Vol. 11, No. 9, pp. 408-413 (1971)

[71-3] Askegaard, V.
"TRANSDUCERS" (in Danish)
Lecturenote No. F 25
Structural Research Laboratory (1971)
Technical University of Denmark

[71-4] Clark, J.A., Durelli, A.J. & Parks, V.J.
"SHEAR AND ROTATION MOIRÉ PATTERNS OBTAINED BY SPATIAL FILTERING OF DIFFRACTION PATTERNS"
Journal of Strain Analysis
Vol. 6, No. 2, pp. 134-142 (1971)

[71-5] Clark, J.A. & Durelli, A.J.
"SEPARATION OF ADDITIVE AND SUBTRACTIVE MOIRÉ PATTERNS"
Journal of Applied Mechanics
Transactions of the A.S.M.E.
Vol. 38, Series E, No. 1, pp. 266-269 (1971)

[71-6] Sciammarella, C.A. & Chang, T.Y.
"OPTICAL DIFFERENTIATION OF THE DISPLACEMENT PATTERNS USING SHEARING INTERFEROMETRY BY WAVEFRONT RECONSTRUCTION"
Experimental Mechanics
Vol. 11, No. 3, pp. 97-104 (1971)

APPENDIX B: DIFFRACTION THEORY, CALCULATION OF DISTRIBUTION OF LIGHT INTENSITY.

In this appendix we will study the theoretical side of the optical methods described in chapter 8. First, an account is given of the concepts of physical optics. This is followed by a survey of some concepts from the Fourier analysis, which is the mathematical tool used in the subsequent calculations.

In section B.3 the relationship between the distribution of the light intensity in a diffraction plane and in the appurtenant diffraction pattern is derived. In B.4, this is followed by a calculation of the diffraction pattern for a line grating, and in B.5, by a calculation of the distribution of the light intensity in the image plane when only certain parts of the diffraction pattern are allowed to pass the focal plane.

In corresponding calculations for two crossed line gratings are discussed in B.6 and B.7.

B.1 Basic Concepts of Physical Optics

Physical optics is based on Maxwell's equations for electro-magnetic fields (see, e.g. Born and Wolf [65-8]). Inter alia these equations govern the propagation of electro-magnetic waves in an arbitrary medium.

The most important of the types of waves fulfilling Maxwell's equations are the two harmonic types, viz. the plane wave and the spherical wave, whose electrical fields are given by:

$$\bar{E} = \bar{E}_o \cos(\bar{r}\cdot\bar{k} - \omega t) \qquad \text{(B.1-1)}$$

$$\bar{E} = \frac{1}{r}\bar{E}_o \cos(\bar{r}\cdot\bar{k} - \omega t) \qquad \text{(B.1-2)}$$

where

$\bar{E}$ = the electrical vector
$\bar{E}_o$ = a constant electrical vector
$\bar{r}$ = the position vector for the point
$\bar{k}$ = the wave vector = $k\,\bar{n}$

$\bar{n}$ = the normal vector of the wave surface
k = the wave number = $\frac{2\pi}{\lambda}$
λ = the wavelength
t = the time
ω = the angular frequency

An alternative way of writing these, which has proved advantageous from the point of view of the calculations, is the complex:

$$\bar{E} = \bar{E}_o \exp\{i(\bar{r}\cdot\bar{k} - \omega t)\} \qquad \text{(B.1-3)}$$

and

$$\bar{E} = \frac{1}{r}\bar{E}_o \exp\{i(\bar{r}\cdot\bar{k} - \omega t)\} \qquad \text{(B.1-4)}$$

where "i" is the imaginary unit and where the real part corresponds to (B.1-1 and B.1-2), while the imaginary part has no physical significance.

The light intensity $I\{\bar{r}\}$ is proportional to the time-averaged value of the square on the length of the light vector, also called the amplitude, i.e.

$$I\{\bar{r}\} = I_o < \bar{E}\cdot\bar{E}^k > \qquad \text{(B.1-5)}$$

where $\bar{E}^k$ denotes the complex conjugate to $\bar{E}$ and I_o is the factor of proportionality.

In the following treatment of the effect of diffraction and image formation, our interest is concentrated on the intensity distribution, and we can, therefore, neglect the time term $\exp\{-i\omega t\}$ in (B.1-3 and B.1-4). Further, in investigating the diffraction we can neglect the direction of the field vector, thereby restricting ourselves to treatment of a wave function in the form

$$U = U_o\{\bar{r}\} \exp\{i\,\bar{r}\cdot\bar{k}\} \qquad \text{(B.1-6)}$$

In the following this is denoted THE OPTICAL DISTURBANCE. $U_o\{\bar{r}\}$ is the amplitude at the point and is constant for plane

waves but is in inverse ratio to the distance from the centre in spherical waves, although only when it is assumed that the medium is not amplitude-absorbent, which is largely the case for atmospheric air.

Diffraction denotes the phenomena in optics that cannot be explained on the basis of the assumption in geometrical optics regarding the straight propagation of light, with sharp shadows, as illustrated in fig. B.1-1. Here, S is a point light source emitting spherical waves, and the question is then, what light intensity this will result in at another point Q when a screen with an opening A-B is placed between the two points.

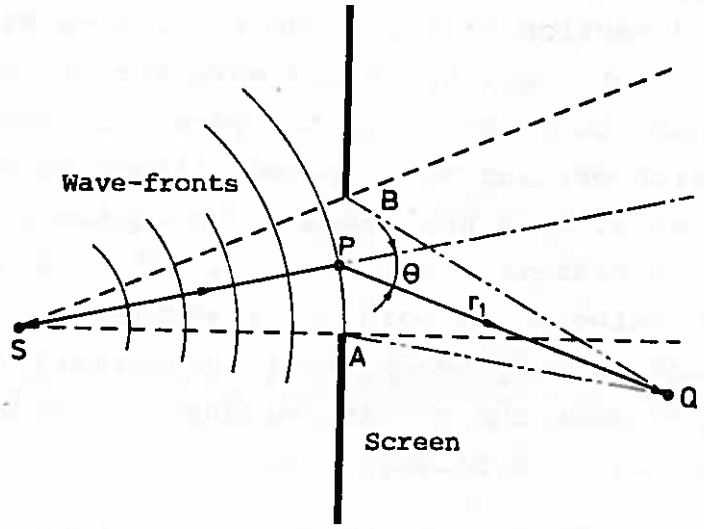

Figure B.1-1

If the question were to be examined on the basis of geometrical optics, the answer would be that no light is received at Q because the point is located in the geometrical shadow area. The fact that light intensity can, nevertheless, be observed in the geometrical shadow area can be explained on the basis of Huygen's principle, which states that all points on a wave surface are points of origin for secondary spherical waves.

The mathematical formulation of this is termed FRESNEL-KIRCHHOFF'S DIFFRACTION FORMULA, according to which the contribution of the primary wave point P to the optical disturbance at Q is given by

$$\boxed{dU_Q = C_o \frac{U_P}{r_1} \exp\{i\,k\,r_1\}\,[\cos\theta + 1]\,dA} \qquad \text{(B.1-7)}$$

where C_o is a constant, $r_1 = PQ$ and θ the angle between the elementary rays SP and PQ.

This can be interpreted as follows: The primary wave gives rise to an optical disturbance U_p at P. From an area element dA on the primary wave surface, a second spherical wave

$$\frac{U_P}{r_1} \exp\{i\,k\,r_1\}\,dA$$

is emitted, the contribution of which at Q has to be corrected by the direction factor $[\cos\theta + 1]$. This direction factor ensures that every spherical wave surface with its centre at S can also be regarded as the result of secondary spherical waves with origins on a second primary wave surface with centre at S. This applies as long as the primary spherical waves can radiate unhindered. If there is a screen with an opening between the point of transmission S and the point of reception Q, only the part of the primary wave surface that passes through the opening with secondary waves contributes to the optical disturbance at Q.

Before calculating the diffraction pattern, let us discuss in brief the Fourier-transforms since these, as mentioned earlier, form the basis for the calculations.

B.2 On Fourier Series, Fourier Transforms and Dirac's Delta Function.

The following is based on Hsu [67-7] and Sneddon [51-1].

According to Fourier Analysis a periodic function f{t} with the period T, i.e.

$$f\{t\} = f\{t + T\} \qquad \text{(B.2-1)}$$

which is piecewise continuous and absolutely integrable over a period T, can also be written

$$\boxed{f\{t\} = \frac{1}{2} a_o + \sum_{n=1}^{\infty} [a_n \cos\{n \omega_o t\} + b_n \sin\{n \omega_o t\}]} \quad (B.2\text{-}2)$$

where $\omega_o = \frac{2\pi}{T}$ = the angular frequency,

$$a_n = \frac{2}{T} \int_{-\frac{T}{2}}^{\frac{T}{2}} f\{t\} \cos\{n \omega_o t\}\, dt \quad (B.2\text{-}3)$$

$$b_n = \frac{2}{T} \int_{-\frac{T}{2}}^{\frac{T}{2}} f\{t\} \sin\{n \omega_o t\}\, dt \quad (B.2\text{-}4)$$

The function f{t}, shown in fig. B.2-1, is needed later, and the Fourier expansion is:

since $a_n = \frac{4}{p} \int_0^{\frac{1}{2}\beta p} E \cos\{n \frac{2\pi}{p} t\}\, dt$

$$= 2 E \beta \frac{1}{n \pi \beta} \sin\{n \pi \beta\}$$

and $b_n = 0$

i.e. $$\boxed{f\{t\} = E\beta [1 + 2 \sum_{n=1}^{\infty} \frac{1}{n \pi \beta} \sin\{n \pi \beta\} \cos\{\frac{2 n \pi t}{p}\}]} \quad (B.2\text{-}5)$$

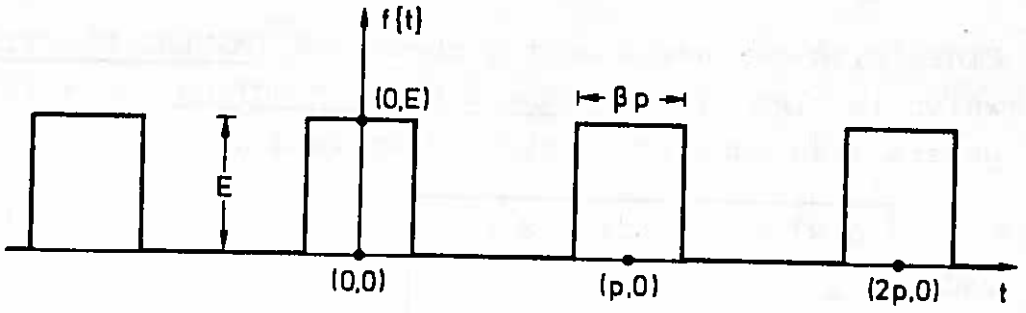

Figure B.2-1

If the function f{t} is piecewise differentiable and absolutely in the interval $-\infty < t < \infty$, a new function F{u} can be formed from it, called the FOURIER TRANSFORM of f{t}, given by

$$F\{u\} = \frac{1}{\sqrt{2\pi}} \int_{-\infty}^{\infty} f\{t\} \exp\{i\,u\,t\}\, dt \qquad \text{(B.2-6)}$$

and, further,

$$f\{t\} = \frac{1}{\sqrt{2\pi}} \int_{-\infty}^{\infty} F\{u\} \exp\{i\,u\,t\}\, du \qquad \text{(B.2-7)}$$

Analogously, the Fourier transforms of a function f{t,s} of two variables is given by

$$F\{u,v\} = \frac{1}{2\pi} \int_{-\infty}^{\infty} \int_{-\infty}^{\infty} f\{t,s\} \exp\{i(u\,t + v\,s)\}\, dt\, ds \qquad \text{(B.2-8)}$$

$$f\{t,s\} = \frac{1}{2\pi} \int_{-\infty}^{\infty} \int_{-\infty}^{\infty} F\{u,v\} \exp\{-i(u\,t + v\,s)\}\, du\, dv \qquad \text{(B.2-9)}$$

An important theorem in Fourier analysis is the so-called CONVOLUTION THEOREM, which states: If the two functions f{t,s} and g{t,s} have the Fourier transforms F{u,v} and G{u,v}, the convolution integral

$$H\{x,y\} = \int_{-\infty}^{\infty} \int_{-\infty}^{\infty} f\{t,x\}\, g\{x - t,\ y - s\}\, dt\, ds \qquad \text{(B.2-10)}$$

can also be written

$$H\{x,y\} = \int_{-\infty}^{\infty} \int_{-\infty}^{\infty} F\{u,v\}\, G\{u,v\} \exp\{-i(x\,u + y\,v)\}\, du\, dv \qquad \text{(B.2-11)}$$

Finally, a few words on the so-called IMPULSE FUNCTION $\delta\{x\}$, which is also called DIRAC'S DELTA FUNCTION. This is a generalized function, which is defined as

$$\delta\{x\} = 0 \quad \text{for} \quad x \neq 0 \qquad \text{(B.2-12)}$$

and

$$\int_{-\infty}^{\infty} \delta\{x\}\, dx = 1 \qquad \text{(B.2-13)}$$

It is thus not a function in the normal understanding of the word, with a given value at a given point. However, it is a considerable aid in the calculations, even though these can only be said to have formal validity.

The following rule of arethmetic applies, inter alia, with the delta function

$$\int_{-\infty}^{\infty} f\{x\}\,\delta\{x - a\}\,dx = f\{a\} \qquad \text{(B.2-14)}$$

$$\int_{-\infty}^{\infty} \delta\{a - x\}\,\delta\{b - x\}\,dx = \delta\{a - b\} \qquad \text{(B.2-15)}$$

$$\int_{-\infty}^{\infty} \delta\{x\}\,\exp\{-i\,v\,x\}\,dx = 1 \qquad \text{(B.2-16)}$$

$$\int_{-\infty}^{\infty} \exp\{i\,v\,x\}\,dv = 2\,\pi\,\delta\{x\} \qquad \text{(B.2-17)}$$

$$\int_{-\infty}^{\infty} \sin\{\omega_o\,x\}\,\exp\{-i\,v\,x\}\,dx = i\,\pi[\delta\{v + \omega_o\} - \delta\{v - \omega_o\}] \qquad \text{(B.2-18)}$$

$$\int_{-\infty}^{\infty} \cos\{\omega_o\,x\}\,\exp\{-i\,v\,x\}\,dx = \pi[\delta\{v + \omega_o\} + \delta\{v - \omega_o\}] \qquad \text{(B.2-19)}$$

The possibility is thus created of calculating with Fourier transforms to the functions $f\{x\} = 1$, $f\{x\} = \sin\{\omega_o\,x\}$ and $f\{x\} = \cos\{\omega_o\,x\}$ despite the fact that they are not absolutely integrable in the interval $-\infty < x < \infty$.

In the special case of the expanded function (B.1-5):

$$f\{t\} = \frac{1}{2}\,a_o + \sum_{n=1}^{\infty} a_n \cos\{n\,\omega_o\,t\} \qquad \text{(B.2-20)}$$

we then get the formal Fourier transform

$$\begin{aligned} F\{u\} &= \frac{1}{\sqrt{2\,\pi}} \int_{-\infty}^{\infty} f\{t\}\,\exp\{-i\,u\,t\}\,dt \\ &= \sqrt{\frac{\pi}{2}}\left[a_o\,\delta\{u\} + \sum_{n=1}^{\infty} a_n[\delta\{u - n\,\omega_o\} + \delta\{u + n\,\omega_o\}]\right] \\ &= \sqrt{\frac{\pi}{2}} \sum_{m=-\infty}^{m=\infty} a_m\,\delta\{u + m\,\omega_o\} \end{aligned} \qquad \text{(B.2-21)}$$

where $a_n = a_m$ with $n = |m|$.

B.3 Fourier Analysis of the Diffraction Pattern

We will now discuss the calculation of the distribution of the light intensity in the focal plane of a lens resulting from the passage of a plane wave through a diffracting plane. The light wave can, for example be produced by means of a laser, and it is assumed to be coherent and monochromatic. This means that the time factor can be neglected and that the wavelength is constant. Under reference to fig. B.3-1, it is assumed that plane waves radiate in the z-direction before encountering the diffracting object plane. In this there are apertures, and the part of the wave front passing through such an aperture gives rise to secondary spherical waves, the onward radiation of which will now be investigated. As the arriving wave front is parallel to the object plane, all secondary waves will start from this with the same phase.

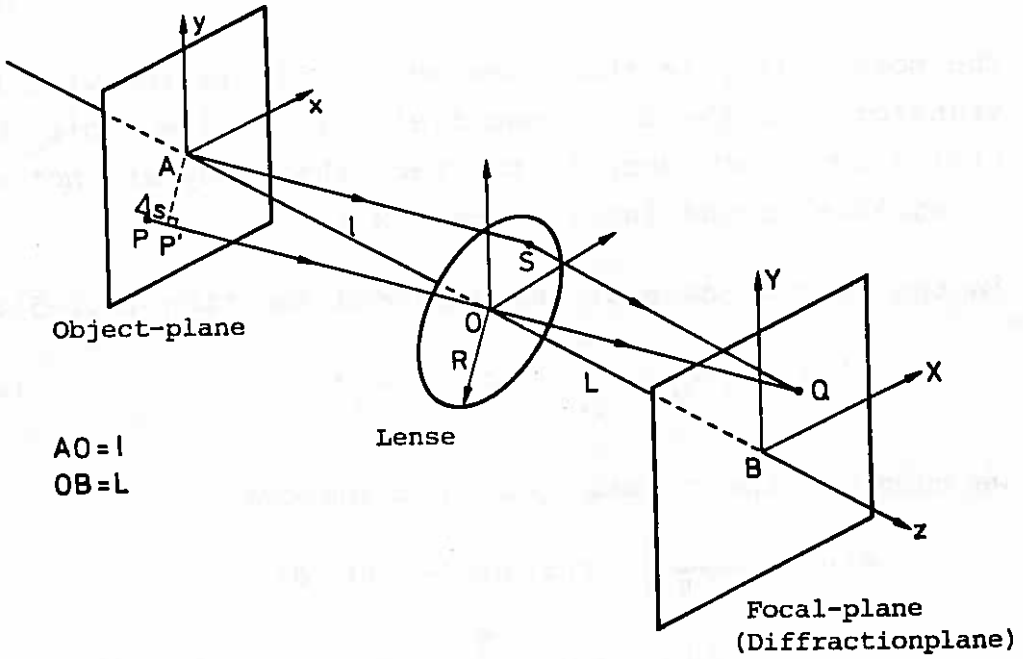

Figure B.3-1

At a distance AO = ℓ from the object plane, a converging lens with a focal length L is placed, and first, we will consider the distribution of the light intensity in the focal plane of

this lens. Optical disturbances from all points in the object plane will arrive at a certain point Q in the focal plane with the coordinates (X,Y).

Every secondary spherical wave from the object plane emits light rays in all directions, the contribution of which to the optical disturbance at Q is governed by the Fresnel-Kirchhoff diffraction formula (B.1-7). We further know from geometrical optics that parallel elementary rays arriving at a lens intersect each other at the same point after passing this.

It is now assumed that the distance OB is so great in relation to the diameter 2 R of the lens that the variation in the direction factor can be neglected. This further means that the variation in the optical distance traversed from the object plan to the focal plan is so small that the reduction in the amplitude by the distance can be taken to be the same for all elementary rays. It is, therefore, only the phase differences between the various wave fronts arriving that give rise to variations in the resulting optical disturbance and, thereby, in the light intensity.

Now the two elementary rays arriving at Q from A and P start with the same phase but traverse different optical distances.

This difference in optical distance Δs is equal to the distance from P to a normal plane through A to the direction of a ray. For the purposes of explanation, we can, for example, imagine that Q (see fig. B.3-2) emits spherical waves. After passing the lens, these become plane waves, and as points on the same wave surface have traversed the same optical distance, the difference in question will be equal to the distance $PP' = \Delta s$.

If the elementary ray leaving the object plane has the direction cosines α, β, and γ, and if the point P has the coordinates (x,y), this difference is given by

$$\Delta s = -(\alpha x + \beta y) \qquad \text{(B.3-1)}$$

in relation to the elementary ray from the point A with $x = y = 0$.

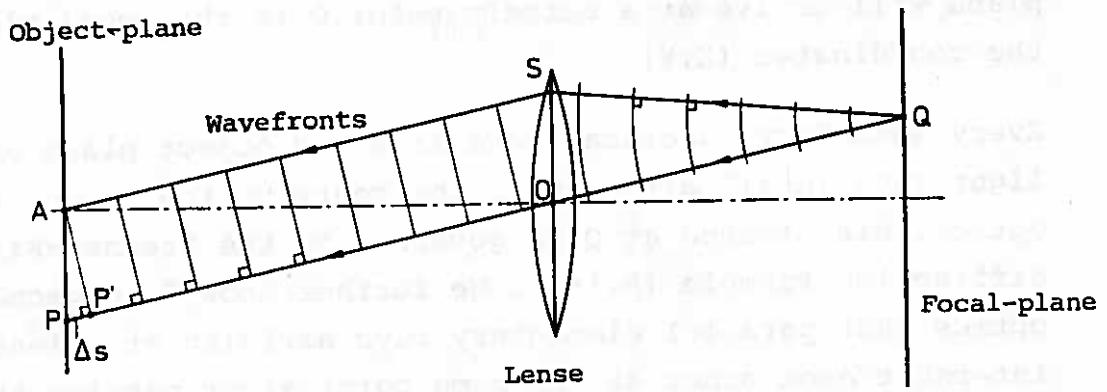

Figure B.3-2

The coordinates (X,Y) to the reception point Q can also be written

$$X \cong \alpha L \quad \text{and} \quad Y \cong \beta L \qquad \text{(B.3-2)}$$

for α and $\beta << 1$

since an elementary ray through the optical midpoint 0 of the lens will pass uninterrupted through the lens. A comparison of (B.3-1 and B.3-2) yields

$$\Delta s = -\left(x\frac{X}{L} + y\frac{Y}{L}\right) \qquad \text{(B.3-3)}$$

It is now practical to introduce two new quantities μ and ν, which are called SPATIAL FREQUENCIES and are defined as

$$\boxed{\mu = k\frac{X}{L} \qquad \nu = k\frac{Y}{L}} \qquad \text{(B.3-4)}$$

where $k = \frac{2\pi}{\lambda}$ = the wave number.

The optical difference in distance is then

$$\boxed{\Delta s = -\frac{1}{k}(x\mu + y\nu)} \qquad \text{(B.3-5)}$$

The phase factor in (B.1-7) $\exp\{i\,k\,r_1\}$ can now be written as follows at the point Q = (X,Y):

$$\exp\{i\,k(r_A + \Delta s)\} = \exp\{i\,k\,r_A\}\exp\{i\,k\,\Delta s\} \qquad \text{(B.3-6)}$$

where r_A is the optical length from A to Q. As this is constant,

the phase factor can also be written as follows, using (B.3-5):

$$\exp\{i\,k\,r_A\}\exp\{i\,k\,\Delta s\} = C_1 \exp\{-i[x\,\mu + y\,\nu]\} \qquad \text{(B.3-7)}$$

The amplitude term is now characterized by means of the TRANSMISSION FUNCTION $g\{x,y\}$ in the object plane, meaning that $g\{x,y\}dx\,dy$ is the amplitude of the diffracted wave originating from the area element $dx\,dy$. In the present case it is equal to a constant in the apertures in the object plane and zero outside these.

In the general theory of diffraction, the transmission function is defined as the ratio between departing and arriving optical disturbance and thus contains information on the phase distribution. With the present assumptions on phase coincidence for departing secondary waves, the definition used is not inconsistent with the general transmission function.

The resulting optical disturbance at point Q = (X,Y) of the focal plane can thus be written

$$U\{\mu,\nu\} = C_2 \int_{-\infty}^{\infty}\int_{-\infty}^{\infty} g\{x,y\}\exp\{-i[x\,\mu + y\,\nu]\}dx\,dy \qquad \text{(B.3-8)}$$

since the point Q is characterized by the spatial frequencies (μ,ν). It will be seen from this that, with the exception of one constant, the optical disturbance (the diffraction pattern) in the focal plane is equal to the Fourier transform of the transmission function.

B.4 The Diffraction Pattern of a Line Grating

Fig. B.4-1 shows an arrangement by which the diffraction pattern of a transmission line grating can be produced. A monochromatic point light source is placed at the focal point of lens 1, and the optical disturbance will, therefore, radiate as plane waves after passing this lens. The diffracting screen is a line grating with the pitch p, with its lines parallel to the x-axis, and with the ratio β between transparent spaces and pitch. The transmission function then

has the same form as fig. B.2-1 and can be written as

$$g\{x,y\} = E\beta[1 + \sum_{n=1}^{\infty} c_n \cos\{n \frac{2\pi}{p} y\}] \qquad (B.4\text{-}1)$$

where

$$c_n = \frac{2}{n\pi\beta} \sin\{n\pi\beta\} \qquad (B.4\text{-}2)$$

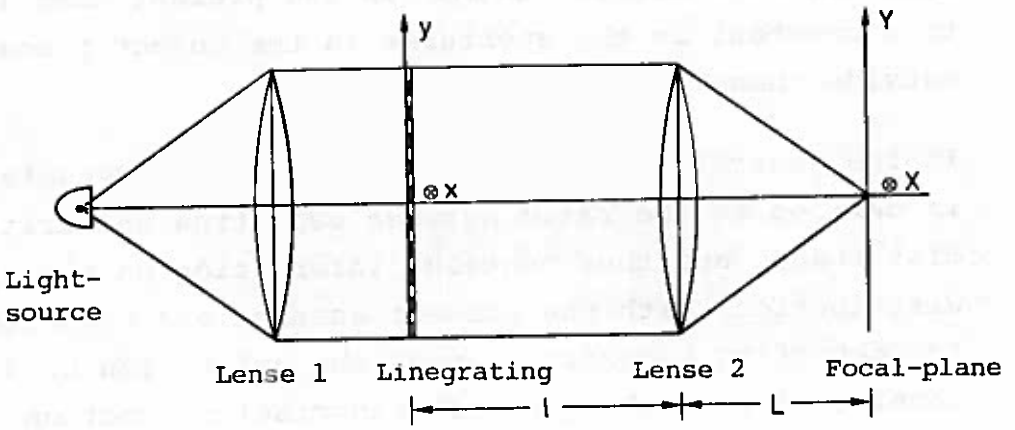

Figure B.4-1

The diffraction pattern of the line grating is obtained as the Fourier transform to (B.4-1), utilizing (B.2-17 and B.2-21):

$$G\{\mu,\nu\} = \frac{1}{2\pi}\int_{-\infty}^{\infty}\int_{-\infty}^{\infty} g\{x,y\} \exp\{-i[x\mu + y\nu]\}dx\,dy$$

$$= E\beta\pi\delta\{\mu\} \sum_{N=-\infty}^{N=\infty} c_N \delta\{\nu - N\frac{2\pi}{p}\} \qquad (B.4\text{-}3)$$

where $c_N = c_n$ with $n = |N|$.

The optical disturbance thus has extreme values at a number of discrete points in the focal plane, as indicated in fig. B.4-2.

The light intensity distributes itself in the same way along the Y-axis and is formally proportional to the square on the amplitude of the optical disturbance at the individual points. The formal calculations give the light intensity an infinitely great value at a number of points, although this is not, of course, the case in reality.

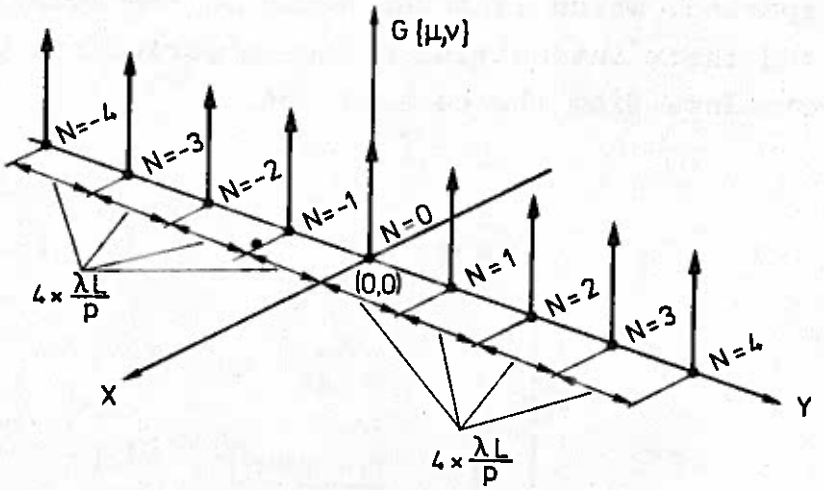

The Optical Disturbance in the Focal Plane

Figure B.4-2

One of the idealizations assumed has been that the grating extended an infinite length in the directions of both axes. If, instead, a finite grating length in the direction of the lines had been assumed, with M grating bars and with a transmission function equal to zero outside this zone, G{μ,ν} would have had the form,

$$G\{\mu,\nu\} = C \frac{\sin\{\frac{1}{2}\nu\beta p\}}{\frac{1}{2}\nu\beta p} \frac{\sin\{\frac{1}{2}M\nu p\}}{\sin\{\frac{1}{2}\nu p\}} \qquad \text{(B.4-4)}$$

This expression is taken from Hsu [67-7], page 277, and is also included in most books on optics. The appurtenant light intensity distribution I{X,Y} is proportional to the square on G{μ,ν}, and is as shown in fig. B.4-3 for $\beta = \frac{1}{4}$. It will be seen to have peak values at the same points as shown in fig. B.4-2. Between these, the distribution has secondary maximum values with function values that are much lower than the peak values.

The various light dots in the focal plane, og which the diffraction pattern is made up, are denoted DIFFRACTION ORDERS and are numbered according to the relevant N-value (cf. fig.

B.4-2 and B.4-3). All orders will be seen to have the same spacing, which is independent on the relative bar-width (1 - β) and their intensities decrease periodically with increasing distance from the central dot.

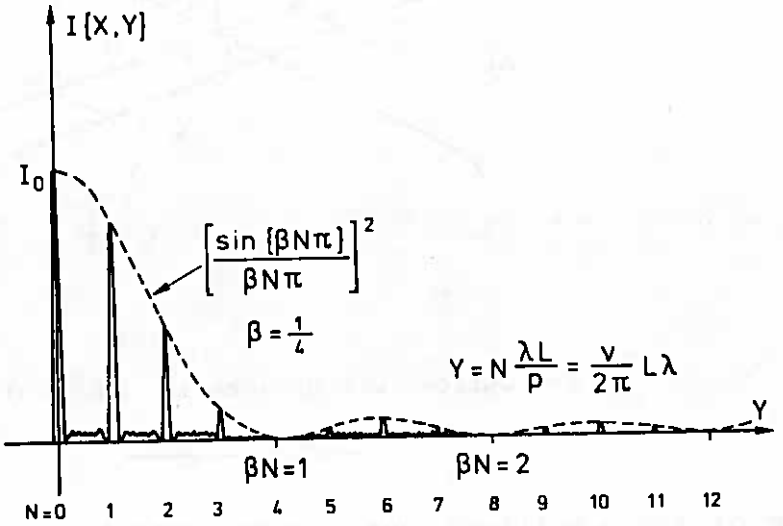

Figure B.4-3

The envelope corresponding to the first term in (B.4-4) has zero points when the product β N assumes integral values. From this it will be seen that the smaller β, the further there will be between the minima of the envelope. As β is the ratio between the grating space width and the pitch, this means that a greater, relative bar width (1 - β) results in increasing distance between minima.

An important factor appearing from the calculations is the relationship between the expansion (B.4-1) of the transmission function and the individual diffraction orders. Here,

> The diffraction orders $\pm N_o$ are produced by the N_o'th harmonic term in the Fourier expansion of the transmission function.

In other words, the central dot (N = 0) in the diffraction pattern is produced by the average disturbance β E in the

object plane. The basic wave (n = 1 in B.4-1) produces N = +1 and N = -1 etc. That is why it is possible to manipulate the image-formation of a grating by only letting selected diffraction orders pass the focal plane.

Finally, it will be seen from the calculations that the N'th diffraction order is produced by waves radiating in the direction

$$(\mu,\nu) = \left(0, N\frac{2\pi}{p}\right) \qquad \text{(B.4-5)}$$

or

$$\boxed{(\alpha,\beta,\gamma) = (0, N\frac{\lambda}{p}, \gamma)} \qquad \text{(B.4-6)}$$

where (α,β,γ) are the direction cosines of the elementary ray. (B.4-6) results from (B.4-5) by means of (B.3-2 and B.3-4)

B.5 Optical Filtering of a Line Grating

The arrangement shown in fig. B.4-1 is now enlarged with a screen, as shown in fig. B.5-1. The line grating is located a distance of twice the focal length from lens 2, and an image of the grating will then be formed at the same distance from the lens on the opposite side of this. In other words, all rays originating from a point on the line grating and passing lens 2 intersect each other at the same point on the image plane, where a screen is arranged to pick up the image. At the selected distance, an image in 1:1 is obtained.

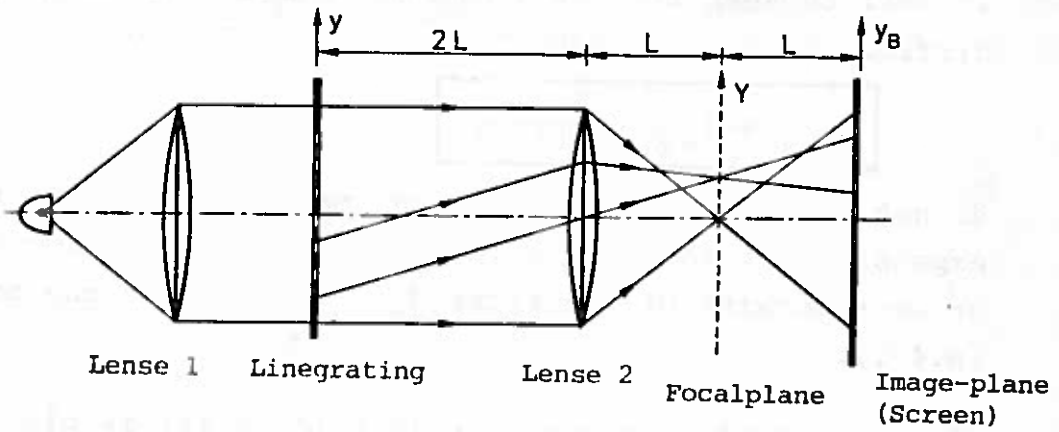

Figure B.5-1

If all light waves emitted from the grating passed through the lens the distribution of the light intensity would be the same in the plane of the grating as in the image plane.

However, part of the light from the plane of the light grating is emitted in the directions outside the lens, and this part must thus be deducted.

Taking a circular area of the grating about the optical axis with radius r, we can immediately find, by means of fig. B.5-2, the directions of radiation that do not pass through the lens. If the lens has an aperture of radius R, we get, for the two

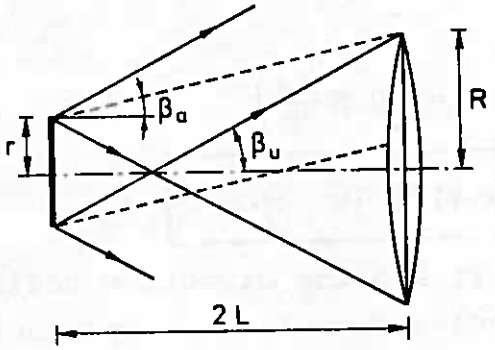

Figure B.5-2

direction cosines β_a and β_u:

$$\beta_a = \frac{R - r}{2L} \qquad \text{(B.5-1)}$$

$$\beta_u = \frac{R + r}{2L} \qquad \text{(B.5-2)}$$

Assuming that R > r, beams with direction cosines smaller than β_a will pass through the lens, while beams with $\beta > \beta_u$ will pass right outside it. For $\beta_a < \beta < \beta_u$, only part of the beam will pass the lens.

It will be seen from (B.4-6) and (B.5-2) that higher diffraction orders than

$$\boxed{N_{max} = \beta_u \frac{p}{\lambda} = \frac{R + r}{2L} \frac{p}{\lambda}} \qquad \text{(B.5-3)}$$

do not occur, and this, in turn, means that the Fourier expansion for the optical disturbance in the image plane will at most consist of the first $N_{max} + 1$ term in the expansion (B.4-1).

If a screen with an aperture (a hole in it) is placed in the focal plane, the aperture being of such a size and location that only the central diffraction dot can pass through it, the question is how the image (pattern) of the line grating will then look.

The optical disturbance in the image plane can either be obtained as the Fourier transform to the first term in (B.4-3) or simply by taking the first term in (B.4-1) since this resulted in the central diffraction order. Denoting the coordinates in the image plane (x_B, y_B), the optical disturbance $u_o\{x_B, y_B\}$ and the intensity $I_o\{x_B, y_B\}$, we get:

$$u_o\{x_B, y_B\} = \beta E \qquad \text{(B.5-4)}$$

$$I_o\{x_B, y_B\} = |u_o|^2 = \beta^2 E^2 \qquad \text{(B.5-5)}$$

in other words, a uniformly illuminated image surface without any grating effect.

If, instead, it is only the diffraction order +1 that slips through the aperture in the focal plane, we get the optical disturbance,

$$u_{+1}\{x_B, y_B\} =$$

$$\frac{1}{2\pi}\int_{-\infty}^{\infty}\int_{-\infty}^{\infty} E\beta\pi c_1 \delta\{\mu\}\,\delta\{\nu - \frac{2\pi}{p}\}\exp\{i(x_B\mu + y_B\nu)\}d\mu\,d\nu =$$

$$\frac{1}{2} E\beta c_1 \exp\{i\frac{2\pi}{p} y_B\} \qquad \text{(B.5-6)}$$

and the light intensity distribution,

$$I_{+1}\{x_B, y_B\} = |u_{+1}|^2 = \left(\frac{c_1}{2}\right)^2 (E\beta)^2 = \left(\frac{c_1}{2}\right)^2 I_o \qquad \text{(B.5-7)}$$

Thus, this, too, results in a uniformly illuminated image surface, but with a reduced light intensity.

If, instead, the screen is provided with two apertures, which allow the orders +1 and -1 through, we get the optical disturbance,

$$u_{\pm 1}\{x_B, y_B\} = E\beta c_1 \cos\left\{\frac{2\pi y_B}{p}\right\} \qquad \text{(B.5-8)}$$

and the light intensity

$$I_{\pm 1}\{x_B, y_B\} = I_o (c_1)^2 \cos^2\left\{\frac{2\pi y_B}{p}\right\} \qquad \text{(B.5-9)}$$

In other words, the image now has a varying light intensity with a distance of $\frac{1}{2}p$ between two maxima or two minima and the image has the character of a grating with half the pitch of the original grating. The line density in the grating has thus been doubled by the filtering. If the filter (the filtering screen in the focal plane) allows the passage of pairs of higher diffraction orders $\pm N$, we get, correspondingly,

$$u_{\pm N} = E\,\beta\,c_N \cos\{N\frac{2\pi}{p}y_B\} \qquad \text{(B.5-10)}$$

$$I_{\pm N} = I_o (c_N)^2 \cos^2\{N\frac{2\pi}{p}y_B\} \qquad \text{(B.5-11)}$$

The image will thus be a grating with $2N$ times as many lines as in the original. This is, in reality, the concept of optical multiplication. N_{max} (B.5-3) at any rate sets an upper bound for the multiplication, but in addition, the intensity is weakened at higher orders.

When the diffraction orders +1, 0 and -1 are allowed to pass the filter a grating with the same line density as the original grating is obtained. In this case,

$$u_{0\pm1}\{x_B, y_B\} = u_o + u_{\pm1} = E\,\beta[1 + c_1 \cos\{\frac{2\pi}{p}y_B\}] \qquad \text{(B.5-12)}$$

or

$$I_{0\pm1}\{x_B, y_B\} = I_o[1 + (c_1)^2 \cos^2\{\frac{2\pi}{p}y_B\} + 2\,c_1 \cos\{\frac{2\pi}{p}y_B\}] \qquad \text{(B.5-13)}$$

It will be seen that the intensity $I_{0\pm1}$ is periodic with the period p.

The difference between this intensity distribution and that of the original grating can be investigated by examining their visibilities V, which are defined by

$$V = \frac{I_{max} - I_{min}}{I_{max} + I_{min}} \qquad \text{(B.5-14)}$$

For the original grating (B.4-1) is

$$I_{max} = E^2 \quad \text{and} \quad I_{min} = 0$$

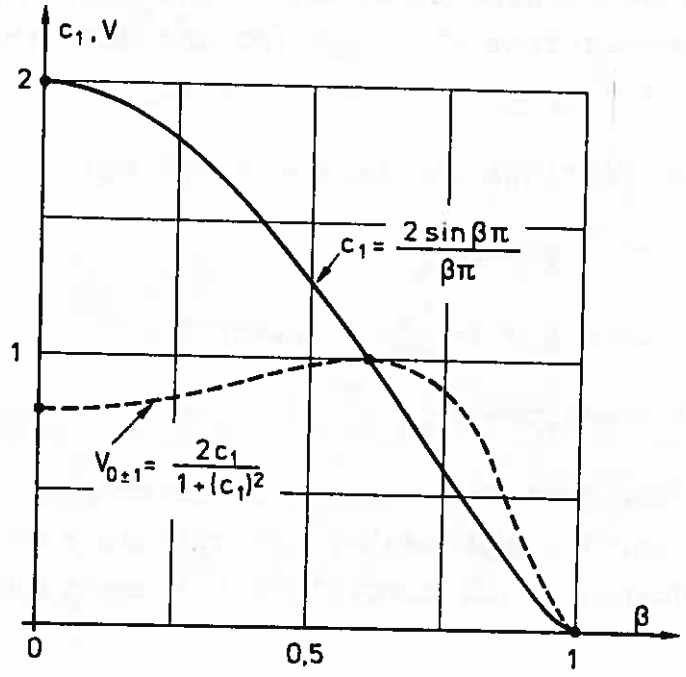

Figure B.5-3

i.e.

$$V_{original} = 1$$

For the grating (B.5-13), we get

$$I_{max} = I_o[1 + (c_1)^2 + 2\,c_1]$$

$$I_{min} = I_o[1 + (c_1)^2 - 2\,c_1]$$

from which

$$V_{0\pm1} = \frac{2\,c_1}{1 + (c_1)^2} \qquad \text{(B.5-15)}$$

This depends on the factor c_1, which in turn depends on the relative spacing width β (cf. (B.4-2)). These relations are shown in fig. B.5-3, and it will be seen that the visibility of the image of the grating is equal to that of the original when $\beta \simeq 0.6$.

B.6 The Diffraction Pattern of Two Crossed Line Gratings

Let us now, instead, place in the object plane in fig. B.5-1, two crossed line gratings (RG and MG), the locations of which in the x,y-system are shown in fig. B.6-1.

The two gratings can be described by:

$$MG : y = m\,p_m \tag{B.6-1}$$

$$RG : y = r\frac{p_r}{\cos\theta} + x\tan\theta \tag{B.6-2}$$

$$RG : y^* = r\,p_r \tag{B.6-3}$$

where the notation is as used in chapter 4. However, in addition, a supplementary coordinate system x* - y* is introduced, which simplifies the description of the grating RG.

If the two grating have the normalized transmission functions $g_m\{x,y\}$ and $g_r\{x,y\}$, the resulting transmission function $h\{x,y\}$ for the superposed gratings will be

$$\boxed{h\{x,y\} = E\,g_m\{x,y\}\,g_r\{x,y\}} \tag{B.6-4}$$

where E is the amplitude of the optical disturbance arriving at the object plane.

Then, from (B.3-8), we find that the optical disturbance $H\{\mu,\nu\}$ in the focal plane can be written:

$$H\{\mu,\nu\} = C\int_{-\infty}^{\infty}\int_{-\infty}^{\infty} g_m\{x,y\}\,g_r\{x,y\}\exp\{-i(x\mu + y\nu)\}dx\,dy \tag{B.6-5}$$

Using the "convolution theorem" (B.2-10 and B.2-11), we see that $H\{\mu,\nu\}$ can also be written

$$\boxed{H\{\mu,\nu\} = C\int_{-\infty}^{\infty}\int_{-\infty}^{\infty} G_m\{\mu - t,\ \nu - s\}\,G_r\{t,s\}dt\,ds} \tag{B.6-6}$$

where

$$G_m\{t,s\} = \frac{1}{2\pi}\int_{-\infty}^{\infty}\int_{-\infty}^{\infty} g_m\{x,y\}\exp\{i(x\,t + y\,s)\}dx\,dy \tag{B.6-7}$$

and analogously for $G_r\{t,s\}$.

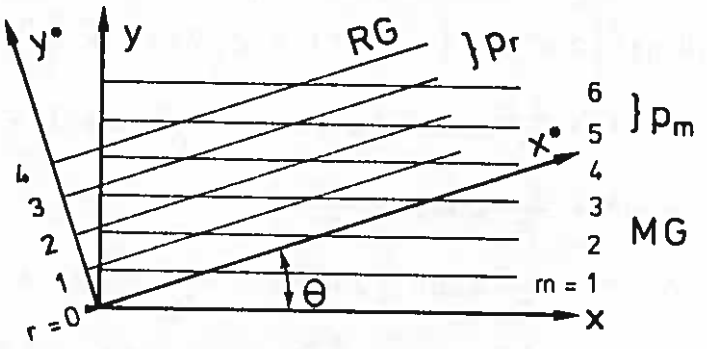

Figure B.6-1

If the relative spacing width (β) is identical for the two gratings, their transmission functions can be written

$$g_m\{x,y\} = \beta[1 + c_1 \cos\{2\pi m\} + c_2 \cos\{2 \cdot 2\pi m\} + \ldots] \qquad \text{(B.6-8)}$$

$$g_r\{x,y\} = \beta[1 + c_1 \cos\{2\pi r\} + c_2 \cos\{2 \cdot 2\pi r\} + \ldots] \qquad \text{(B.6-9)}$$

which is obtained from (B.4-1) with E = 1. In addition, it is assumed that

$$m = \frac{y}{p_m} \qquad \text{(B.6-10)}$$

$$r = \frac{1}{p_r}(y\cos\theta - x\sin\theta) = \frac{y^*}{p_r} \qquad \text{(B.6-11)}$$

If only the first two terms in (B.6-8 and B.6-9) are included, then analogously to (B.4-3), $G_m\{t,s\}$ and $G_r\{t^*,s^*\}$ become

$$G_m\{t,s\} = \beta\pi\delta\{t\}\left[2\delta\{s\} + c_1\delta\{s + \frac{2\pi}{p_m}\} + c_1\delta\{s - \frac{2\pi}{p_m}\}\right] \qquad \text{(B.6-12)}$$

and

$$G_r\{t^*,s^*\} = \beta\pi\delta\{t^*\}\left[2\delta\{s^*\} + c_1\delta\{s^* + \frac{2\pi}{p_r}\} + c_1\delta\{s^* - \frac{2\pi}{p_r}\}\right] \qquad \text{(B.6-13)}$$

Substituted in (B.6-6) we get:

$$
\begin{aligned}
H\{\mu,\nu\} = \\
& C(\beta\pi)^2\Big[2\,\delta\{\mu^*\}\Big(2\,\delta\{\nu^*\} + c_1\,\delta\{\nu^* + \frac{2\pi}{p_r}\} + c_1\,\delta\{\nu^* - \frac{2\pi}{p_r}\}\Big) \\
& + c_1\,\delta\{\mu^* + \frac{2\pi}{p_m}\sin\theta\}\Big(2\,\delta\{\nu^* + \frac{2\pi}{p_m}\cos\theta\} + c_1\,\delta\{\nu^* + \frac{2\pi}{p_m}\cos\theta + \frac{2\pi}{p_r}\} \\
& + c_1\,\delta\{\nu^* + \frac{2\pi}{p_m}\cos\theta - \frac{2\pi}{p_r}\}\Big) \\
& + c_1\,\delta\{\mu^* - \frac{2\pi}{p_m}\sin\theta\}\Big(2\,\delta\{\nu^* - \frac{2\pi}{p_m}\cos\theta\} + \\
& + c_1\,\delta\{\nu^* - \frac{2\pi}{p_m}\cos\theta + \frac{2\pi}{p_r}\} + c_1\,\delta\{\nu^* - \frac{2\pi}{p_m}\cos\theta - \frac{2\pi}{p_r}\}\Big)\Big]
\end{aligned}
$$

(B.6-14)

where

$$\mu^* = \mu\cos\theta + \nu\sin\theta$$

$$\nu^* = -\mu\sin\theta + \nu\cos\theta$$

The diffraction pattern is shown in fig. B.6-2, where the points in the focal plane at which the amplitude of the optical disturbance is infinite are plotted. There are 9 points in all. Had more of the terms in the expressions for the transmission function (B.6-8 and B.6-9) been included in the calculation of G_m and G_r in (B.6-12 and B.6-13), there would have been a correspondingly greater number of points in the diffraction pattern.

The nine points in fig. B.6-2 are provided with "the coordinates" [M,R], where M is the diffraction order in the diffraction pattern of the line grating MG to which the point corresponds, and analogously for R. It will be seen that the points [+1,0], [0,0] and [-1,0] are the diffraction pattern that would be produced by the line grating MG only, while RG on its own would give the points [0,+1], [0,0] and [0,-1]. The remaining four points, on the other hand, are due to the interplay between the two superposed line gratings.

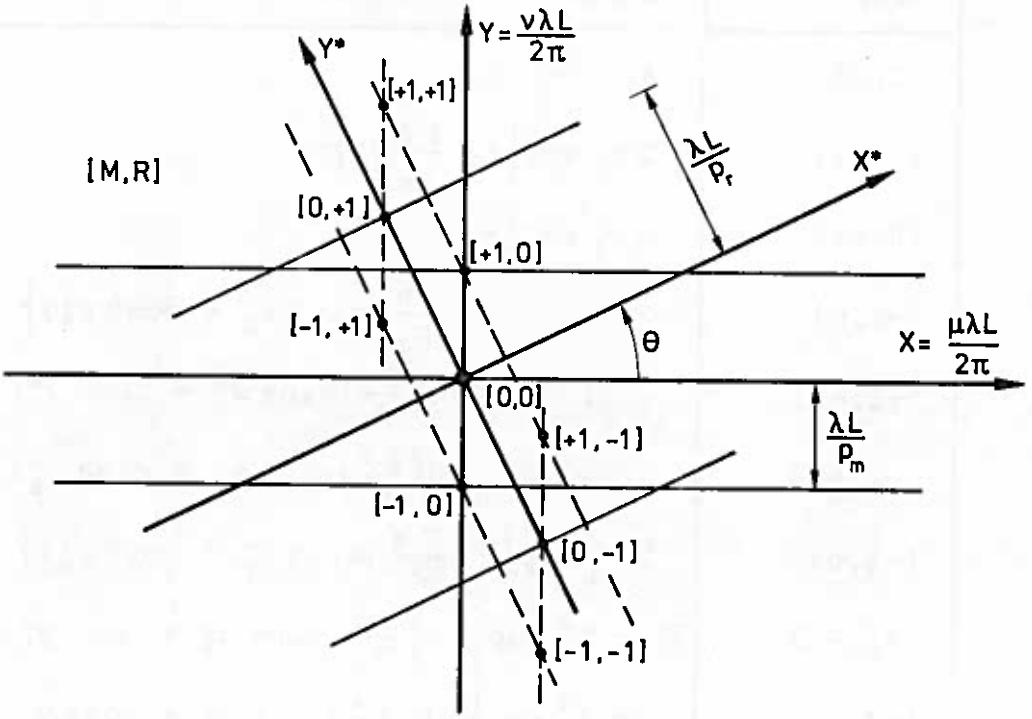

Diffraction pattern for two crossed line gratings

Figure B.6-2

B.7 Optical Filtering of a Moiré Pattern

As in the case of the filtering of the line grating in B.5, the image of two crossed gratings can be varied by suitable choice of diffraction patterns. The contributions of the various diffraction orders to the optical disturbance in the image plane are obtained, as earlier, by taking the Fourier transform of the corresponding term in (B.6-14). The contributions are as follows in table B.7-1.

Diffraction Order	Contribution to Optical Disturbance in the Image Plane. Factor $\frac{1}{2} C \pi \beta^2$
[0,0]	4
[0,-1]	$2 c_1 \exp\left\{- i \frac{2\pi}{p_r} y_B^*\right\}$
[0,+1]	$2 c_1 \exp\left\{+ i \frac{2\pi}{p_r} y_B^*\right\}$
[-1,0]	$2 c_1 \exp\left\{- i \frac{2\pi}{p_m} (\sin\theta\, x_B^* + \cos\theta\, y_B^*)\right\}$
[-1,-1]	$(c_1)^2 \exp\left\{- i\left(\frac{2\pi}{p_m}(\sin\theta\, x_B^* + \cos\theta\, y_B^*) + \frac{2\pi}{p_r} y_B^*\right)\right\}$
[-1,+1]	$(c_1)^2 \exp\left\{- i\left(\frac{2\pi}{p_m}(\sin\theta\, x_B^* + \cos\theta\, y_B^*) - \frac{2\pi}{p_r} y_B^*\right)\right\}$
[+1,0]	$2 c_1 \exp\left\{+ i \frac{2\pi}{p_m} (\sin\theta\, x_B^* + \cos\theta\, y_B^*)\right\}$
[+1,-1]	$(c_1)^2 \exp\left\{+ i\left(\frac{2\pi}{p_m} (\sin\theta\, x_B^* + \cos\theta\, y_B^*) - \frac{2\pi}{p_r} y_B^*\right)\right\}$
[+1,+1]	$(c_1)^2 \exp\left\{+ i\left(\frac{2\pi}{p_m} (\sin\theta\, x_B^* + \cos\theta\, y_B^*) + \frac{2\pi}{p_r} y_B^*\right)\right\}$

Table B.7-1

For the purposes of clarification, the following quantities will now be introduced:

$$r_B = \frac{1}{p_r} y_B^* \qquad \text{(B.7-1)}$$

$$m_B = \frac{1}{p_m} (\sin\theta\, x_B^* + \cos\theta\, y_B^*) \qquad \text{(B.7-2)}$$

which will be seen to describe two line gratings in the coordinate system (x_B^*, y_B^*) of the image plane. These are the images of the two line gratings in fig. B.6-1.

Table B.7-1 can now be written as shown in table B.7-2.

Diffraction Order	Contribution to Optical Disturbance in the Image Plane. Factor $\frac{1}{2} C \pi \beta^2$
[0,0]	4
[0,-1]	$2 c_1 \exp\{- i 2 \pi r_B\}$
[0,+1]	$2 c_1 \exp\{+ i 2 \pi r_B\}$
[-1,0]	$2 c_1 \exp\{- i 2 \pi m_B\}$
[-1,-1]	$(c_1)^2 \exp\{- i 2 \pi (m_B + r_B)\}$
[-1,+1]	$(c_1)^2 \exp\{- i 2 \pi (m_B - r_B)\}$
[+1,0]	$2 c_1 \exp\{+ i 2 \pi m_B\}$
[+1,-1]	$(c_1)^2 \exp\{+ i 2 \pi (m_B - r_B)\}$
[+1,+1]	$(c_1)^2 \exp\{+ i 2 \pi (m_B + r_B)\}$

Table B.7-2

Table B.7-3 gives the light intensity distribution for a number of related diffraction orders.

It will be seen from cases a, b and c that two or three diffraction orders corresponding to the same model grating diffraction order (M) will give an image with the same orientation as the reference grating. The period will also be the same if the order R = 0 is included (case a), while it will be halved if this is omitted (b and c). An analogous case for orders with the same R-value is shown in case f.

It will be seen that in case d, the diffraction orders [+1,+1], [0,0] and [-1,-1] vary periodically with the quantity $n_B^+ = r_B + m_B$ with the period $\Delta n_B^+ = 1$. It is precisely the additive moiré pattern formed by two line gratings with the parameters r_B and m_B that is given by this parametric description, and we have thus succeeded in producing this pattern by means of the optical filtering. Omitting the

Diffraction Order	Diffraction Pattern	Variation in Light Intensity in the Image Plane
a) [0,+1] + [0,0] + [0,-1]		$16[1 + (c_1)^2 \cos^2\{2\pi r_B\} + 2c_1\{2\pi r_B\}]$ (reference grating)
b) [0,+1] + [0,-1]	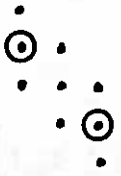	$16(c_1)^2 \cos^2\{2\pi r_B\}$ (reference grating doubled)
c) [+1,+1]+ [+1,-1]		$4(c_1)^2 \cos^2\{2\pi r_B\}$ (reference grating doubled)
d) [+1,+1]+ [-1,-1]+ [0,0]		$4[1 + (c_1)^2 \cos^2\{2\pi(r_B + m_B)\} + 2c_1 \cos\{2\pi(r_B + m_B)\}]$ (additive moiré pattern)
e) [+1,+1]+ [-1,-1]	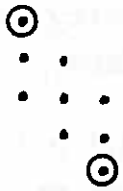	$4(c_1)^2 \cos^2\{2\pi(r_B + m_B)\}$ (additive moiré pattern doubled)
f) [+1,0] + [-1,0]		$16(c_1)^2 \cos^2\{2\pi m_B\}$ (model grating doubled)
g) [0,+1] + [+1,0]	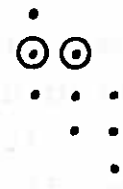	$8(c_1)^2 [1 + \cos\{2\pi(m_B - r_B)\}]$ (subtractive moiré pattern)
h) [-1,+1]+ [+1,-1]	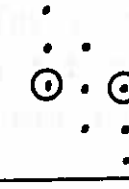	$4(c_1)^2 \cos^2\{2\pi(m_B - r_B)\}$ (subtractive moiré pattern doubled)

Table B.7-3

central order [0,0], we get, as shown in case e, the same orientation in the pattern as in case d, but the period is halved. The additive pattern has thus been multiplied by the factor 2. Cases g and h show entirely analogous conditions, in which the light intensity varies with the quantity $\bar{n}_B = m_B - r_B$. This corresponds to the subtractive moiré pattern formed by the two line gratings RG and MG, i.e. the pattern which is normalle observed as the moiré pattern for small values of θ and $p_m - p_r$, and on which the whole of chapter 4 of the report is based.

It is important to note here that the original grating lines have been filtered off in the patterns depicted.

Only the first two terms in (B.6-8 and B.6-9) were included in the calculations, i.e. the transmission function for the gratings is assumed to have a cosine variation with a period equal to the pitch. If further terms are included, a correspondingly greater number of diffraction orders will be obtained, and by optical filtering of these, we can obtain moiré patterns corresponding to the pitches that are fractions of those used here.

APPENDIX C

BRIGHT AND DARK MOIRÉ-FRINGES, OR VICE VERSA

As mentioned in connexion with fig. 2.5-1 of section 2.5, the formally bright moiré-fringes can, in some cases, appear as the darkest fringes in a moiré-pattern. As far as is known, this phenomenon has only been described and explained by Rieder and Ritter in [65-9] and Pelzer-Bawin in [68-16]. (Termed by the latter "Une particularité photographique dans la domaine du moiré".)

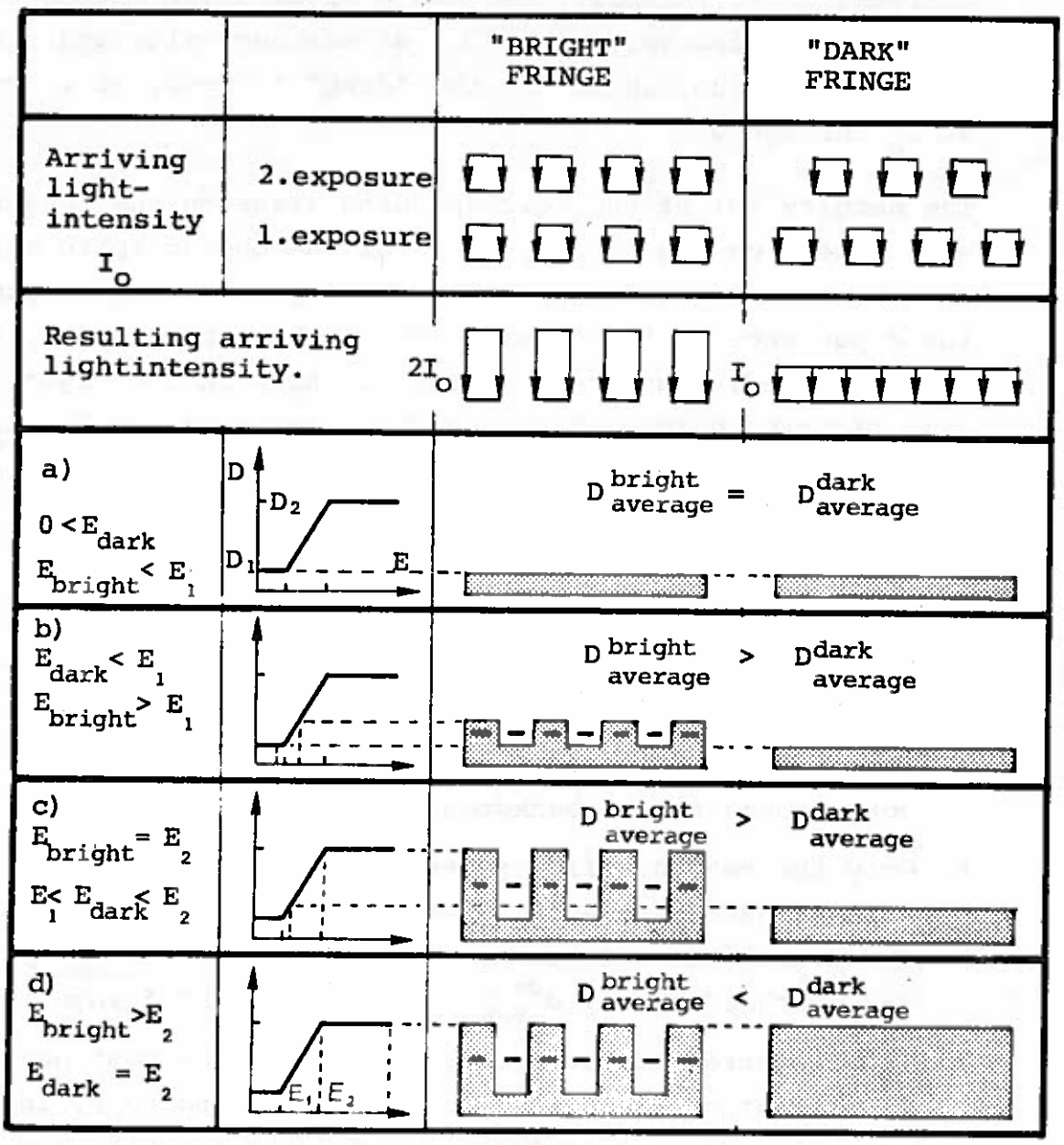

Figure C-1

Fig. C-1 provides an explanation of the case "double exposure" of a negative, where the grating photographed is, for example, rotated between the two exposures.

The top of the figure shows the arriving light intensity, which is equal to I_o, where there are spaces, and zero where there are grating bars. The "bright" fringes are formed where spaces from the 2nd exposure coincide with spaces from the 1st exposure, while the "dark" fringes are formed where grating bars fall in spaces. The resulting arriving light intensity becomes a block distribution for the "bright" fringes, with $2\,I_o$ as maximum value and zero as minimum value, while for the "dark" fringes, it is constant at I_o throughout.

The density (D) of the corresponding areas on the negative will depend on the density curve of the photographic material and the exposure time (Δt). The density curve, which expresses the dependence of the density (D) on the exposure (E), has the idealized, non-linear character shown in the figure, with background fogging D_1, which is constant for $E < E_2$. The exposure (E) is equal to the light intensity (I) times the exposure time (Δt), i.e.

$$E = I\,\Delta t$$

Fig. C.1-a, C.1-b and C.1-c show the density for various exposure times:

a) The exposure time is so short that the density only corresponds to the background fogging throughout.

b) Only the most heavily exposed areas in the "bright" fringes have become denser than the background fogging. The average density in the "bright" fringes $D^{bright}_{average}$ exceeds the average density $D^{dark}_{average}$ for the "dark" fringes.

c) The exposure time is increased wo that the most heavily exposed areas reach the density limit, and here, increased exposure will not increase the density further. The "bright" fringes are now fully developed, while with further

exposure, the "dark" fringes will increase in density until they, too, reach the density limit.

d) The dark fringes have now also reached the density limit, and for an exposure time of between Δt_c and Δt_d, $D^{dark}_{average}$ has become greater than $D^{bright}_{average}$.

In the case of further copying, the resulting positive will have its bright parts, where the average density of the negative is maximum. If the negative is exposed corresponding to case c), $D^{bright}_{average}$ will be greatest, and the "bright" fringes will be brightest on the positive, while exposure corresponding to d) will make the "dark" fringes brightest.

It will be seen from this that <u>if a negative is over-exposed, the "dark" fringes</u> on the final positive <u>will appear as the "brightest" fringes, and vice versa.</u>

AFDELINGEN FOR BÆRENDE KONSTRUKTIONER
DANMARKS TEKNISKE HØJSKOLE

Structural Research Laboratory
Technical University of Denmark, DK-2800 Lyngby

RAPPORTER (Reports)

(1970 -

R 11.	Bræstrup, Mikael W.: The Cosserat Surface and Shell Theory. 1970.	Out of print
R 12.	Askegaard, Vagn: Anvendelse af modelanalyse. 1970.	
R 13.	Solnes, Julius: The Spectral Character of Earthquake Motions. 1970.	Out of print
R 14.	Bræstrup, Mikael W.: Yield Lines in Discs, Plates and Shells. 1970.	Out of print
R 15.	Møllmann, J.: Beregning af hængekonstruktioner ved hjælp af deformationsmetoden. 1970.	Out of print
R 16.	Byskov, Esben: The calculation of Stress Intensity Factors Using the Finite Element Method with Cracked Elements. 1970.	
R 17.	Askegaard, V.: Grundlaget for adhæsion. 1970.	
R 18.	Summaries of Lecture Notes on Experimental Stress Analysis. 1970.	Out of print
R 19.	Sørensen, Hans Christian: Forskydning i jernbeton-bjælker. 1970.	
R 20.	Sørensen, Hans Christian: Forskydningsforsøg med 12 jernbetonbjælker med T-tværsnit. 1971.	
R 21.	Møllmann, H.: Analysis of Hanging Roofs Using the Displacement Method. 1971.	Out of print
R 22.	Haurbæk, Poul E.: Dæmpede svingninger i spændbeton-bjælker. Svingningsforsøg med simpelt understøttede bjælker.	Publication pending
R 23.	Bræstrup, M.W.: Yield-line Theory and Limit Analysis of Plates and Slabs. 1971.	
R 24.	Dyrbye, Claës: Pendulum Vibration. 1971.	Out of print
R 25.	Møllmann, H.: Analytical Solution for a Cable Net over a Rectangular Plan. 1971.	
R 26.	Nielsen, J.: Silotryk. 1972.	Out of print
R 27.	Askegaard, V., M. Bergholdt and J. Nielsen: Problems in connection with pressure cell measurements in silos. 1972.	
R 28.	Ramirez, H. Daniel: Buckling of plates by the Ritz methods using piecewise-defined functions. 1972.	
R 29.	Thomsen, Kjeld & Henning Agerskov: Behaviour of butt plate joints in rolled beams assembled with prestressed high tensile bolts. 1972.	
R 30.	Julius Solnes and Ragnar Sigbjörnsson: Structural response to stochastic wind loading. 1972.	
R 31.	H. J. Larsen og H. Riberholt: Forsøg med uklassificeret konstruktionstræ. 1972.	

R 32. Vagn Askegaard: Programme and methods of teaching of experimental mechanics. 1972. Out of print

R 33. Julius Solnes and Ole Holst: Weight optimization of framed structures under earthquake loads. 1972.

R 34. Rostam, Steen and Esben Byskov: Cracks in Concrete Structures. A Fracture Mechanics Approach. 1973.

R 35. Sørensen, Hans Chr.: Efficiency of Bent-up Bars as Shear Reinforcement. 1973.

R 36. Krenk, Steen: Singulær integralformulering af nogle plane friktionsfri kontaktproblemer. 1973.

R 37. Philipsen, Claus: An investigation of the stability of columns with thin-walled open cross-section. 1973.

R 38. Theilgaard, Esko: Integralligningsmetoder anvendt på problemer inden for bygningsstatikken. 1973.

R 39. Henrichsen, Lars: Linearly viscoelastic finite elements. 1973.

R 40. Bryndum, Mads: Litteraturstudium vedrørende let konstruktionsbeton. 1973.

R 41. Holst, Ole: Beregning af plane rammekonstruktioner med geometrisk ikkelinearitet. 1973.

R 42. Krenchel, Herbert: Rupture criteria for FRC-materials. 1973.

R 43. Borchersen, Egil: Moire pattern deformation theory and optical filtering techniques. 1974.

R 44. Brøndum-Nielsen, Troels: Optimum design of reinforced concrete shells and slabs. 1974.

R 45. Pedersen, Flemming Bligaard: Dynamic properties of anti-vibration mountings. 1974.

R 46. Philipsen, Claus: Interferensholografisk bestemmelse af legemers form og flytningsfelt. 1974.

R 47. Larsen, H.J. og H. Riberholt: Tværbæreevne af søm og dykkere i spån- og træfiberplader. 1974.

R 48. Poulsen, P.E.: The photo-elastic effect in three--dimensional states of stress. 1974.

R 49. Nielsen, J.: Modellove for kornede medier med særligt henblik på silomodeller. 1974.